Fabrication of dense polymer derived mullite ceramics by fused deposition modeling (FDM) method

Inaugural dissertation
of the Faculty of Science,
University of Bern

presented by

Fateme Sarraf

from Iran

Supervisors of the doctoral thesis:

Prof. Dr. Sergey V. Churakov
University of Bern, Paul Scherrer Institut (PSI)

Dr. Frank Clemens
Empa- Swiss Federal Laboratories for Materials Science and Technology

Fabrication of dense polymer derived mullite ceramics by fused deposition modeling (FDM) method

Inaugural dissertation
of the Faculty of Science,
University of Bern

presented by

Fateme Sarraf
from Iran

Supervisors of the doctoral thesis:

Prof. Dr. Sergey V. Churakov
University of Bern, Paul Scherrer Institut (PSI)

Dr. Frank Clemens
Empa- Swiss Federal Laboratories for Materials Science and Technology

Accepted by the Faculty of Science.

Bern, 08.09.2023 The Dean
Prof. Dr. Marco Herwegh

Acknowledgement

I would like to express my gratitude to my thesis advisor at Empa, Dr. Frank Clemens, for giving me the chance to start as a PhD researcher in their group. I got familiar with Dr. Clemens during my internship in 2017 at Empa and I learned a lot from our scientific discussions. Coming to Empa for a PhD position, their invaluable guidance and support continued throughout the entire research process. Their insightful feedback and constructive criticism have played a crucial role in shaping this thesis.

I would like to sincerely thank my academic advisor in the University of Bern, Prof. Sergey V. Churakov, for supporting me through this PhD thesis. Their mentorship and encouragement have been instrumental in shaping the direction of my study.

I would also like to extend my sincere appreciation to the members of my thesis committee, the external reviewer, Prof. Enrico Bernardo to accept reviewing this PhD thesis and Prof. Jörg Hermann for chairing the defense session. I appreciate their valuable input and suggestions, which greatly contribute to the improvement of this work.

I am grateful to SNFS organization for funding this project and Empa for providing the necessary resources, facilities, and opportunities that enabled me to conduct this research.

I would like to acknowledge the assistance and cooperation of Dr. Amir Hadian and Dr. Frank Gfeller who contributed their time and expertise to this study. Their involvement has been instrumental in obtaining meaningful results and insights. Also, I would like to thank Mr. Nikolajs Toropovs, Dr. Amy Jenelle Knorpp and Dr. John Bell as I learned a lot from our discussions in the lab.

I would like to express my heartfelt thanks to my friends Sara, Saeed, Neda, Maria, Sena, Hossein, Abdi, Zahra, Bahar, Somashree, Elham, Laura, Arun and Ehsan for their unwavering support, encouragement, and understanding throughout this academic journey and always being there for me.

I would like to thank my parents, Mahdi and Akram for being my biggest support during these 30 years and giving me all their love and support through my hard times, and Faeze, for being my best friend since she was born!

Abstract

Using preceramic polymers (PCP) for additive manufacturing of oxide and non-oxide ceramics has attracted a lot of attention since a few years ago due to their extraordinary properties. Various kinds of polymer derived ceramics produced by utilizing different PCPs have shown excellent thermal stability, corrosion and oxidation resistance at high temperatures, biocompatibility, dielectric properties and so on.

Thermoplastic properties of PCPs provide the plasticity and flowability desired for the additive manufacturing (AM) shaping processes.

Fabrication of PDCs using material extrusion based additive manufacturing (MEX-AM) method, formerly called fused deposition modeling (FDM) or fused filament fabrication (FFF) process, has been addressed in a very limited set of studies with a narrow focus. Further investigations are needed to explore the full potential of this method for the fabrication of dense, crack-free polymer derived ceramics.

This PhD thesis aimed to develop a fused deposition modeling (FDM) process for fabricating polymer-derived mullite ceramics, with a focus on achieving dense sintered parts with high wall thickness. The research questions addressed in this study are 1) the promotion of densification through the addition of MgO sintering aid, 2) the evaluation of ceramic yield and the effect of heating rate on the polymer derived mullite material, and 3) the prevention of structural defects through the creation of interconnected small pores.

In this study, it was demonstrated that the addition of 1.0 wt% MgO significantly influenced the sinterability of mullite ceramics, resulting in increased densification and improved flexural strength. Furthermore, the impact of printing orientation on mechanical properties was mitigated by the presence of MgO. However, defects in the cross-section of the sintered samples, attributed to trapped water molecules, were still present. Therefore, the utilization of submicron alumina powder as an active filler, combined with a small amount of MgO, was necessary to obtain a pure mullite phase after sintering.

Further, the ceramic yield of commercially available methyl-silsesquioxane (SILRES MK) was evaluated under different atmospheres and heating rates. Stable yields were observed under inert atmospheres and at higher heating rates in air, while lower heating rates led to decreased yields in air atmosphere. The heating rate was found to influence the composition of Si-O-Si bonds, with slower rates resulting in the dominance of cages over network structures. This

finding suggested that volatile polyhedral silsesquioxanes (POSS) molecules were more likely to evaporate during the heat-treatment at lower heating rates.

Finally, a new approach involving the modification of the thermoplastic binder system was proposed. By adding a water-soluble polyvinyl alcohol (PVA) grade, interconnected porous channels were formed, enabling the escape of released gases during post-processing. The use of a screw-based FDM printer facilitated the printing of feedstocks in the form of pellets, allowing for the fabrication of bulk polymer-derived ceramics without restrictions related to filament production. The choice of suitable ethylene vinyl alcohol (EVA) properties influenced the removal of gaseous products and the printability of the feedstocks.

In general, the research presented in this thesis contributes to the development of FDM-based fabrication of polymer-derived mullite ceramics, and the methods and findings presented have the potential for application in the manufacturing of ceramic objects with diverse shapes using a range of plastic-forming technologies.

List of abbreviations

3D	Three-dimensional
AM	Additive manufacturing
CS	Calcium silicate
DIW	Direct ink writing
DLP	Digital light processing
EVA	Ethylene vinyl acetate
FDM	Fused Deposition Modeling
FFF	Fused filament fabrication
FTIR	Fourier-transform infrared
MEX_AM	Material extrusion based additive manufacturing
M	Monomer
NMR	Solid-state nuclear magnetic resonance
PDC	Polymer derived ceramic
PCP	Preceramic polymer
PI	Photo initiator
PVA	Poly(vinyl alcohol)
SEM	Scanning electron microscopy
SL	Stereolithography
SLS	Selective laser sintering
TG	Thermogravimetry
TPP	Two-photon polymerization
XRD	X-ray diffraction

Table of Contents

Chapter 1- Introduction

Ceramic art has been a part of human culture since prehistoric times. The term "ceramic" originated from a Greek keramos, referring to "pottery" or "potter's clay". For thousands of years, mixing clay and water, tableware, tiles, bricks and sanitaryware were shaped and fired at high temperatures. Producing the first silica refractories in 1822, the word "ceramic" was used for other materials, which contained no clay, but were processed similarly [1]. During the 20th century, accelerated development in producing technical ceramics created a demand to explore new synthetic plasticizers and binder additives, as technical ceramic powders like Al_2O_3, ZrO_2, SiC, or Si_3N_4 did not show the plasticity of clays, necessary for the shaping process when using water [2]. As a result, shaping ceramics came a long way from making handmade pieces out of clay by casting, pressing and thermoplastic shaping toward more advanced free-forming techniques, called additive manufacturing (AM).

It is worthwhile to mention that for shaping ceramics, an organic binder system is used in most cases to compensate for the lack of plasticity and have an efficient green strength to hold the ceramic particles together after shaping [3]. The organic binder, however, has to be removed in a debinding step before sintering (densification at high temperatures) to provide a uniform and strong ceramic part. To make ceramic materials, natural minerals are processed into powders or they can be synthesized by different methods including solid-state synthesis, coprecipitation, reactions in molten salts, sol-gel, hydrothermal synthesis, etc. [4].

Alternatively, ceramics can be produced by polymer pyrolysis using some organic compounds, called preceramic polymers (PCPs), too. PCPs, specifically Si-based PCPs, are polymeric compounds containing C, O, N, B, or H atoms grafted in their main structure [5]. Thermal treatment of PCPs results in crosslinking and pyrolysis, yielding Si-C, Si-O or Si-O-C, Si-N and Si-B based ceramics depending on the starting precursor and the atmosphere during the heat treatment [6]. Fillers such as alkali metal oxides, hydroxide, carbonates, sulfates and nitrates can react with the remained ceramic yield from pyrolysis of PCP and produce new ceramic phases by heating at higher temperatures. Using PCPs, a wide range of oxide or non-oxide ceramics such as mullite ($3Al_2O_3.2SiO_2$) [7-9], cordierite ($2MgO.2Al_2O_3.5SiO_2$) [10] [11], wollastonite ($CaSiO_3$) [12], silicon carbide (SiC) [13-15], silicon nitride (Si_3N_4) [16], silicon carbonitride (SiCN), silicon oxycarbide (SiOC) [17, 18], silicoboron carbonitride (SiBCN) [19, 20], SiBCO [21, 22] and sialon (SiAlON) [23], etc. can be achieved. Employing these classes of ceramics for chemical, thermal and mechanical applications requires good

chemical and thermal stability, mechanical properties, and low tolerances to maintain high quality [24]. When shaping PDCs for advanced applications, conventional polymer processing shaping methods can be used, including additive manufacturing (AM). AM has been introduced as a bottom-up approach to overcome the limitations in shaping materials and enabling the creation of free-form geometries for many years. However, despite its longevity, the full potential of AM has yet to be fully realized, and there is still much to be explored in this field. Various AM techniques have been developed to shape PDCs, including light-assisted techniques such as stereolithography [18, 25, 26] and digital light processing (DLP) [27, 28], laser-assisted methods like selective laser sintering [29], and material extrusion-based AM techniques such as fused deposition modeling [7, 30] and direct ink writing [31]. There have been significant advances in developing innovative methods to shape PDCs. However, choosing a proper post-processing including debinding and sintering steps can be difficult depending on the geometry and composition of the part.

FDM process for the shaping of PDCs has been not studied in detail so far. Using FDM process, in particular, which contains a thermoplastic binder system to hold the particles together during the printing process, post-processing can be challenging when debinding and sintering large pieces. During the debinding step, shape instability problems (e.g. deformation of structure) due to remelting the binder and impact of gravity forces during the post-printing steps can occur, which leads to distortion in large and dense structures if not carefully controlled. Shape stability and avoiding structural defects in produced parts are of more importance where specifically technical ceramics are involved.

In this thesis, the investigation of FDM process for PDCs will be studied in more detail to be able to print larger dense ceramic structures in the future for different applications like ceramic matrix composites, electromagnetically transparent materials for high-temperature applications, biomedical components, etc. [24].

1.1. The motivation for the thesis

Fused deposition modeling/fused filament fabrication (FDM/FFF), later named as material extrusion based additive manufacturing (MEX-AM) shaping method by ASTM standard has been rarely explored for PDC materials [7, 30]. For polymer materials, FDM/FFF is one of the most common methods to achieve larger structures in a short time. There are several studies that address the application of FDM/FFF for metal and ceramic materials [32-34]. In this process, feedstocks in the form of continuous filaments or pellets can be used to feed the printer

[35, 36]. Filament extruders are used to feed a 1.75 or 2.85mm filament into the printer head via drive wheels. The material is guided through a hot-end zone which includes a heater that melts the thermoplastic binder, provides a viscous material to flow through a nozzle and deposits the feedstock on a printing bed. When spooling filament is not possible due to brittleness, a pellet extruder is used [36]. In this case, the material is fed into a hopper and transported by an auger screw to the hot end zone.

Using PCP for FDM/FFF process is interesting, because of their natural thermoplastic properties [37]. In principle, this would enable us to use the thermoplastic PCP binder system to achieve plasticity and flowability during the shaping process and as a raw material to synthesize PDCs by sintering. However, Gorjan et al. could demonstrate that still 60 vol% organic binder content is recommended to achieve a stable printing process [7]. The results showed that PDCs can be fabricated by FDM/FFF process but the process needed to be further investigated to be able to achieve dense structures without structural defects (e.g. closed pores).

1.2. Research aims and objectives

This thesis investigates the fabrication of 3D printed mullite based structures using PCPs and FDM/FFF technique. To approach this subject, the following three research questions were investigated in more detail:

- **How sintering additives affect the densification and mullite formation during the sintering process?**

The low bulk and grain-boundary diffusion coefficients of Si^{4+} and Al^{3+} cations hinder the sintering process of mullite ceramics, making it difficult to achieve high densities at lower temperatures [38]. To overcome this challenge, sintering oxides such as MgO (magnesium oxide), Y_2O_3 (yttrium oxide) [39], TiO_2 (Titanium oxide) [40] and La_2O_3 (lanthanum oxide) [41] are often introduced to facilitate the densification of mullite ceramics. According to research findings, MgO has shown the most promising results so far. Studies have indicated that the addition of MgO can result in the formation of a liquid phase that enhances the diffusion of SiO_2 and Al_2O_3 species, enabling densification at lower temperatures [42].

- **How to design the thermal post-printing process to control the ceramic yield of PCP materials for silicate based ceramic materials?**

The composition of PDCs is influenced by thermal treatment parameters like heating rate, dwell temperatures, and dwell times at lower temperatures (< 800°C) because of the ceramic yield variation of the PCP (Si-O containing oligomers can escape) [6].

- **How to optimize FDM process to fabricate dense large PDCs structures?**

Shaping PDCs is mainly limited to coatings [43], thin structures [7], foams and porous structures [44-46]. Fabrication of dense structures can be quite challenging due to intensive gas release during their crosslinking and pyrolysis steps and causes cracks, blisters, or bubbles when processing larger parts [47]. The presence of cracks formed during pyrolysis is also affected by the heating rate. Hence, it is crucial to implement an appropriate heating program with relatively low rates (e.g., 2K/min or less) for the pyrolysis of the preceramic polymer (PCP), especially when dealing with larger parts (above a few mm^3) to ensure a gradual release of gases during the ceramization process, which is desirable. Using PCP as the silica source, Gorjan et al. observed macro-voids in the center of printed samples after sintering [7]. These pores can come from the printing process or debinding step. Therefore, the closed pores need to be removed before sintering step.

The following experiments and characterization methods were set up to answer these research questions:

(i) investigation of MgO as a sintering aid to improve sinterability of mullite, (ii) investigation of post-printing processing steps to prevent macro-voids in the final sintered PDC structures, (iii) investigation of thermal treatment parameters on preceramic polymer yield to be able to adjust the ceramic composition of PDC based silicate ceramics, (iv) investigation of a suitable binder system to avoid pore formation during debinding step.

1.3. Structure outline

The thesis is structured into seven chapters, as shown in Fig. 1. Chapter 1 presents a general overview of the topic, motivation, research questions and objectives. In chapter 2, a comprehensive literature survey is conducted to provide an overview of relevant studies, with a particular focus on PDCs and additive manufacturing techniques. This section offers an in-depth review of state-of-the-art research in this field. Chapters 3 to 5 include the results of this study as appended papers including the effect of MgO sintering additive content on enhancing

the densification and phase purity of polymer derived 3:2 mullite (chapter 3). In the second step, thermal decomposition of the PCP material was studied to optimize the effect of thermal treatment parameters (atmosphere and heating rate) and achieve a stable high ceramic yield after pyrolysis (chapter 4). After that, debinding step was investigated in more detail to find a solution for structural defects like cracks and closed pores before densification during sintering, and modify the binder system to control the gas removal during heat treatment of the PCP (chapter 5). Chapter 6 provides a detailed conclusion and an outlook. In collaboration with other scientists, chapter 7, presents the collaborative studies for the development of characterization methods to improve the FDM/FFF process for other ceramic materials. To enhance readability, the references are located at the end of each chapter.

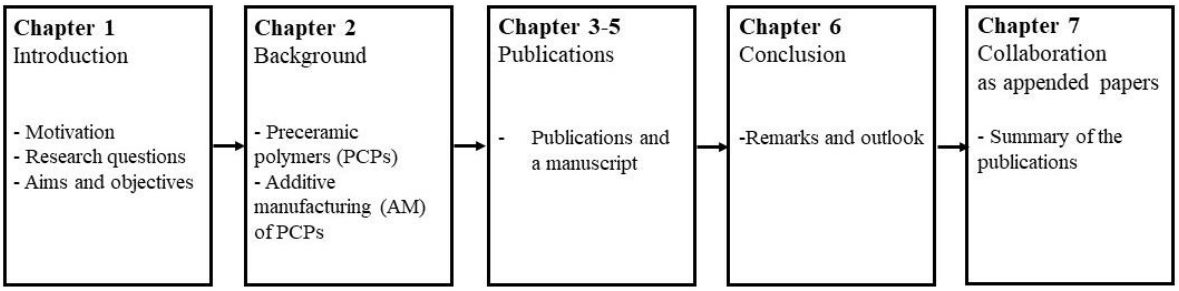

Fig. 1. The structure of this thesis, with emphasis on the main topics covered in each chapter.

References

[1] C.B. Carter, M.G. Norton, Ceramic materials: science and engineering, Springer2007.

[2] S. Blackburn, D.I. Wilson, Shaping ceramics by plastic processing, Journal of the european Ceramic Society 28(7) (2008) 1341-1351.doi: https://doi.org/10.1016/j.jeurceramsoc.2007.12.013.

[3] J.A. Lewis, Binder removal from ceramics, Annual Review of Materials Science 27(1) (1997) 147-173.doi: https://doi.org/10.1146/annurev.matsci.27.1.147.

[4] D. Segal, Chemical synthesis of ceramic materials, Journal of Materials Chemistry 7(8) (1997) 1297-1305.doi: https://doi.org/10.1039/A700881C.

[5] G. Mera, E. Ionescu, Silicon-containing preceramic polymers, Encyclopedia of polymer science and technology (2002).doi: https://doi.org/10.1002/0471440264.pst591.

[6] P. Colombo, G. Mera, R. Riedel, G.D. Soraru, Polymer-derived ceramics: 40 years of research and innovation in advanced ceramics, Ceramics Science and Technology (2013) 245-320.

[7] L. Gorjan, R. Tonello, T. Sebastian, P. Colombo, F. Clemens, Fused deposition modeling of mullite structures from a preceramic polymer and γ-alumina, Journal of the European Ceramic Society 39(7) (2019) 2463-2471.doi: https://doi.org/10.1016/j.jeurceramsoc.2019.02.032.

[8] J. Schmidt, A.A. Altun, M. Schwentenwein, P. Colombo, Complex mullite structures fabricated via digital light processing of a preceramic polysiloxane with active alumina fillers, Journal of the European Ceramic Society 39(4) (2019) 1336-1343.doi: https://doi.org/10.1016/j.jeurceramsoc.2018.11.038.

[9] E. Bernardo, P. Colombo, E. Pippel, J. Woltersdorf, Novel mullite synthesis based on alumina nanoparticles and a preceramic polymer, Journal of the American Ceramic Society 89(5) (2006) 1577-1583.doi: https://doi.org/10.1111/j.1551-2916.2006.00963.x.

[10] G. Parcianello, E. Bernardo, P. Colombo, Cordierite ceramics from silicone resins containing nano-sized oxide particle fillers, Ceramics International 39(8) (2013) 8893-8899.doi: https://doi.org/10.1016/j.ceramint.2013.04.083.

[11] I.-H. Song, M.-J. Kim, H.-D. Kim, Y.-W. Kim, Processing of microcellular cordierite ceramics from a preceramic polymer, Scripta Materialia 54(8) (2006) 1521-1525.doi: https://doi.org/10.1016/j.scriptamat.2005.12.039.

[12] E. Bernardo, P. Colombo, E. Dainese, G. Lucchetta, P.F. Bariani, Novel 3D wollastonite-based scaffolds from preceramic polymers containing micro-and nano-sized reactive particles, Advanced Engineering Materials 14(4) (2012) 269-274.doi: https://doi.org/10.1002/adem.201100241.

[13] R.M. Laine, F. Babonneau, Preceramic polymer routes to silicon carbide, Chemistry of materials 5(3) (1993) 260-279.

[14] Y.J. Lee, J.H. Lee, S.R. Kim, W.T. Kwon, H. Oh, J.-h.P. Klepeis, S.J. Teat, Y. Kim, Synthesis and characterization of novel preceramic polymer for SiC, Journal of materials science 45 (2010) 1025-1031.doi: https://doi.org/10.1007/s10853-009-4034-2.

[15] H. Chen, X. Wang, F. Xue, Y. Huang, K. Zhou, D. Zhang, 3D printing of SiC ceramic: Direct ink writing with a solution of preceramic polymers, Journal of the European Ceramic Society 38(16) (2018) 5294-5300.doi: https://doi.org/10.1016/j.jeurceramsoc.2018.08.009.

[16] M. Wang, C. Xie, R. He, G. Ding, K. Zhang, G. Wang, D. Fang, Polymer-derived silicon nitride ceramics by digital light processing based additive manufacturing, Journal of the American Ceramic Society 102(9) (2019) 5117-5126.doi: https://doi.org/10.1111/jace.16389.

[17] G. Pierin, C. Grotta, P. Colombo, C. Mattevi, Direct Ink Writing of micrometric SiOC ceramic structures using a preceramic polymer, Journal of the European Ceramic Society 36(7) (2016) 1589-1594.doi: https://doi.org/10.1016/j.jeurceramsoc.2016.01.047.

[18] E. Zanchetta, M. Cattaldo, G. Franchin, M. Schwentenwein, J. Homa, G. Brusatin, P. Colombo, Stereolithography of SiOC ceramic microcomponents, Advanced Materials 28(2) (2016) 370-376.doi: https://doi.org/10.1002/adma.201503470.

[19] O. Majoulet, J.G. Alauzun, L. Gottardo, C. Gervais, M.E. Schuster, S. Bernard, P. Miele, Ordered mesoporous silicoboron carbonitride ceramics from boron-modified polysilazanes: Polymer synthesis,

processing and properties, Microporous and mesoporous materials 140(1-3) (2011) 40-50.doi: https://doi.org/10.1016/j.micromeso.2010.09.008.

[20] X.-B. Yan, L. Gottardo, S. Bernard, P. Dibandjo, A. Brioude, H. Moutaabbid, P. Miele, Ordered mesoporous silicoboron carbonitride materials via preceramic polymer nanocasting, Chemistry of Materials 20(20) (2008) 6325-6334.doi: https://doi.org/10.1021/cm703114y.

[21] M.A. Schiavon, N.A. Armelin, I.V.P. Yoshida, Novel poly (borosiloxane) precursors to amorphous SiBCO ceramics, Materials Chemistry and Physics 112(3) (2008) 1047-1054.doi: https://doi.org/10.1016/j.matchemphys.2008.07.041.

[22] V. Liebau, R. Hauser, R. Riedel, Amorphous SiBCO ceramics derived from novel polymeric precursors, Comptes Rendus Chimie 7(5) (2004) 463-469.doi: https://doi.org/10.1016/j.crci.2003.11.012.

[23] E. Bernardo, P. Colombo, S. Hampshire, SiAlON-based ceramics from filled preceramic polymers, Journal of the American Ceramic Society 89(12) (2006) 3839-3842.doi: https://doi.org/10.1111/j.1551-2916.2006.01287.x.

[24] Y. Guo, Y. Sugahara, Polymer-derived ceramics for electrocatalytic energy conversion reactions, International Journal of Applied Ceramic Technology 20(1) (2023) 8-23.doi: https://doi.org/10.1111/ijac.14262.

[25] Z.C. Eckel, C. Zhou, J.H. Martin, A.J. Jacobsen, W.B. Carter, T.A. Schaedler, Additive manufacturing of polymer-derived ceramics, Science 351(6268) (2016) 58-62.doi: https://doi.org/10.1126/science.aad2688.

[26] S.A. Brinckmann, N. Patra, J. Yao, T.H. Ware, C.P. Frick, R.S. Fertig III, Stereolithography of SiOC polymer-derived ceramics filled with SiC micronwhiskers, Advanced Engineering Materials 20(11) (2018) 1800593.doi: https://doi.org/10.1002/adem.201800593.

[27] J. Schmidt, P. Colombo, Digital light processing of ceramic components from polysiloxanes, Journal of the European Ceramic Society 38(1) (2018) 57-66.doi: https://doi.org/10.1016/j.jeurceramsoc.2017.07.033.

[28] S. Li, W. Duan, T. Zhao, W. Han, L. Wang, R. Dou, G. Wang, The fabrication of SiBCN ceramic components from preceramic polymers by digital light processing (DLP) 3D printing technology, Journal of the European Ceramic Society 38(14) (2018) 4597-4603.doi: https://doi.org/10.1016/j.jeurceramsoc.2018.06.046.

[29] T. Friedel, N. Travitzky, F. Niebling, M. Scheffler, P. Greil, Fabrication of polymer derived ceramic parts by selective laser curing, Journal of the European Ceramic Society 25(2-3) (2005) 193-197.doi: https://doi.org/10.1016/j.jeurceramsoc.2004.07.017.

[30] H. Mei, Y. Yan, L. Feng, K.G. Dassios, H. Zhang, L. Cheng, First printing of continuous fibers into ceramics, Journal of the American Ceramic Society 102(6) (2019) 3244-3255.doi: https://doi.org/10.1111/jace.16234.

[31] H. Xiong, H. Chen, L. Zhao, Y. Huang, K. Zhou, D. Zhang, SiCw/SiCp reinforced 3D-SiC ceramics using direct ink writing of polycarbosilane-based solution: Microstructure, composition and mechanical properties, Journal of the European Ceramic Society 39(8) (2019) 2648-2657.doi: https://doi.org/10.1016/j.jeurceramsoc.2019.02.045.

[32] M. Allahverdi, S. Danforth, M. Jafari, A. Safari, Processing of advanced electroceramic components by fused deposition technique, Journal of the European Ceramic Society 21(10-11) (2001) 1485-1490.doi: https://doi.org/10.1016/S0955-2219(01)00047-4.

[33] S.J. Kalita, S. Bose, H.L. Hosick, A. Bandyopadhyay, Development of controlled porosity polymer-ceramic composite scaffolds via fused deposition modeling, Materials Science and Engineering: C 23(5) (2003) 611-620.doi: https://doi.org/10.1016/S0928-4931(03)00052-3.

[34] A. Bellini, L. Shor, S.I. Guceri, New developments in fused deposition modeling of ceramics, Rapid Prototyping Journal (2005).doi: https://doi.org/10.1108/13552540510612901.

[35] K.S. Boparai, R. Singh, H. Singh, Development of rapid tooling using fused deposition modeling: a review, Rapid Prototyping Journal 22(2) (2016) 281-299.doi: https://doi.org/10.1108/RPJ-04-2014-0048.

[36] J. Gonzalez-Gutierrez, S. Cano, S. Schuschnigg, C. Kukla, J. Sapkota, C. Holzer, Additive manufacturing of metallic and ceramic components by the material extrusion of highly-filled polymers: A review and future perspectives, Materials 11(5) (2018) 840.doi: https://doi.org/10.3390/ma11050840.

[37] P. Colombo, K. Perini, E. Bernardo, T. Capelletti, G. Maccagnan, Ceramic microtubes from preceramic polymers, Journal of the American Ceramic Society 86(6) (2003) 1025-1027.doi: https://doi.org/10.1111/j.1151-2916.2003.tb03413.x.

[38] M.D. Sacks, N. Bozkurt, G.W. Scheiffele, Fabrication of mullite and mullite-matrix composites by transient viscous sintering of composite powders, Journal of the American Ceramic Society 74(10) (1991) 2428-2437.doi: https://doi.org/10.1111/j.1151-2916.1991.tb06780.x.

[39] V. Viswabaskaran, F. Gnanam, M. Balasubramanian, Effect of MgO, Y2O3 and boehmite additives on the sintering behaviour of mullite formed from kaolinite-reactive alumina, Journal of Materials Processing Technology 142(1) (2003) 275-281.

[40] S. Maitra, J. Roy, Effect of TiO2 and V2O5 additives on chemical mullite, Adv. Ceram. Sci. Eng.(ACSE) 2(3) (2013).

[41] H. Ji, M. Fang, Z. Huang, K. Chen, Y. Xu, Y.g. Liu, J. Huang, Effect of La2O3 additives on the strength and microstructure of mullite ceramics obtained from coal gangue and γ-Al2O3, Ceramics International 39(6) (2013) 6841-6846.doi: https://doi.org/10.1016/j.ceramint.2013.02.016.

[42] L. Montanaro, J. Tulliani, C. Perrot, A. Negro, Sintering of industrial mullites, Journal of the European Ceramic Society 17(14) (1997) 1715-1723.doi: https://doi.org/10.1016/S0955-2219(97)00043-5.

[43] G. Barroso, T. Kraus, U. Degenhardt, M. Scheffler, G. Motz, Functional coatings based on preceramic polymers, Advanced Engineering Materials 18(5) (2016) 746-753.doi: https://doi.org/10.1002/adem.201500600.

[44] L. Fiocco, H. Elsayed, L. Ferroni, C. Gardin, B. Zavan, E. Bernardo, Bioactive Wollastonite-Diopside Foams from Preceramic Polymers and Reactive Oxide Fillers, Materials, 2015, pp. 2480-2494.

[45] J. Zeschky, T. Höfner, C. Arnold, R. Weißmann, D. Bahloul-Hourlier, M. Scheffler, P. Greil, Polysilsesquioxane derived ceramic foams with gradient porosity, Acta Materialia 53(4) (2005) 927-937.doi: https://doi.org/10.1016/j.actamat.2004.10.039.

[46] P. Colombo, M. Modesti, Silicon oxycarbide ceramic foams from a preceramic polymer, Journal of the American Ceramic Society 82(3) (1999) 573-578.doi: https://doi.org/10.1111/j.1151-2916.1999.tb01803.x.

[47] P. Colombo, G. Mera, R. Riedel, G.D. Sorarù, Polymer-Derived Ceramics: 40 Years of Research and Innovation in Advanced Ceramics, Journal of the American Ceramic Society (2010) no-no.doi: https://doi.org/10.1111/j.1551-2916.2010.03876.x.

Chapter 2- Background

2.1. Preceramic polymers

The idea of using molecular precursors to produce ceramic structures was first introduced by Ainger and Herbert in 1960 [1]. Pyrolysis of organosilicon polymers to produce ceramic materials for use in high-temperature applications was presented by Verbeek in the early 1970s, specifically designed to make Si_3N_4/SiC ceramic fibers [2]. The research work of Yajima et al. in 1975 on the synthesis of SiC-based fibers from polycarbosilane, marked a major advancement in the area of polymer pyrolysis for the production of polymer derived ceramics (PDCs) [3]. Since then, preceramic polymers (PCPs), more specifically organosilicon polymers, have been widely acknowledged as an effective method to create advanced ceramics. It is worthwhile to mention that different terms have been used for organosilicon polymers [4, 5] such as Si-based polymers [6, 7], Si-based preceramic polymers [8, 9] and silicone resins [10, 11].

2.1.1. Si-based preceramic polymers

The first step for the fabrication of Si-based polymer derived ceramics is to synthesize the proper organosilicon polymer. By grafting different elements such as oxygen, nitrogen and carbon to the Si backbone structure, various types of Si-based polymers can be achieved [1, 2], as shown in Fig. 1. These polymers serve as starting precursors for producing a wide range of ceramic compositions, including SiC, SiO_2, Si_3N_4, SiOC, SiCN, SiBCN, SiBOC, SiAlON, and other [2]. The most frequently used organosilicon polymers, their chemical formula, synthesis routes and applications are listed in Table 1.

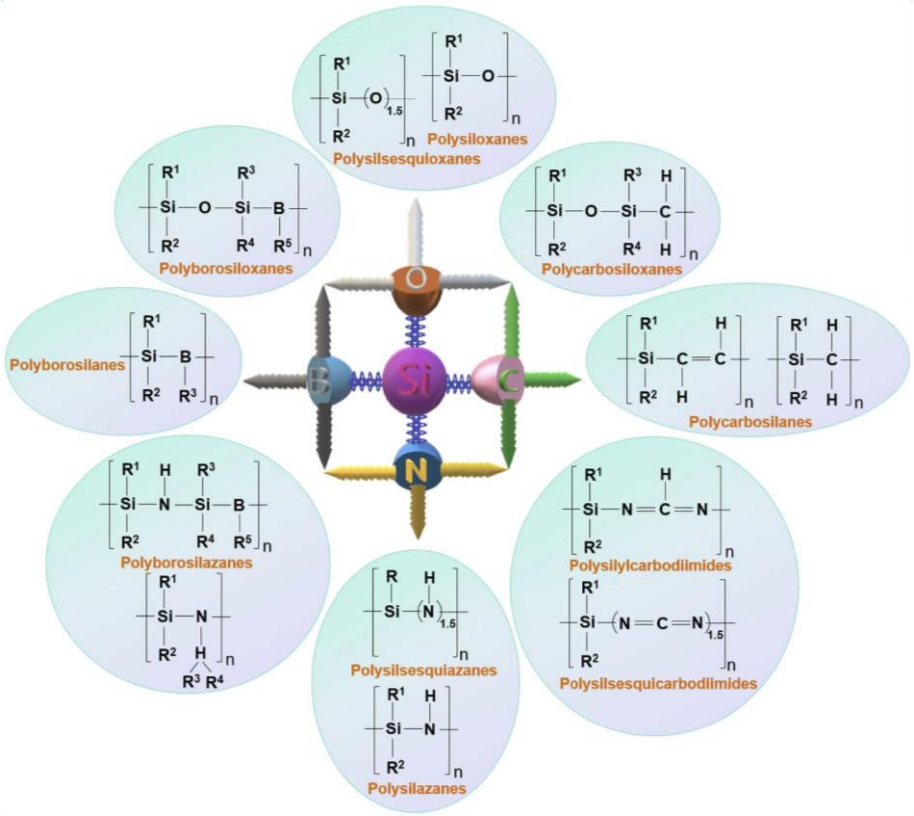

Fig. 1. Different types of Si-based preceramic polymers (reprinted from [2] with permission from Elsevier).

Only high molecular weight polymers that are capable of crosslinking can be used for the fabrication of polymer derived ceramics [3]. A brief description of the important classes of preceramic polymers including polysilane, polycarbosilane, polysilazane, and polysiloxane is mentioned below:

Polysilanes

Polysilanes having a one-dimensional silicon backbone are basic precursors for synthesis of SiC ceramics. Each silicon atom is attached to R_1 and R_2 substituents. Polysilanes are typically prepared using a commonly employed method known as Wurtz-type coupling of halosilanes [12]. This synthetic approach involves the reaction of chlorosilanes with sodium or lithium dispersion, resulting in the reduction process that leads to the formation of polysilane. The reaction occurs within a high boiling point inert solvent, such as toluene, benzene, or tetrahydrofuran, under reflux conditions. Polysilanes have been proposed for various applications such as photoresists, photoconductors, and semiconductors [5]. Their σ-conjugation due to electron delocalization on silicon-silicon bonds results in distinctive optoelectronic and photoelectric properties. The properties of polysilane stem from two primary

factors: the side chain groups attached to the backbone and the molecular weight of the polymer [2].

Polycarbosilanes

Polycarbosilanes with a Si-C backbone, contain branched chains such as methylene, vinylidene and phenylene that make them more complex compared to polysilanes [13]. The most common way to synthesize these polymers is thermal decomposition of polysilanes under pressure using Kumada mechanism. However, the accumulation of decomposition gaseous products (e.g. methane, Me_3SiH, SiH_4) can lead to a dangerous increase of pressure in the autoclave. Synthesis of polycarbosilanes by pyrolysis of polydimethylsilane in a nitrogen atmosphere was performed at ambient pressure through catalytic processes (using polyborodiphenylsiloxane) in a reflux condenser [14]. This class of organosilicon polymers has been widely used for the fabrication of SiC based components like fibers, composites, powders and so on.

Polysilazanes

Using polysilazanes with C-containing side chains attached to a Si-N backbone, SiCN ceramics are synthesized. If a C- free polysilazane polymer like perhydridopolysilazane is utilized, Si_3N_4 ceramics can be produced. Fabrication of SiCN fibers from polycarbosilazanes was first demonstrated by Verbeek et al. in the 1970s [15] where oxidation resistance up to 1200°C, significant strength and elastic modulus were achieved.

Remarkable thermal stability, scratch resistance, corrosion resistance, and high hardness of polysilazanes make them ideal for various applications including protective and heat-resistant coatings in industries such as electronics, automotive, and aerospace as well as heat exchanger barriers [16] and for protecting steel against oxidation [17].

Polysiloxanes and polysilsesquioxanes

Polysiloxanes (Fig. 2a) with a general formula of $[R_2SiO]_n$ are inexpensive, widely used class of Si-based PCPs for synthesis of silicone oxycarbide and oxynitride ceramics [2].

Equation 2.1 describes the formation of polysiloxanes through the reaction of chlorosilane precursors with water.

$$n\ Si(CH_3)_2Cl_2 + nH_2O \rightarrow [Si(CH_3)_2O]_n + 2n\ HCl \qquad (2.1)$$

Ring opening polymerization of cyclic trimers and tetramers has been reported as a successful alternative to the hydrolysis approach [18]. Crosslinked polysiloxanes and polysilsesquioxanes can be obtained using the sol-gel process via hydrolysis and condensation reactions of organically modified silicon alkoxides, depending on their functional side chain.

Polysilsesquioxanes with a chemical formula of $[RSiO_{3/2}]_n$, as implied by their name, consist of a silicon atom (sil-), bonded to one and a half (-sesqui-) oxygen atom (-ox-), and a hydrocarbon group (-ane) [19]. R can be either H atom or an organic functional group such as methyl, phenyl, ethoxy, or hydroxyl. The nature of the organic ligands attached to the Si atoms determines the packing of the molecules and the intermolecular forces between them, which ultimately determine the physical state of the material. As a result, pure polysilsesquioxanes can be found in the form of liquid, crystalline or amorphous powder. These hybrid organic-inorganic materials can have random, ladder, partial cage and cage structures [20, 21] (Fig. 2b). Random structures are polymeric precursors that lack long-range order. The Ladder ones consist of alternating silicon and oxygen atoms in an oligomeric scale arranged in a ladder-like structure. The process of hydrolysis and condensation of organosilanes results in the formation of partial cage structures. These structures, despite being partially condensed, still have silanol groups present at one or more corners of the cage. Cage structures contain no silanol groups (-OH) as they are fully crosslinked.

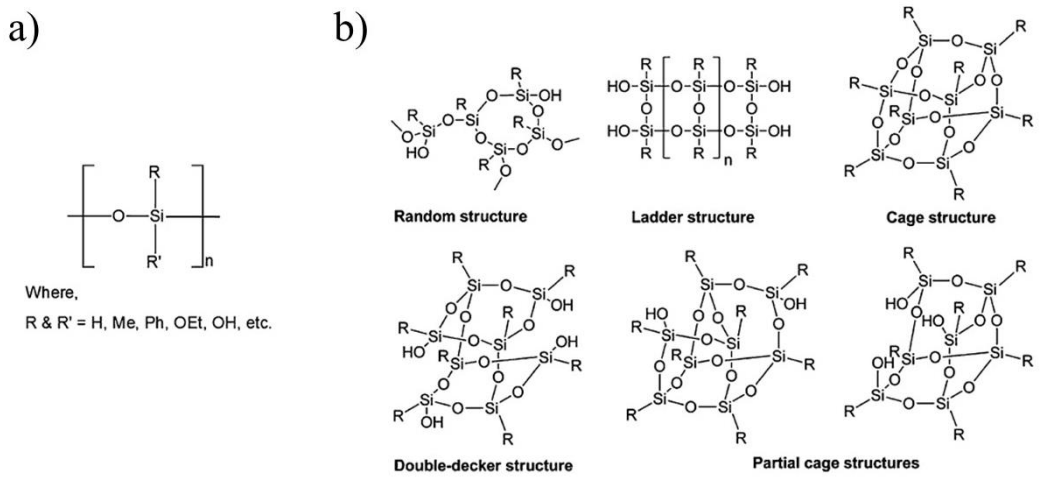

Fig. 2. General structure of a) polysiloxanes, and b) polysilsesquioxanes (reproduced from [21] with permission from Springer Nature).

Pyrolysis of polysiloxanes and polysilsesquioxanes results in the formation of siliconoxycarbide (SiOC) glasses [22]. Mechanical properties of carbon-rich SiOC glasses,

particularly creep resistance have been extremely improved compared to fused SiO_2 [23]. The addition of ceramic or metallic particles allows for modification of the mechanical and physical properties of the SiOC matrix [24].

In addition to SiOC ceramics, silicate ceramics can be fabricated by introducing fillers to the polysiloxane/polysilsesquioxanes polymers [1].

Table 1. Various organosilicon polymers are used for the fabrication of PDCs (synthesis methods, obtained ceramics and their applications) (reproduced from [5]). Open access CC-BY 4.0.

Organosilicon polymer	**Backbone structure**	**Synthesis methods**	**Applications**
Polysilane	$-R_1R_2Si-$	Wurtz-type coupling of halosilanes anionic polymerization of masked disilenes catalytic dehydrogenation of silanes reduction of dichlorosilanes	Photoresists, photo conductors, semiconductors and precursors for synthesis of polycarbosilane
Polycarbosilane	$-R_1R_2Si-C-$	Kumada rearrangement of polysilanes ring opening polymerization Dehydrocoupling reaction of trimethylsilane hydrosilylation of vinylhydridosilanes grignard coupling reaction of (chloromethyl)-triethoxysilane and vinylmagnesium bromide	Precursors for preparation of SiC, electric or photo conductors, photoresist nonlinear optical materials
Polysilazane	$-R_1R_2Si-N=$	Ammonolysis reactions of chlorosilanes with ammonia or by aminolysis ring opening polymerization of cyclic polysilanane	Precursors for preparation of Si_3N_4 or SiCN, barrier for heat exchanger or on steel against oxidation
Polysiloxane	$-R_1R_2Si-O-$	Ring-open polymerization of cyclic silaethers polycondensation of linear silanes	Precursors for preparation of SiOC, medicine electronics, textile chemistry
Polysilylcarbodiimides	$-R_1R_2Si-N=C=N-$	Pyridine-catalyzed polycondensation reaction of chlorosilanes with bis(trimethylsilylcarbodiimide)	Precursors for preparation of SiCN
Polyborosilazane	$-R_1R_2Si-N(R_3R_4B)-$	Co-condensation reaction of boron trichloride, organodichlorosilanes, and hexamethyldisilazane	Precursors for preparation of SiCBN

2.1.2. Properties of Si-based polymers

The unique properties of PCPs offer potential solutions for different applications where thermal stability is a necessity or the material experiences a harsh environment [5]. An intriguing aspect that encourages the utilization of PCPs is the possibility to modify the functional groups within the starting precursor, thereby promoting its properties [2]. Using Si-based polymers, PDCs in the form of powders, fibers, coatings, composites and complex three-dimensional (3D) structures can be produced. Diverse processing techniques have been implemented for the fabrication of PDCs as they can be melted and crosslinked or dissolved in many solvents [2].

Due to their viscoelastic behavior versus temperature and the miscibility with other polymers, various thermoplastic shaping methods can be utilized. Blending preceramic polymers with organic/inorganic additives facilitates the preparation of homogenous compounds for fabrication of PDCs. Substituting PCPs for ceramic powders, it is feasible to mix the materials at lower temperatures, while concurrently reducing abrasion within the machinery involved [25].

By dissolving PCPs in compatible organic solvents, mixed with other organic/inorganic additives, homogeneous ink, gel, or dried sediments (after drying) can be achieved. The obtained mixture can then be used for subsequent shaping or synthesis steps.

To fabricate polymer derived ceramic (PDC) 3D structures, organosilicon precursors need to have certain properties in order to be effective. One of these properties is the ability to crosslink. Following the shaping process, these polymers undergo a crosslinking stage to preserve the shape during subsequent thermal treatment [26]. A preceramic polymer with a high molecular weight is advantageous as more crosslinks can form, resulting in a thermoset that has a high shape stability during the thermal debinding process [5]. Utilizing preceramic polymers to create PDCs, it is possible to do machining of the parts before ceramization [27]. In this way, the occurrence of brittle fractures during machining of the ceramic part can be prevented.

By pyrolysis and sintering of PCPs in either air or an inert atmosphere at relatively lower temperatures (800-1200°C), a wide range of oxide and non-oxide ceramics can be obtained. Since the density values for the polymer (1-1.2 g/cm^3) and ceramic phases (2-3.2 g/cm^3) vary significantly, the resulting ceramic residue after pyrolysis may experience shrinkage of up to 70% in volume that leads to the development of considerable porosity or cracks. Therefore, achieving a minimum ceramic yield of 60% is expected after pyrolysis of preceramic polymers; however, a yield of 80% is more favorable for the PDC route [28] as the resulting PDCs are likely to show reduced shrinkage and lower occurrence of defects such as cracks and bubbles

[29]. The release of gaseous products during the crosslinking and pyrolysis of the PCPs is another factor contributing to the formation of micro/macro porosity and cracks in the fabricated PDCs [30].

To overcome the pore formation during crosslinking and pyrolysis, as well as the volume shrinkage of the PCPs during polymer to ceramic conversion [31], fillers have been commonly used for near-net-shape fabrication of PDCs by decreasing their freedom to shrink as first introduced by Greil et al. in the 1990s [32, 33] (Fig. 3). By adding fillers to the PCP matrix, its mechanical, thermal, or other desired properties can be improved. They are typically incorporated inside the matrix before the pyrolysis process. Depending on the specific application, desired characteristics and compatibility with the PCP matrix, a wide range of fillers can be utilized.

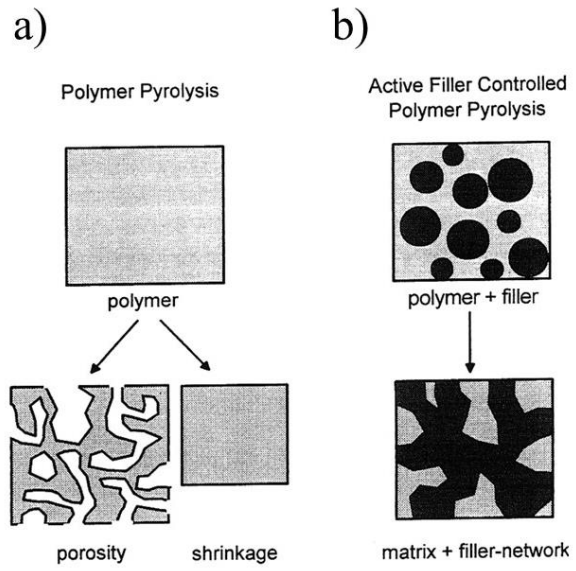

Fig. 3. Microstructure evolution during polymer to ceramic conversion (pyrolysis step): a) without, and b) with filler (reprinted from [33] with permission from Wiley).

Different shapes of fillers including powders, platelets, nanotubes, chopped and long fiber and so on can be added to the PCP matrix before shaping. Fillers are divided into four groups as shown in Fig. 4 [34]:

- passive fillers: this group of fillers does not react at all and only controls the shrinkage and presence of macro defects during pyrolysis such as SiC and Si_3N_4.

- active fillers: using active fillers, on the other hand, a new phase compared to the starting PCP can be achieved. Carbides, nitrides, silicates, oxides and silicides can be produced as a result of

a reaction between the filler and atmosphere or PCP residue after pyrolysis or the gaseous products during pyrolysis itself.

- meltable fillers: this category of fillers consists of meltable materials, typically glasses. When subjected to high temperatures, the glass phase melts or softens and effectively fills the porosity and enhances the density. This approach protects the part against oxidation and corrosion. When meltable fillers are used in coatings, their softening at elevated temperatures reduces the Young's modulus, allowing for the relaxation of thermomechanical stresses arising from mismatches in thermal expansion between the substrate, coating, and fillers within the precursor matrix. They may also undergo chemical reactions with other components in the system, acting as active fillers.

- sacrificial fillers: These organic compounds are mixed with the PCP and after crosslinking, are removed through thermal decomposition or dissolution in a solvent. Introducing porosity in the PDC part is their main application.

The choice of fillers depends on the desired properties of the final ceramic material and the compatibility with the preceramic polymer matrix. The amount and dispersion of fillers within the polymer matrix also play a crucial role in determining the overall performance of the resulting ceramic material.

Ceramic powders such as silicon carbide (SiC) [35], silicon nitride (Si_3N_4) [36], alumina (Al_2O_3) [37-39] and boron nitride (BN) [40] can be added to create composite or new phases after pyrolysis and enhance the mechanical properties. Using carbon-based fillers like carbon fibers and carbon nanotubes (CNTs) have been employed to improve the mechanical properties, electrical conductivity, and thermal stability of the preceramic polymers [30, 41]. Incorporating metallic powders or particles, mixed with a PCP as a reactive binder, PCP can improve wear resistance and corrosion resistance properties of the metal part [30]. Addition of fillers such as molybdenum disilicide ($MoSi_2$) [42] and iron silicide (FeSi), can be introduced to adjust electrical conductivity or magnetic properties. Polymeric fillers like cellulose fibers can be used as fillers to modify the rheological properties, processability, or combustibility of the preceramic polymer [43]. Also, Kim et al. in 2005 used poly (methyl methacrylate-co-ethylene glycol dimethacrylate) microbeads to create partially interconnected microcellular ceramics [44].

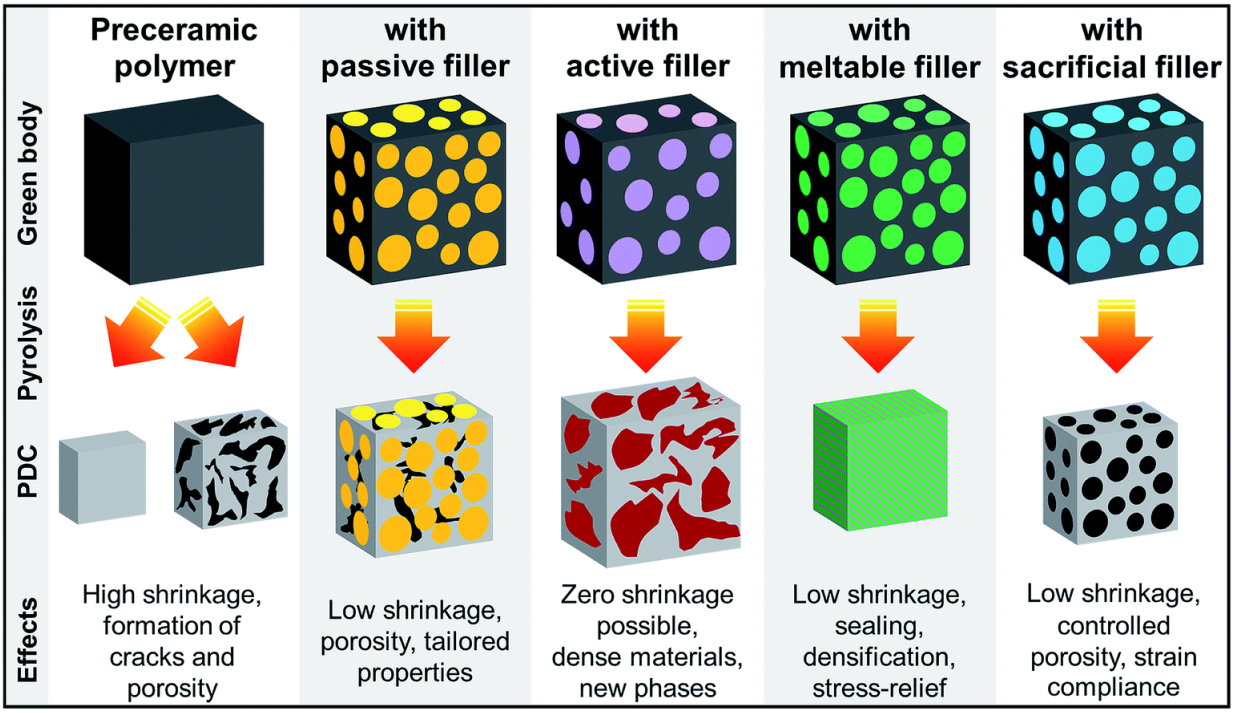

Fig. 4. Different types of fillers and their application in the fabrication of PDCs (reprinted from [34] with permission from Wiley).

Due to the thesis's objective to investigate the manufacturing process of mullite 3D ceramic structures using polysilsesquioxane through material extrusion-based additive manufacturing (MEX-AM) technique, the state-of-the-art, in the following sections mainly focus on the synthesis of oxide and silicate ceramics, to gain a better understanding of the current advancements and developments made in this specific area.

2.1.3. Synthesis of silicate ceramics using polysiloxane and polysilsesquioxanes

In recent years, there has been a lot of interest in polymer derived silicate ceramics by incorporating active fillers into PCP matrix. As can be seen in Table 2, various types of silicate ceramics have been successfully produced using polysilsesquioxanes. It should be noted that the fabrication of silicates using organosilicon polymers requires handling and heat treatment in an air atmosphere.

In 2006, Bernardo et al. [38] reported the use of nano fillers to enhance the reactivity between the PCP and the active filler. Their study employed a mixture of methyl-silsesquioxanes, namely SILRES MK (MK), and γ-Al_2O_3 (average particle size of 15nm) to produce dense 3:2 mullite disks (d≈31mm, h≈5mm). At a temperature of 1250°C, mullitization, with a volume

fraction of 96%, was already observed. This percentage increased to 99.5% at temperatures exceeding 1350°C.

Table 2. Fabricated silicate and oxynitride ceramics from preceramic polymers and fillers.

Silicate ceramic	Preceramic polymer	Active filler	Additive	Ref
Mullite ($3Al_2O_3.2SiO_2$)	MK YR3370 MK+H62C H62C	 γ- Al_2O_3	- - - Borax	[38, 39] [44] [1]
ZTM (Zirconia Toughened Mullite)	MK	γ- Al_2O_3	ZrO_2 and TiO_2	[45]
Wollastonite ($CaO.SiO_2$)	MK Mk+H62C	- CaO $CaCO_3$ $CaCO_3$	Ca-acetate - Hap TEOS	[46] [47] [48]
Yttrium mono-silicate ($Y_2O_3.SiO_2$) Yttrium di-silicate ($Y_2O_3.2SiO_2$)	MK	Y_2O_3 - -	Eu_2O_3 - -	[49] [1]
Zircon ($ZrO_2.SiO_2$)	MK, H62C	ZrO_2	TiO_2 Zircon seeds	[50]
Forsterite ($2MgO.SiO_2$)	MK, H62C	MgO	TiO_2	[51]
Willemite ($2ZnO.SiO_2$)	MK	ZnO	Mn-acetate	[1]
Cordierite ($2MgO.2Al_2O_3.5SiO_2$)	MK, H62C	γ-Al_2O_3, MgO	-	[52]
Gehlenite ($2CaO.Al_2O_3.SiO_2$)	MK	γ-Al_2O_3, $CaCO_3$	Eu_2O_3, CeO_2	[53]
Akermanite	MK, H62C	MgO, $CaCO_3$	m-Hap, Borax	[54]
Hardystonite ($2CaO.ZnO.2SiO_2$)	MK	γ-Al_2O_3, ZnO	Eu_2O_3	[1]
β′-SiAlON	MK, H44	γ-Al_2O_3	Si_3N_4, AlN, SiC	[55-57]
Y-Si-O-Ns	MK	Y_2O_3	Eu_2O_3, CeO_2	[25]
wollastonite-based silicate bioceramic	MK	$CaCO_3$	AP40 glass (apatite–wollastonite system)	[58]
wollastonite and hardystonite-based ceramics	MK	ZnO, $CaCO_3$	AP40 glass (apatite–wollastonite system)	[59]
Wollastonite-Diopside foam	H62C, MK	$Mg(OH)_2$, $CaCO_3$, Na_2 $HPO_4{\cdot}7H_2O$	Ca/Mg-rich silicate glass	[60]
Lithium orthosilicate (Li_4SiO_4)	PMS	Lithium carbonate (Li_2CO_3)	-	[61]
Biosilicate glass-ceramic	MK+ H62C	$CaCO_3$, Na_2CO_3 and anhydrous sodium phosphate	Biosilicate® glass frit powder	[62]

By sintering at 1550°C for 2.5 hours, complete mullitization was achieved, with only a remaining volume fraction of 0.1% silicate glass. Presence of residual cristobalite was previously reported [37, 63, 64]. Absence of cristobalite impurity in this study was attributed to the effective dispersion of highly active nano alumina within the PCP matrix. Colombo et al.

reported the fabrication of different silicate ceramics using nano active fillers [25]. Pure mullite, zircon, cordierite, fosterite and yttrium-silicates with low grain size were achieved at low sintering temperatures and dwell times as a result of highly favorable reaction kinetics. However, the issue with densification in the polymer-derived silicates persists due to the typical poor ionic interdiffusion in silicates. Therefore, submicron pores appear between densified areas.

Fig. 5 illustrates the porosity values for pure mullite derived from MK and nano-sized γ-Al_2O_3 (more than 20%). By incorporating a secondary inert filler (i.e. ZrO_2), zirconia-toughened mullite with higher density was obtained. Addition of secondary fillers reduces the amount of PCP. In this way, less gaseous products are generated during PCP transformation to PDC and fewer pores are expected. Although the porosity is reduced to 15% or less, the material remains porous. Introducing TiO_2 as a sintering additive, transient viscous sintering occurs (above 1200°C) that enhances the sinterability of the mullite phase as well as zircon ($ZrSiO_4$) [50] and forsterite (Mg_2SiO_4) [51].

Substituting a fraction of MK for SIRLES H62C, a relative density of 97% was achieved. The authors explained this observation by varying levels of network connectivity and defects in the amorphous silica phase of different organosilicon polymers, as a more defective silica network is favorable for accommodating the Si-O network containing fragments into the mullite structure [1].

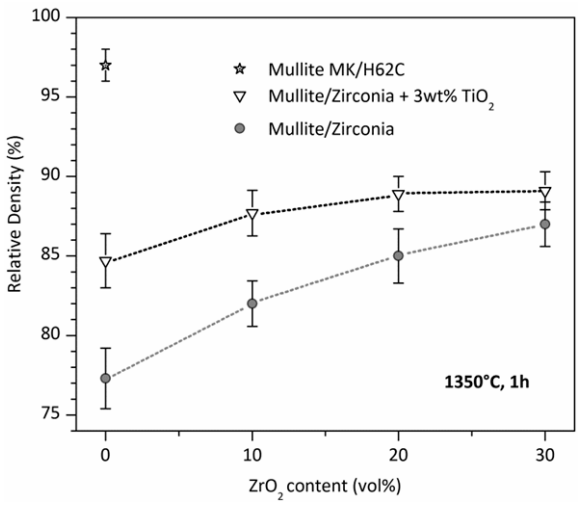

Fig. 5. Fabrication of mullite-based ceramics from MK polymer filled with nano γ-Al2O3: the impact of incorporating secondary filler (ZrO_2), sintering additive (TiO_2), and partial modifications in the starting polymer composition (mixing MK and H62C) [1]. Open access CC-BY.

Same approach has been used to prevent the extensive cracking of zircon [50], forsterite [51] and cordierite [52] ceramics. Partial replacement of MK by SILRES H62C (H62C) enhanced the compactness due to different molecular arrangements of the PCPs, leading to diverse possibilities to rearrange the molecular structure. Also, H62C goes through different crosslinking reactions that avoid gas release during pyrolysis. In this way, local pressure accumulation from generated gaseous products is eliminated. A Crosslinking step (at 250°C for 30min) prior to shaping can be beneficial due to a certain amount of gas release and shrinkage before pyrolysis step.

The microstructure of polymer-derived mullite ceramics typically exhibits equiaxed grain morphology, which can be attributed to limited cation interdiffusion. It has been demonstrated that addition of B_2O_3 can shift the mullitization to lower temperatures and encourage the anisotropic grain growth by lowering the viscosity of the intergranular phase [65]. Bernardo et al. demonstrated the fabrication of acicular mullite fibers by adding 3wt% hydrated sodium borate to the mixture of MK and nano γ-Al_2O_3 [1]. Such interlocking grown fibers can be a candidate for fabrication of highly porous materials. Acicular mullite ceramics, which are typically produced through complex thermo-chemical processes can be replaced by the polymer derived cellular ceramics [66].

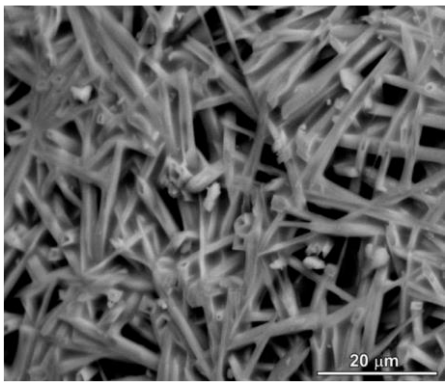

Fig. 6. Microstructure of polymer derived mullite ceramic, based on the mixture of MK, nano γ-Al_2O_3 and borax [1]. Open access CC-BY.

To improve the relative density of mullite based ceramics from 93% to 97%, Riedel et al. used MK polymer filled with functionalized nano γ-Al_2O_3 (added octylsilane groups on the surface) [67] and obtained a high amount of mullite crystals already at 1300 °C, attributed to the better distribution of functionalized γ-Al_2O_3 within the initial PC compared to unfunctionalized fillers. Due to heat treatment of the mixture in a nitrogen atmosphere, silicon oxycarbide (SiOC) was

yielded from MK which transformed into SiC crystals due to the interaction with γ-Al_2O_3. The resulting SiC-mullite monoliths can be an alternative for SiC/mullite nano-composites derived from polymethylsiloxane gels filled with α-Al_2O_3. The obtained crack-free monoliths can be potential candidates for complex-shaped ceramic, resistant to high temperatures and corrosion. Ternary SiC-mullite composite containing nano α- Al_2O_3 crystals was obtained by substituting nano aluminum fillers for γ-Al_2O_3 [68].

In binary systems consisting of silica and a metal oxide, the formation of multiple silicate phases requires having a specific molar ratio between silica and the metal oxide. For instance, when silica is combined with CaO, various silicates such as $CaO{\cdot}SiO_2$, $3CaO{\cdot}2SiO_2$, $2CaO{\cdot}SiO_2$, and $3CaO{\cdot}SiO_2$ can be produced depending on the CaO/SiO_2 molar ratios. These silicates can be mainly used for biomaterial applications [46]. Using a filler like $CaCO_3$, can result in the formation of a silicate with a higher CaO/SiO_2 ratio than intended. For example, when micro-sized $CaCO_3$ is used in a filler/PCP formulation, the desired wollastonite ($CaO{\cdot}SiO_2$) phase is replaced with di-calcium silicate ($2CaO{\cdot}SiO_2$) due to localized concentrations of CaO. Conversely, almost pure wollastonite was obtained using nano-sized $CaCO_3$ under the same conditions [45].

The choice of PCP has been found to influence the polymorphism of calcium silicates. Using H62C with a low molecular weight instead of MK, a trace of α-phase or "pseudowollastonite was detected alongside the β-phase typically obtained at the temperature range of 900-1100 °C [46]. The polymer with a lower molecular weight consists of short Si-O fragments that promote the formation of ring-structured silicate variants like the α-phase [69].

Synthesis of binary ceramic compositions such as forsterite and yttrium silicates has been reported as well. A highly reactive combination of PCP filled with nano-sized MgO enables the formation of forsterite for biomaterials [70] and dielectric applications [71] at temperatures as low as 800 °C. Due to the limited ionic interdiffusion in silicates, however, some MgO remains unreacted. As a result, enstatite forms in MgO-poor regions. The inclusion of nano-sized TiO_2, not only improves densification (by forming $Mg_2Si_{0.9}Ti_{0.1}O_4$ solid solution) but also plays a crucial role in eliminating unreacted MgO and enstatite impurities [51].

Combination of yttria (Y_2O_3) and silica (SiO_2) can produce mono- and di-silicates such as $Y_2O_3{\cdot}SiO_2$ (or Y-MS) and $Y_2O_3{\cdot}2SiO_2$ (Y-DS) [49]. Y-MS is monophasic, undergoing a dislocative transformation between the X1 (low temperature) and X2 (high temperature) phases. Y-DS, however, exhibits multiple polymorphs (y, α, β, γ, δ, z), with each form stable within a specific temperature range. Depending on the processing, different polymorphs can be obtained [72]. Sol-gel method encourages the formation of the α-phase [73, 74], while hydrothermal

synthesis enables the development of the y-phase [75]. Mixing MK with nano Y_2O_3, it is possible to achieve both silicates at lower temperatures (1000-1350 °C) [49].

Synthesis of ternary systems is quite challenging due to the potential formation of multiple silicate phases resulting from combinations of silica and various oxides. For instance, in the CaO-MgO-SiO_2 system, diopside ($CaMgSi_2O_6$) and akermanite ($Ca_2MgSi_2O_7$) can form. In the case of Cordierite ($2MgO{\cdot}2Al_2O_3{\cdot}5SiO_2$) and gehlenite ($2CaO{\cdot}Al_2O_3{\cdot}SiO_2$), presence of silica-free compounds such as Mg and Ca aluminates, respectively, is probable. Presence of such silica-free phases hinders the full interaction between oxides and polymer-derived silica, increasing the risk of residual SiO_2 in the final product. To address this issue, firing temperature has been modified. For example, firing polymer-derived cordierite at 1350 °C can eliminate $MgAl_2O_4$ phase. Alternatively, the ionic interdiffusion was promoted by generating solid solutions with more "open" crystal structures. An example of this approach involves the partial substitution of Ca^{2+} ions with Eu^{3+} ions to produce luminescent materials. Formation of $Ca_{2-2x}Eu_{2x}Al(Al_{1+2x}Si_{1-2x}O_7)$ solid solutions by adjusting the Al/Si ratio, can significantly reduce the Ca-aluminate content [114].

2.1.4. Processing of preceramic polymers

Using preceramic polymers to fabricate 3D ceramic structures, several steps need to be taken including shaping the material, followed by crosslinking and pyrolysis. After that, a sintering step can be implemented if necessary. Fig. 7 demonstrates all the processing steps to achieve polymer derived ceramic (PDC) components.

Shaping

One of the advantages of PCPs is their viscoelastic behavior rising from their polymeric nature. As a result, PCPs are well-suited for a wide range of thermoplastic shaping techniques such as casting, injection molding, pressing, tape casting, extrusion, fiber drawing and coating [30]. More recently, using additive manufacturing techniques for shaping PCPs attracted interest among researchers as well. This topic will be discussed in more detail in section 2.2. Utilizing PCPs also eliminates the concerns from powder-based and sol-gel approaches. They prevent drying issues and long processing times for gelation and drying as well as maintaining constant rheological properties within the processing time window. PCPs also minimize the need for

flammable solvents and special handling processes. Furthermore, their solutions remain stable for extended periods and fillers can be easily incorporated to produce composite ceramics.

Crosslinking

Crosslinking is the process by which polymer chains are linked together, forming a three-dimensional network. This process is important for almost all the fabrication processes of PDC structures because it allows the precursor to transform from a flexible, thermoplastic organic material (necessary for shaping) into a rigid and insoluble, thermoset and preserve the structure during post-processing [20]. Crosslinking can occur through a variety of mechanisms, most commonly by thermal crosslinking in the range of 100-250°C under airflow, crosslinking with chlorosilane, or curing with radiation [31]. Presence of functional groups such as Si-H, Si-OH and Si-vinyl, PCPs can be spontaneously crosslinked below 200°C by hydrosilylation (addition) or silanol-silanol reactions (condensation) [26]. Crosslinking in an air atmosphere has traditionally been a popular method for curing PCPs to provide SiO_2 yield. This process, however, is not suitable for the fabrication of non-oxide ceramics due to the drawback of leaving up to 15 wt% oxygen in the final PDC [76-78]. This residual oxygen content can adversely affect the thermal stability of the non-oxide PDCs, weakening their overall performance.

The utilization of a catalyst offers the advantage to crosslink the preceramic polymers at lower temperatures. Moreover, the early linking of volatile oligomers, facilitated by the catalyst, contributes to the shape stability by increasing the yield of obtained ceramic as the volatile oligomers, which would typically evaporate or degrade, are effectively incorporated into the crosslinked network [78].

Crosslinking by UV radiation is applicable when PCP contains photosensitive functional groups in its backbone structure. This method can be mostly effective for crosslinking of fibers and thin structures as the penetration depth is limited [79, 80]. Another common crosslinking mechanism called "free radical polymerization" is utilized for vat photopolymerization AM technique. This method involves the absorption of UV photons by a photoinitiator (PI). This process generates highly reactive free radicals (R*) that react with the monomer (M), leading to the formation of polymer chains and subsequent completion of the polymerization process.

Pyrolysis

Shaping and crosslinking of PCPs is followed by a pyrolysis step, known as ceramization, in which the PCP is transformed into a ceramic material through various thermal processes. These processes include hot pressing, spark plasma sintering, chemical vapor deposition, plasma spraying, rapid thermal annealing, laser pyrolysis, microwave heating, and the most commonly used method, pyrolysis in an argon or nitrogen atmosphere. Pyrolysis in such inert atmospheres leads to the formation of amorphous covalent ceramics by the gradual removal of generated gases from the decomposition of organic side chains (methyl/phenyl/vinyl groups) and Si–H, Si–OH, or Si–NHx groups at elevated temperatures (600-1000 °C). The reaction mechanisms during pyrolysis can be studied using solid-state nuclear magnetic resonance (NMR), Fourier transform infrared spectroscopy (FTIR), Raman spectroscopy, and thermogravimetric analysis (TGA) coupled with mass spectroscopy. Using ion irradiation to eliminate hydrogen atoms through the cleavage of C-H bonds is an alternative non-thermal process for ceramization where any remaining carbon is transformed to diamond-like carbon clusters. Pyrolysis atmosphere can modify the composition of the final ceramic component. Pyrolysis in air can be employed for the formation of silicate ceramics using active metal oxide fillers.

During the ceramization process of PCPs, important parameters such as heating rate, reaction atmosphere, reaction temperature, and dwell time influence the phase composition and microstructure of the final ceramics. They influence the extent of crystallization, carbothermal reduction reactions, and filler reactions within the material.

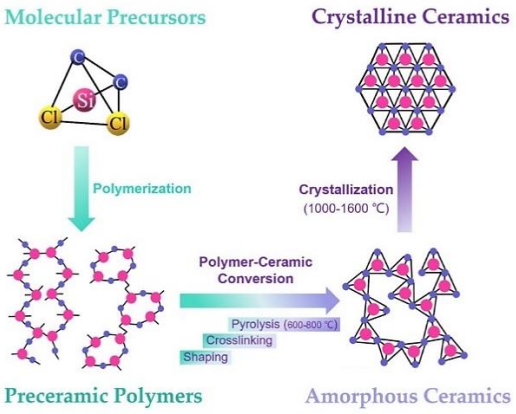

Fig. 7. Processing steps for fabrication of PDC components, from shaping and crosslinking to pyrolysis and crystallization (sintering) (reprinted from [2] with permission from Elsevier).

This doctoral thesis focuses on the investigation of pyrolysis of filled polysiloxanes (MK) with γ-Al_2O_3 as an active filler, with a particular emphasis on conducting the pyrolysis in air atmosphere. Consequently, the following section mainly highlights studies that have employed pyrolysis in air environment.

2.2. Additive manufacturing of preceramic polymers

The versatility of polymer-forming technologies allows for shaping preceramic polymers in various ways, thereby eliminating the limitations and drawbacks associated with traditional ceramic processing. Shaping methods such as extrusion, injection molding, foaming [62], joining, infiltration, pressing, coating, spinning, and more recently additive manufacturing (AM). Using AM, a 3D model can be replicated as a complex and detailed geometry to a three-dimensional (3D) structure by depositing the material layer by layer. A summary of different AM methods used for the fabrication of PDCs by polysiloxane/polysilsesquioxane is presented in Table 3.

Table 3. Additive manufacturing methods for fabrication of polymer derived ceramics (reproduced from [2,81] with permission from Elsevier).

AM technique	Features	Feedstock form	Forming method	Printing requirements	Resolution
Direct ink writing (DIW)	Easy operation, low cost, wide choice of materials, highly accurate and complex 3D architectures	Slurry	Extrusion	Appropriate viscosity and elastic properties	Few 100 μm to mm
Fused deposition modeling	Low operating cost, high speed and large size capability, reuse waste, low printing precision, limited extrusion temperature range	Filament	Extrusion	In filament/pellet state	mm
Stereolithography (SL)/ Digital light Processing (DLP)	moderate cost, high efficiency, good surface quality and ease of processability	Slurry	polymerization	Dissolvable and possess sufficient photocurable moieties	
Two-photon Polymerization (TPP)	High surface quality, high printing precision, low speed	Slurry	Non-linear polymerization	Dissolvable, crosslinkable by two-photon absorption moieties	sub μm
Selective laser sintering (SLS)	Complex 3D structures, slow speed, low shrinkage, low curing temperature, high dimensional accuracy	Powder	Powder fusion	Meltable by laser and curable via reactive groups	μm to mm
Binder Jetting	Complex 3D structures, limited strength, and rough surfaces	Powder and slurry	Binder bonding	Dissolvable in solvents and act as binders	μm to mm
Inkjet printing	High printing resolution, low material waste, limited by printable inks, low printing speed	Slurry	Binder bonding	Low viscosity, rapid crosslinking and high ceramic yield	Few 100 μm to mm
Laminated object manufacturing	Large-scale production, no complicated chemical/physical processes, low speed, low precision, high anisotropy	sheet	Binder Bonding and laser cutting	In sheet state	mm

2.2.1. Light assisted AM (vat photopolymerization)

Vat photopolymerization techniques including the first invented stereolithography (SL) method [82] followed by digital light processing (DLP) and two-photon polymerization (TPP) as derivatives of SL technique can provide accurate 3D replicas with fine details and utilize similar principles but have some key differences in their implementation [83].

PCPs are highly compatible with AM involving vat photopolymerization [84]. In SL of PCPs, precise patterning of PCPs and subsequent conversion to ceramics through pyrolysis results in complex PDCs with a high resolution. The PCP needs to be photosensitive, soluble in compatible solvents and provide proper rheological behavior. Ensuring a homogeneous dispersion of PCPs in the liquid phase also helps minimize scattering, resulting in a high-quality surface finish for the final PDC components.

A general description of these printing methods and the existing research on using SL and DLP for manufacturing parts with polysiloxane/polysilsesquioxane materials are provided in the following:

Stereolighography (SL)

Stereolithography (SL) enables the creation of precise objects with defined edge quality. SL method is based on photopolymerization of liquid resins containing monomers and oligomers that are sensitive to a specific wavelength of light [85]. These so-called photopolymers undergo a chemical reaction by exposing to a specific wavelength and the liquid transforms into a solid polymer. In this process, a thin layer of photopolymer is deposited on the build platform. This layer of resin is exposed to a specific pattern of light typically ultraviolet (UV) light using a point-by-point scanning method, where the laser beam sequentially cures the resin. The photoinitiator in the resin absorbs the light energy and cures the resin in the defined areas to form a solid layer. After curing one layer, the platform moves down to create space for the next layer of liquid resin. Each cured layer bonds to the previous layer, creating a cohesive structure. This process continues layer by layer until the desired 3D structure is achieved. After printing, the printed form is placed in the proper solvent to remove the extra uncured resin. Using SL technique for 3D printing of PCPs, a high print resolution (20 μm or less) can be achieved [86]. However, the full potential of this method is still not clear due to a limited number of proper photocurable PCPs.

Ożóg et al. in 2022 fabricated highly porous gyroid scaffolds obtained by masked stereolithography [87]. In this study, Biosilicate® glass-ceramics were produced using a phenyl

silicone resin (H44)/photocurable liquid acrylate blends at a ratio of H44/SB/IPA= 1/1/0.5. Calcium carbonate ($CaCO_3$), sodium carbonate (Na_2CO_3) and sodium phosphate ($Na_4P_2O_6$) were used as the fillers. Pyrolysis was performed in nitrogen atmosphere (0.5 °C/min up to 500 °C for 5 h, followed by heating at 2 °C/min up to 1000 °C for 1 h).

Rosado et al. in 2023 reported utilizing a commercial silica polyacrylic resin and nano Al_2O_3 to produce mullite-based scaffolds using stereolithography [88]. One approach involved infiltrating a colloidal alumina sol into the printed porous silica components. A second more effective method follows the printing silica/alumina components using a photocurable alumina resin mixed with the silica resin. Presence of higher alumina concentration and larger reaction surface results in a higher degree of mullitization in the final parts.

SiOC microlattice and honeycomb cellular structures were fabricated in a notable work by Eckel et al. in 2016 [89]. A combination of (mercaptopropyl) methylsiloxane and vinylmethoxysiloxane was printed after the addition of a UV free-radical photoinitiator, free-radical inhibitor and UV absorber. Subsequently, samples went through a pyrolysis step at 1000°C in an argon atmosphere. Final SiOC amorphous structures were dense and defect-free with only 30% linear shrinkage. The mechanical properties of the obtained SiOC microlattices are comparable with commercial SiC, aluminosilicate and SiOC foams.

Although complex structures with fine details are produced by SL method, due to the discrete layer-by-layer photopolymerization process, obstacles such as anisotropy in shape and mechanical properties have been observed. The nature of SL method reduces the printing speed and can cause a staircase effect in the printing sample. By introducing slant beam rotation (SBR) scanning, Aerif et al. in 2009 suggested a different approach to reduce the roughness in the stair-stepped object [90]. In this method, a UV light beam is angled to create slanted edges within each layer and add an extra degree of freedom in the scanning mechanism to rotate 360 degrees inside the resin.

Digital light processing (DLP)

Digital Light Processing (DLP) technique shares similarities with SL. However, it uses a different approach to achieve layer-by-layer printing [91]. In DLP, the light source is a digital projector with a digital micromirror device (DMD) that projects a patterned image of an entire layer onto a vat (the container of liquid resin) that allows for higher resolutions without the need for complex scanning mechanisms. That is why DLP offers a higher printing speed compared to SL since the whole layer can be exposed to light simultaneously. Here also a photopolymer

resin sensitive to light, specifically to a certain wavelength such as ultraviolet (UV) or visible light is used. To start the printing process, the build platform is lowered into the vat, submerging a thin layer of liquid resin. The digital projector then projects the patterned image onto the resin surface. Selective curing of the resin happens in the illuminated areas. The exposed resin undergoes photopolymerization, transforming from a liquid to a solid state to create the desired pattern. The platform is then incrementally raised or lowered to deposit a new layer. The process is repeated until the 3D form is completed. Then, the printed object is typically removed from the vat and rinsed to remove any excess or uncured resin.

Fabrication of complex mullite structures (Fig. 8) using DLP method has been reported by Schmidt et al. in 2019 [92]. A mixture of highly acrylated, liquid photocurable polysiloxane (TEGO RC711) and nano γ-Al_2O_3 was printed and cured with a UV lamp for 2 minutes. Samples were debound by heating up to 500 °C at 1 °C/min to decompose the polymer network and then fired between 1300-1400°C to produce 3D printed mullite structure. Using nano γ-Al_2O_3, pure mullite was achieved at 1300°C. By increasing the filler size to micron-sized γ-Al_2O_3, remaining alumina phase was detected.

Although the authors showed more desirable mullitization using nano fillers, it was found that the suspensions containing nanoparticles had some drawbacks for 3D printing [92]. A higher amount of solvent was used for nano fillers, which resulted in a low ceramic yield and the formation of a weak polymerized acrylate network. Due to these reasons, printed samples suffered from low printing resolution, cracking, and structure collapse during sintering. This issue was solved by employing micro-sized alumina powder to achieve dense and crack-free bulk components, as well as porous components with complex shapes. The porous components exhibited a total porosity of 90 vol% and compression strength of 1.8 ± 0.3 MPa.

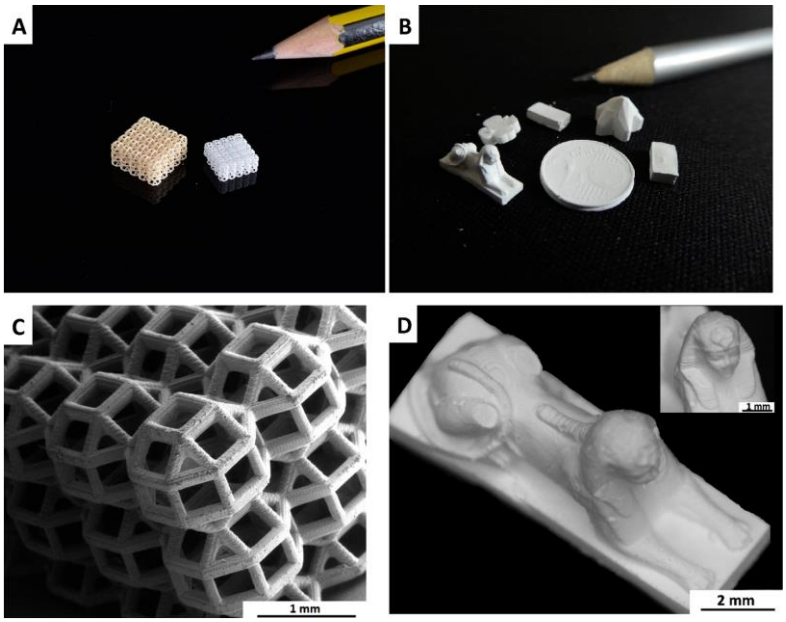

Fig. 8. Complex porous structure fabricated by DLP before (A,left) and after (A,C) sintering, and bulk parts (after sintering (B,D)). The coin in Fig. 8B was manufactured by soft-lithography (reprinted from [92] with permission from Elsevier).

Fabrication of different bioactive scaffolds has been reported [93]. Dasan et al. fabricated Akermanite scaffolds [93] using H44 or H62C silicone resin. Fillers such as $CaCO_3$, $Mg(OH)_2$ micro-powders, nano MgO powder and borax. After printing, samples were sintered up to 1100°C using a stepwise heat treatment. Using 4.5 wt.% $Na_2B_4O_7$ borax inside the compound with H44 polymer, crack-free and phase-pure scaffolds with microporous struts were achieved. The compressive strength of scaffold with this composition was comparable with the values for silicate scaffolds having the same porosity level [94].

Crack-free glass-ceramics scaffolds have been developed for use in tissue engineering applications [95]. A mix of glass powders containing WB and 'silica-defective' variant, WB-15 was mixed with MK (responsible for binding the glass powder) was printed. Ceramization of MK at elevated temperatures generates an amorphous silica phase up to 800°C. Formed silica promotes shape stability even at sintering temperatures when glass powders are softened.

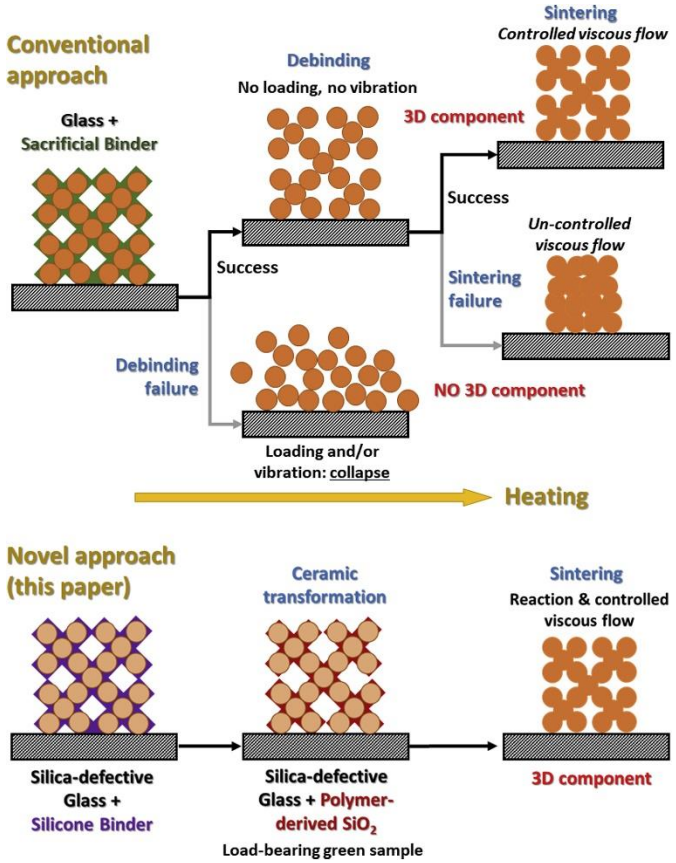

Fig. 9. Fabrication of glass ceramic scaffold with conventional method and by using silica-defective glasses (re-printed from [95] with permission from Elsevier).

Ultrathin (with a thickness of 1.5 mm) scaffolds, containing 60 vol% porosity, were fabricated by Wang et al. for orbital bone repair via DLP method [96]. The dilute magnesium-substituting wollastonite (CSi-Mg) scaffolds showed strong mechanical strength and stable biodegradability under a relatively low sintering temperature. The obtained scaffold with CSi-Mg composition was proposed as a good candidate for osteoconduction.

He et al. printed zirconia/calcium silicate (CS) composite scaffolds using DLP method [97]. After sintering the calcium silicate phase was embedded between the ZrO_2 grains. The presence of CS phase improved the cell proliferation and differentiation of ZrO_2 ceramic. Degradation of the scaffold resulted in the deposition of apatite which was favorable for the integration of the scaffold with living bone. The obtained ZrO_2/CS composite scaffold can be a good candidate for 3D printing bone repair scaffolds due to their enhanced biocompatibility compared to the ZrO_2 scaffold.

Two-photon polymerization (TPP)

Using Two-photon polymerization (TPP), high-resolution, complex three-dimensional structures can be achieved at micro/nanoscale level [98]. In this method, a photosensitive material absorbs a femtosecond laser beam in the near-infrared range with a high photon energy density. The beam excites the material molecules on a specific point and creates a voxel (volume pixel) by the two-photon absorption process [99]. In this way, each layer is built by curing the photopolymer point by point until the full 3D form is obtained. Using this method, the fabrication of 3D structures with exceptional Two-photon polymerization is an ideal technique for various applications in fields such as microelectronics, photonics, biomedicine, and other areas that require precise fabrication at the micro- and nanoscale. These applications encompass tissue-engineered scaffolds, micro medical devices like microswimmers and needle arrays, optical devices, and more [99]. Using TPP method, only SiOC ceramics were obtained [89, 100, 101].

2.2.2. Selective laser sintering (SLS)

Using selective laser sintering (SLS) technique, a laser beam facilitates the fusion or sintering of powdered materials together to build 3D structures [102]. First, a thin layer of powder is deposited on the build platform. A high-powered laser beam is exposed on the powder bed, which accurately follows the points to achieve the desired object on the powder. Consequently, particles stick together because of generated heat below the material's melting point and selective fusion in defined areas. After sintering each layer, the platform is lowered to prepare a new layer of powder for sintering. After the sintered full 3D structure is cooled down, it is removed to be further processed, e.g. remove the excess powder and finish the surface followed by heat treatment, depending on the material and desired specifications.

The research from Friedel et al. in 2005 is the only reported study on using SLS specifically for curing PCPs [103]. They referred to this process as selective laser curing (SLC). A poly(methylsilsesquioxane) (MK) mixed with SiC passive filler was SLS printed and cured using a CO_2 laser beam at 400°C. MK was cured due to a condensation reaction between hydroxyl and ethoxyl groups, transforming the resin from a thermoplastic resin into a thermosetting material. An additional advantage of working with molten MK is its ability to blend uniformly with fillers, facilitating the formation of a homogeneous raw material for printing, followed by the subsequent pyrolysis process. The cured structure was subsequently pyrolyzed up to 1200°C in an argon atmosphere to obtain Si-O-C/SiC ceramic. The presence

of SiC filler decreased the amount of shrinkage. Infiltrating molten Si into the structure resulted in a higher density and improved the bending strength significantly to 220MPa. Due to low linear shrinkage of 3% after pyrolysis, they proposed the SLC approach for near-net-shape forming of ceramics.

2.2.3. Laminated object manufacturing (LOM)

In this method, thin sheets of material bond together to form 3D objects. A stack of sheets can be first laminated and then cut (cut-off-the-stack) or each sheet is cut and then laminated (cut-then-bond) together [104]. The cutting is computer-controlled and follows the contour of the object's shape in each sheet and removes the excess part to achieve the desired shape. In the cut-then-bond method, a layer of adhesive is applied to bond the sheets together. After that, heat and pressure are applied using heated platens or rollers to ensure the firm fusing of the sheets. The process from cutting to bonding repeats after each sheet is cut until the full 3D object is built. Trimming by mechanical or laser cutting, depending on the material and desired specifications, may be required. LOM is commonly used for simple geometries and large-scale object fabrication in various industries.

Sieber et al. in 2000 achieved SiOC ceramics by infiltrating cleaning papers with a PCP-based slurry [105]. The slurry includes a polymethylsiloxane (NH21), Si powder as an active and α-SiC as a passive filler. Dried sheets after infiltration were laminated at 230°C by hot pressing for 20min followed by pyrolysis in an argon atmosphere at 1450°C. Converted cellulose fiber to carbon fibers reacted with Si powder in the slurry and produced a SiC phase. By modifying the filler content in the slurry, laminated composites with low shrinkage were successfully demonstrated. Windsheimer in 2007 fabricated Si-SiC Composites by LOM method [43]. Cellulosic PCP sheets were made using 76.8 wt% SiC powder, 20 wt% cellulose pulp, and 3.2 wt% retention agent and binder. To bind the sheets, a polysiloxane based adhesive coating was sprinkled on the surface followed by heating at 90°C to distribute the coating homogenously. Laminated Si-SiOC composites were first sintered at 800°C under a nitrogen atmosphere followed by infiltration of Molten Si at 1500°C to reduce the porosity. Fabrication of the highly dense composites, however, is dependent on the layer orientations and loading directions and varies the bending strength from 150 to 315 MPa. Based on the good and comparable results achieved by Windsheimer, it may be possible to substitute commonly used binders for fabrication of laminated composites with PCPs.

2.2.4. Extrusion based AM

As mentioned earlier, PCPs exhibit thermoplastic behavior because of their polymeric nature. As a result, extrusion based additive manufacturing techniques can be utilized to create PDC parts [106]; however, they behave differently compared to the typical engineering polymers due to their low glass transition temperature and lack of chain entanglements. Additionally, temperature significantly influences their viscoelastic properties [5].

Direct ink writing (DIW)

Direct ink writing (DIW), also called robocasting [107], involves a controlled deposition of inks and pastes to create 3D objects [108]. The ink or paste is typically a mixture of polymers and fillers such as ceramics, metals, or composites with a careful formulation to achieve the desired rheological properties. In this process, a deposition system controls the flow and pressure of the ink extruded from the nozzle. The extruded material flows as a stream or filament and is deposited on a build platform. Movements of the extrusion system in multiple axes are controlled through a computer and follow a specific path to achieve the desired shape. The ink should have the necessary flow characteristics, including a proper yield stress and storage modulus to be extruded through a printing nozzle. Depending on the nature of the ink or paste, a post-processing step such as curing or drying is required to achieve proper mechanical properties. DIW method is a common option for applications where surface quality is not of the highest priority. The following is a summary of the existing research on the Direct Ink Writing (DIW) technique of polysiloxane and polysilsesquioxane PCPs:

Wei et al. in 2019 used UV-assisted DIW to fabricate SiOC cellular structures using a mixture of commercial polymethylsilsesquioxane (MK) and 3-(trimethoxysilyl)propyl methacrylate (TMSPM) [109]. After synthesis of UV-curable MK-TMSPM by sol-gel reactions, Trimethylolpropane triacrylate (TMPTA) was added as a low viscosity curing agent to enhance the curing and achieve a proper viscosity. Photoinitiators of 1-hydroxy cyclohexyl phenylketone and ethyl phenyl(2,4,6-trimethylbenzoyl) phosphinate were also used to increase the absorption range of the UV light. The prepared mixture was printed with a filament size of 200 μm. In order to attain simultaneous and uniform curing, the laser beam is split into two beams with equal intensity and positioned on either side of the printing needle. Direct crosslinking of the material during printing prevented the formation of cracks during the pyrolysis process and resulted in only linear shrinkage of 25% and a mass loss of 30%.

By adding active fillers, various silicate compositions in the form of scaffolds were printed using polymethylsilsesquioxane (MK) as a polysilsesquioxane. Zocca et al. in 2016 used a MK mixed with ZnO and $CaCO_3$ to produce hardystonite ($Ca_2ZnSi_2O_7$) bioceramic scaffolds [110]. After ball milling the components in isopropanol medium, the homogenous obtained ink was deposited in a non-wetting oil bath using a nozzle with a diameter of 0.41 mm, and scaffolds with dimensions of 15 mm × 5 mm × 5 mm were fabricated. In another study, Fiocco et al. in 2017 fabricated silica-bonded calcite scaffolds by DIW technique [111]. MK was mixed with fused silica and $CaCO_3$. The same mixing and printing parameters were used to achieve scaffolds. Elsayed et al. in 2019 used a mixture of methyl-siloxane (MK) and methyl-phenyl-siloxane (H62C) as silica sources to produce Biosilicate® scaffolds [62]. A nozzle with a diameter of 0.81mm was used for printing. More studies on Akermanite ($Ca_2MgSi_2O_7$)-based 3D scaffolds were fabricated by Dasan et al. in 2019 [112]. 3D scaffolds were fabricated using DIW by synthesis of a bioactive glass-ceramic from a mixture of MK and a CaO-Na_2O-B_2O_3-SiO_2 glass system [113]. Complex hardystonite glass-ceramic scaffolds were obtained by DIW [114]. The amorphous phase obtained by SIRLES MK exhibited better reactivity with other additives compared to conventional silica sources. In most of the mentioned studies, fused silica was added to the ink as a thixotropic agent to adjust the viscosity for DIW process. To achieve a hierarchical SiOC porous structure, MK and Polymethyl methacrylate (PMMA) sacrificial microbeads with a diameter of 0.46 μm were used [115].

Table 5. Summary of printed polysiloxane/polysilsesquioxanes using DIW technique.

PCPs	**Fillers**	**Obtained ceramic**	**Print resolution (μm)**	**Porosity (vol%)**	**Compressive strength (MPa)**	**Ref**
MK	ZnO and $CaCO_3$	hardystonite ($Ca_2ZnSi_2O_7$)	300-500	Up to 80%	0.6±0.2	[110]
MK	$CaCO_3$	silica-bonded calcite	450	56%–64%	2.9–5.5	[111]
MK	Active: $CaCO_3$, Na_2CO_3 and anhydrous sodium phosphate Passive: Biosilicate® glass frit powder (<5 μm)	Biosilicate glass-ceramic	600	60%	Average 6.7	[62]
MK	$CaCO_3$, MgO	Akermanite ($Ca_2MgSi_2O_7$)		72.4 ± 2.9%	3.3 ± 0.6	[112]
MK and H62C	Active: ZnO, $CaCO_3$, $SrCO_3$, $Mg(OH)_2$ Passive: glass powder	Sr/Mg-doped hardystonite	840	73±1	2.3±0.7	[116]
MK	PMMA sacrificial microbeads	SiOC	400	74.9 ± 3.2	8.19 ± 3.06	[115]

Fused deposition modeling (FDM)

Fused Deposition Modeling (FDM), also called fused filament fabrication (FFF) is based on extruding and deposition of thermoplastic materials [117]. FDM is one of the most widely used and accessible methods of 3D printing. In this method, thermoplastic feedstocks containing organic binder and ceramic powder in form of filaments or pellets are fed into an extrusion chamber inside a heat zone where the feedstock is melted (see Fig. 6). The melted filament/pellets are pushed further and extruded through a small nozzle on a build platform layer by layer. The movements of nozzle along the X and Y axes, follow the pre-determined path of the object's digital model. Each layer solidifies directly after deposition and bonds with the previous layer to ensure the structural integrity of the object. This layer-by-layer approach continues until the entire object is formed. After that, the printed object requires a debinding step to remove the organic thermoplastic component.

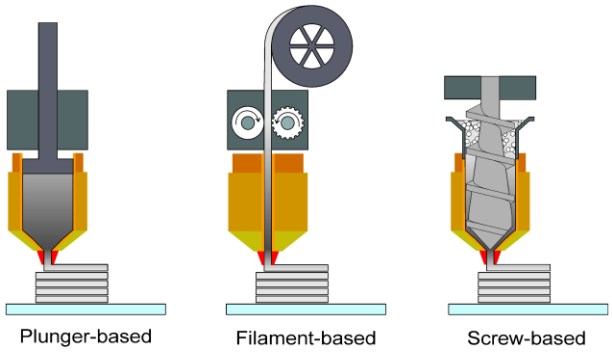

Fig. 10. Different possibilities for extrusion based additive manufacturing [118]. Open access CC-BY.

FDM printing of PDCs has remained an unexplored area because the commonly used filament printers require spooling of the feedstock into filaments. Considering the high glass transition temperature (>50 °C) and melting temperature range (approximately 70 to 250 °C) of PCPs, their filaments can be brittle and hard to spool. On the other hand, the thermoplastic nature of PCPs is favorable for adjusting the viscosity and elastic properties of filaments. To address this topic, Gorjan et al. [39] used a mixture of polymethylsiloxane (MK) and ethylene vinyl acetate (EVA) as thermoplastic components to produce PCP-based filaments for FDM process. Mullite honeycomb structure and cylindric porous scaffolds were achieved by employing MK as a silica source and γ-Al_2O_3 as an active filler. After printing the structure using a 1.0mm nozzle diameter at 170 °C, heat treatment with a gradual heating program was performed up to 1000°C in air to crosslink and pyrolyze the preceramic on one hand and eliminate the organic

components, on the other hand. Further sintering up to 1550°C in the air was required to form mullite ceramic components through the reaction of alumina and polymer derived silica. The resulting ceramic components exhibited no shape distortions or cracks. This work represented PCPs as viable candidates for filament preparation. Nevertheless, further research is necessary to obtain defect-free PDCs [18,39].

Gorjan et al. in 2019 used two different alumina sources with D50 of 5.3μm and 14.8μm to produce mullite ceramics. Complete mullitization was achieved at 1550°C, as the reaction pathway necessitated higher temperatures in comparison to when nano-sized alumina particles were employed [38]. Using alumina with D50 of 5.3μm, residual corundum peak was observed even at 1550°C. It seems that mixing the components in a solvent (dissolving the PCP in a proper solvent) and mixing with fillers is more effective for achieving a homogenous dispersion. The use of a solvent to mix the components, specifically dissolving the PCP, and subsequently combining it with fillers, appears to be a more efficient approach for achieving a uniform dispersion and higher mulitization [38].

References

[1] E. Bernardo, L. Fiocco, G. Parcianello, E. Storti, P. Colombo, Advanced Ceramics from Preceramic Polymers Modified at the Nano-Scale: A Review, Materials, 2014, pp. 1927-1956.

[2] R.P. Chaudhary, C. Parameswaran, M. Idrees, A.S. Rasaki, C. Liu, Z. Chen, P. Colombo, Additive manufacturing of polymer-derived ceramics: Materials, technologies, properties and potential applications, Progress in Materials Science 128 (2022) 100969.doi: https://doi.org/10.1016/j.pmatsci.2022.100969.

[3] S. Yajima, K. Okamura, J. Hayashi, Structural analysis in continuous silicon carbide fiber of high tensile strength, Chemistry Letters 4(12) (1975) 1209-1212.doi: https://doi.org/10.1246/cl.1975.1209.

[4] M. Monthioux, O. Delverdier, Thermal behavior of (organosilicon) polymer-derived ceramics. V: Main facts and trends, Journal of the European Ceramic Society 16(7) (1996) 721-737.

[5] S. Fu, M. Zhu, Y. Zhu, Organosilicon polymer-derived ceramics: An overview, Journal of advanced ceramics 8 (2019) 457-478.doi: https://doi.org/10.1007/s40145-019-0335-3.

[6] Q. Wen, F. Qu, Z. Yu, M. Graczyk-Zajac, X. Xiong, R. Riedel, Si-based polymer-derived ceramics for energy conversion and storage, Journal of Advanced Ceramics 11 (2022) 197-246.

[7] J. Pivin, P. Colombo, A. Martucci, G. Soraru, E. Pippel, M. Sendova-Vassileva, Ion beam induced conversion of Si-based polymers and gels layers into ceramics coatings, Journal of sol-gel science and technology 26(1-3) (2003) 251-255.

[8] G. El Chawich, J. El Hayek, V. Rouessac, D. Cot, B. Rebière, R. Habchi, H. Garay, M. Bechelany, M. Zakhour, P. Miele, C. Salameh, Design and Manufacturing of Si-Based Non-Oxide Cellular Ceramic

Structures through Indirect 3D Printing, Materials, 2022.
[9] K.L. Martin, M.J. Parvulescu, T.A. Patel, P. Mogilevsky, T.S. Key, C.M. Thompson, M.B. Dickerson, Bioinspired crosslinking of preceramic polymers via metal ion coordination bonding, Journal of the European Ceramic Society 41(13) (2021) 6366-6376.
[10] M. Narisawa, Silicone resin applications for ceramic precursors and composites, Materials 3(6) (2010) 3518-3536.
[11] J. Koo, M. Miller, J. Weispfenning, C. Blackmon, Silicone polymer composites for thermal protection system: fiber reinforcements and microstructures, Journal of composite materials 45(13) (2011) 1363-1380.
[12] R.G. Jones, S.J. Holder, High-yield controlled syntheses of polysilanes by the Wurtz-type reductive coupling reaction, Polymer international 55(7) (2006) 711-718.
[13] K. Okamura, Ceramic fibres from polymer precursors, Composites 18(2) (1987) 107-120.
[14] S. Yajima, Y. Hasegawa, K. Okamura, T. Matsuzawa, Development of high tensile strength silicon carbide fibre using an organosilicon polymer precursor, Nature 273(5663) (1978) 525-527.
[15] H.J. Kleebe, H. Störmer, S. Trassl, G. Ziegler, Thermal stability of SiCN ceramics studied by spectroscopy and electron microscopy, Applied organometallic chemistry 15(10) (2001) 858-866.
[16] M. Hörz, A. Zern, F. Berger, J. Haug, K. Müller, F. Aldinger, M. Weinmann, Novel polysilazanes as precursors for silicon nitride/silicon carbide composites without “free” carbon, Journal of the European Ceramic Society 25(2-3) (2005) 99-110.
[17] M. Günthner, T. Kraus, A. Dierdorf, D. Decker, W. Krenkel, G. Motz, Advanced coatings on the basis of Si (C) N precursors for protection of steel against oxidation, Journal of the European Ceramic Society 29(10) (2009) 2061-2068.
[18] Y. Abe, T. Gunji, Oligo-and polysiloxanes, Progress in Polymer Science 29(3) (2004) 149-182.
[19] L. Fan, X. Wang, D. Wu, Polyhedral oligomeric silsesquioxanes (POSS)-based hybrid materials: molecular design, solution self-assembly and biomedical applications, Chinese Journal of Chemistry 39(3) (2021) 757-774.
[20] R.H. Baney, M. Itoh, A. Sakakibara, T. Suzuki, Silsesquioxanes, Chemical Reviews 95(5) (1995) 1409-1430.
[21] S. Packirisamy, K. Sreejith, D. Devapal, B. Swaminathan, Polymer-derived ceramics and their space applications, Handbook of Advanced Ceramics and Composites: Defense, Security, Aerospace and Energy Applications (2020) 975-1080.
[22] C. Stabler, E. Ionescu, M. Graczyk-Zajac, I. Gonzalo-Juan, R. Riedel, Silicon oxycarbide glasses and glass-ceramics:“All-Rounder” materials for advanced structural and functional applications, Journal of the American Ceramic Society 101(11) (2018) 4817-4856.
[23] G.D. Sorarù, E. Dallapiccola, G. D'Andrea, Mechanical Characterization of Sol–Gel-Derived Silicon Oxycarbide Glasses, Journal of the American Ceramic Society 79(8) (1996) 2074-2080.
[24] R. Melcher, P. Cromme, M. Scheffler, P. Greil, Centrifugal casting of thin-walled ceramic tubes

from preceramic polymers, Journal of the American Ceramic Society 86(7) (2003) 1211-1213.
[25] P. Colombo, E. Bernardo, G. Parcianello, Multifunctional advanced ceramics from preceramic polymers and nano-sized active fillers, Journal of the European Ceramic Society 33(3) (2013) 453-469.
[26] P. Colombo, G. Mera, R. Riedel, G.D. Sorarù, Polymer-Derived Ceramics: 40 Years of Research and Innovation in Advanced Ceramics, Journal of the American Ceramic Society (2010) no-no.doi: https://doi.org/10.1111/j.1551-2916.2010.03876.x.
[27] R.M.d. Rocha, P. Greil, J.C. Bressiani, A.H.d.A. Bressiani, Complex-shaped ceramic composites obtained by machining compact polymer-filler mixtures, Materials Research 8 (2005) 191-196.
[28] D. Seyferth, Preceramic polymers: past, present and future, Massachusetts Inst of Tech Cambridge Dept of Chemistry, 1992.
[29] C.A. Lewinsohn, P. Colombo, I. Reimanis, Ö. Ünal, Stresses occurring during joining of ceramics using preceramic polymers, Journal of the American Ceramic Society 84(10) (2001) 2240-2244.
[30] P. Colombo, G. Mera, R. Riedel, G.D. Soraru, Polymer-derived ceramics: 40 years of research and innovation in advanced ceramics, Ceramics Science and Technology (2013) 245-320.
[31] P. Greil, Polymer derived engineering ceramics, Advanced engineering materials 2(6) (2000) 339-348.doi: https://doi.org/10.1002/1527-2648(200006)2:6<339::AID-ADEM339>3.0.CO;2-K.
[32] P. Greil, M. Seibold, Modelling of dimensional changes during polymer-ceramic conversion for bulk component fabrication, Journal of Materials Science 27(4) (1992) 1053-1060.doi: 10.1007/BF01197660.
[33] P. Greil, Active-filler-controlled pyrolysis of preceramic polymers, Journal of the American Ceramic Society 78(4) (1995) 835-848.doi: https://doi.org/10.1111/j.1151-2916.1995.tb08404.x.
[34] G. Barroso, Q. Li, R.K. Bordia, G. Motz, Polymeric and ceramic silicon-based coatings–a review, Journal of materials chemistry A 7(5) (2019) 1936-1963.
[35] P. Colombo, T. Gambaryan-Roisman, M. Scheffler, P. Buhler, P. Greil, Conductive ceramic foams from preceramic polymers, Journal of the American Ceramic Society 84(10) (2001) 2265-2268.
[36] M. Mirkhalaf, H. Yazdani Sarvestani, Q. Yang, M.B. Jakubinek, B. Ashrafi, A comparative study of nano-fillers to improve toughness and modulus of polymer-derived ceramics, Scientific reports 11(1) (2021) 6951.
[37] D. Suttor, H.J. Kleebe, G. Ziegler, Formation of mullite from filled siloxanes, Journal of the American Ceramic Society 80(10) (1997) 2541-2548.
[38] E. Bernardo, P. Colombo, E. Pippel, J. Woltersdorf, Novel mullite synthesis based on alumina nanoparticles and a preceramic polymer, Journal of the American Ceramic Society 89(5) (2006) 1577-1583.doi: https://doi.org/10.1111/j.1551-2916.2006.00963.x.
[39] L. Gorjan, R. Tonello, T. Sebastian, P. Colombo, F. Clemens, Fused deposition modeling of mullite structures from a preceramic polymer and γ-alumina, Journal of the European Ceramic Society 39(7) (2019) 2463-2471.doi: https://doi.org/10.1016/j.jeurceramsoc.2019.02.032.
[40] R.L. LEHMAN, Ceramic matrix fiber composites, Treatise on Materials Science & Technology,

Elsevier1989, pp. 229-291.
[41] E. Ionescu, A. Francis, R. Riedel, Dispersion assessment and studies on AC percolative conductivity in polymer-derived Si–C–N/CNT ceramic nanocomposites, Journal of materials science 44 (2009) 2055-2062.
[42] J. Cordelair, P. Greil, Electrical characterization of polymethylsiloxane/MoSi2-derived composite ceramics, Journal of the American Ceramic Society 84(10) (2001) 2256-2259.
[43] H. Windsheimer, N. Travitzky, A. Hofenauer, P. Greil, Laminated object manufacturing of preceramic-paper-derived Si? SiC composites, Advanced Materials 19(24) (2007) 4515-4519.
[44] Y.W. Kim, H.D. Kim, C.B. Park, Processing of microcellular mullite, Journal of the American Ceramic Society 88(12) (2005) 3311-3315.doi: https://doi.org/10.1111/j.1551-2916.2005.00597.x.
[45] G. Parcianello, E. Bernardo, P. Colombo, Mullite/zirconia nanocomposites from a preceramic polymer and nanosized fillers, Journal of the American Ceramic Society 94(5) (2011) 1357-1362.
[46] E. Bernardo, E. Tomasella, P. Colombo, Development of multiphase bioceramics from a filler-containing preceramic polymer, Ceramics International 35(4) (2009) 1415-1421.doi: https://doi.org/10.1016/j.ceramint.2008.07.003.
[47] E. Bernardo, P. Colombo, I. Cacciotti, A. Bianco, R. Bedini, R. Pecci, K. Pardun, L. Treccani, K. Rezwan, Porous wollastonite–hydroxyapatite bioceramics from a preceramic polymer and micro-or nano-sized fillers, Journal of the European Ceramic Society 32(2) (2012) 399-408.
[48] E. Bernardo, P. Colombo, E. Dainese, G. Lucchetta, P.F. Bariani, Novel 3D wollastonite-based scaffolds from preceramic polymers containing micro-and nano-sized reactive particles, Advanced Engineering Materials 14(4) (2012) 269-274.doi: https://doi.org/10.1002/adem.201100241.
[49] E. Bernardo, G. Parcianello, P. Colombo, Novel synthesis and applications of yttrium silicates from a silicone resin containing oxide nano-particle fillers, Ceramics International 38(7) (2012) 5469-5474.
[50] G. Parcianello, E. Bernardo, P. Colombo, Low temperature synthesis of zircon from silicone resins and oxide nano-sized particles, Journal of the European Ceramic Society 32(11) (2012) 2819-2824.doi: https://doi.org/10.1016/j.jeurceramsoc.2011.11.028.
[51] E. Bernardo, L. Fiocco, G.A. Giffin, V. Di Noto, P. Colombo, Microstructure Development and Dielectric Characterization of Forsterite-Based Ceramics from Silicone Resins and Oxide Fillers, Advanced Engineering Materials 16(6) (2014) 806-813.
[52] G. Parcianello, E. Bernardo, P. Colombo, Cordierite ceramics from silicone resins containing nano-sized oxide particle fillers, Ceramics International 39(8) (2013) 8893-8899.doi: https://doi.org/10.1016/j.ceramint.2013.04.083.
[53] E. Bernardo, L. Fiocco, A. Prnová, R. Klement, D. Galusek, Gehlenite: Eu3+ phosphors from a silicone resin and nano-sized fillers, Optical Materials 36(7) (2014) 1243-1249.
[54] E. Bernardo, J.-F. Carlotti, P.M. Dias, L. Fiocco, P. Colombo, L. Treccani, U. Hess, K. Rezwan, Novel akermanite-based bioceramics from preceramic polymers and oxide fillers, Ceramics International 40(1) (2014) 1029-1035.

[55] E. Bernardo, P. Colombo, S. Hampshire, SiAlON-based ceramics from filled preceramic polymers, Journal of the American Ceramic Society 89(12) (2006) 3839-3842.doi: https://doi.org/10.1111/j.1551-2916.2006.01287.x.
[56] E. Bernardo, P. Colombo, S. Hampshire, Advanced ceramics from a preceramic polymer and nano-fillers, Journal of the European Ceramic Society 29(5) (2009) 843-849.
[57] E. Bernardo, G. Parcianello, P. Colombo, J. Adair, A. Barnes, J. Hellmann, B. Jones, J. Kruise, J. Swab, SiAlON ceramics from preceramic polymers and nano-sized fillers: Application in ceramic joining, Journal of the European Ceramic Society 32(7) (2012) 1329-1335.
[58] A. Zocca, H. Elsayed, E. Bernardo, C. Gomes, M. Lopez-Heredia, C. Knabe, P. Colombo, J. Günster, 3D-printed silicate porous bioceramics using a non-sacrificial preceramic polymer binder, Biofabrication 7(2) (2015) 025008.doi: 10.1088/1758-5090/7/2/025008.
[59] H. Elsayed, A. Zocca, E. Bernardo, C.M. Gomes, J. Günster, P. Colombo, Development of bioactive silicate-based glass-ceramics from preceramic polymer and fillers, Journal of the European Ceramic Society 35(2) (2015) 731-739.doi: 10.1016/j.jeurceramsoc.2014.09.020.
[60] L. Fiocco, H. Elsayed, L. Ferroni, C. Gardin, B. Zavan, E. Bernardo, Bioactive wollastonite-diopside foams from preceramic polymers and reactive oxide fillers, Materials 8(5) (2015) 2480-2494.
[61] A. Choudhary, S.P. Sahoo, S.K. Behera, Lithium orthosilicate ceramics with preceramic polymer as silica source, Ceramics International 43(10) (2017) 7951-7957.doi: 10.1016/j.ceramint.2017.03.093.
[62] H. Elsayed, P. Rebesan, M.C. Crovace, E.D. Zanotto, P. Colombo, E. Bernardo, Biosilicate® scaffolds produced by 3D-printing and direct foaming using preceramic polymers, Journal of the American Ceramic Society 102(3) (2019) 1010-1020.doi: https://doi.org/10.1111/jace.15948.
[63] T. Michalet, M. Parlier, F. Beclin, R. Duclos, J. Crampon, Elaboration of low shrinkage mullite by active filler controlled pyrolysis of siloxanes, Journal of the European Ceramic Society 22(2) (2002) 143-152.
[64] E. Bernardo, P. Colombo, E. Manias, SiOC glass modified by montmorillonite clay, Ceramics International 32(6) (2006) 679-686.
[65] S.-H. Hong, W. Cermignani, G. Messing, Anisotropic grain growth in seeded and B2O3-doped diphasic mullite gels, Journal of the European Ceramic Society 16(2) (1996) 133-141.
[66] A.J. Pyzik, C.S. Todd, C. Han, Formation mechanism and microstructure development in acicular mullite ceramics fabricated by controlled decomposition of fluorotopaz, Journal of the European Ceramic Society 28(2) (2008) 383-391.
[67] R. Riedel, L. Toma, C. Fasel, G. Miehe, Polymer-derived mullite–SiC-based nanocomposites, Journal of the European Ceramic Society 29(14) (2009) 3079-3090.
[68] L. Toma, C. Fasel, S. Lauterbach, H.-J. Kleebe, R. Riedel, Influence of nano-aluminum filler on the microstructure of SiOC ceramics, Journal of the European Ceramic Society 31(9) (2011) 1779-1789.
[69] E. Mazzucato, A. Gualtieri, Wollastonite polytypes in the CaO-SiO 2 system. Part I. Crystallisation kinetics, Physics and Chemistry of Minerals 27 (2000) 565-574.

[70] S. Ni, L. Chou, J. Chang, Preparation and characterization of forsterite (Mg2SiO4) bioceramics, Ceramics International 33(1) (2007) 83-88.
[71] K. Song, X. Chen, Phase evolution and microwave dielectric characteristics of Ti-substituted Mg2SiO4 forsterite ceramics, Materials Letters 62(3) (2008) 520-522.
[72] Z. Sun, Y. Zhou, J. Wang, M. Li, γ-Y2Si2O7, a machinable silicate ceramic: mechanical properties and machinability, Journal of the American Ceramic Society 90(8) (2007) 2535-2541.
[73] M. Dıaz, I. Garcia-Cano, S. Mello-Castanho, J. Moya, M. Rodrıguez, Synthesis of nanocrystalline yttrium disilicate powder by a sol–gel method, Journal of non-crystalline solids 289(1-3) (2001) 151-154.
[74] J. Moya, M. Díaz, C. Serna, S. Mello-Castanho, Formation of nanocrystalline yttrium disilicate powder by an oxalate gel method, Journal of the European Ceramic Society 18(9) (1998) 1381-1384.
[75] A.I. Becerro, M. Naranjo, A.C. Perdigón, J.M. Trillo, Hydrothermal chemistry of silicates: Low-temperature synthesis of y-yttrium disilicate, Journal of the American Ceramic Society 86(9) (2003) 1592-1594.
[76] T. Taki, S. Maeda, K. Okamura, M. Sato, T. Matsuzawa, Oxidation curing mechanism of polycarbosilane fibres by solid-state 29 Si high-resolution NMR, Journal of materials science letters 6 (1987) 826-828.
[77] H. Ly, R. Taylor, R. Day, F. Heatley, Conversion of polycarbosilane (PCS) to SiC-based ceramic Part 1. Characterisation of PCS and curing products, Journal of Materials science 36(16) (2001) 4037-4043.
[78] N. Janakiraman, F. Aldinger, Fabrication and characterization of fully dense Si–C–N ceramics from a poly (ureamethylvinyl) silazane precursor, Journal of the European Ceramic Society 29(1) (2009) 163-173.
[79] M. Schulz, M. Börner, J. Göttert, T. Hanemann, J. Haußelt, G. Motz, Cross linking behavior of preceramic polymers effected by UV-and synchrotron radiation, Advanced Engineering Materials 6(8) (2004) 676-680.
[80] B. Eick, J. Youngblood, SiC nanofibers by pyrolysis of electrospun preceramic polymers, Journal of materials science 44 (2009) 160-165.
[81] S. Zhou, H. Mei, P. Chang, M. Lu, L. Cheng, Molecule editable 3D printed polymer-derived ceramics, Coordination Chemistry Reviews 422 (2020) 213486.
[82] C.W. Hull, S.T. Spence, D.J. Albert, D.R. Smalley, R.A. Harlow, P. Steinbaugh, H.L. Tarnoff, H.D. Nguyen, C.W. Lewis, T.J. Vorgitch, Methods and apparatus for production of three-dimensional objects by stereolithography, Google Patents, 1991.
[83] S. Nohut, M. Schwentenwein, Vat photopolymerization additive manufacturing of functionally graded materials: a review, Journal of Manufacturing and Materials Processing 6(1) (2022) 17.
[84] A. Al Rashid, W. Ahmed, M.Y. Khalid, M. Koc, Vat photopolymerization of polymers and polymer composites: Processes and applications, Additive Manufacturing 47 (2021) 102279.

[85] J. Huang, Q. Qin, J. Wang, A review of stereolithography: Processes and systems, Processes 8(9) (2020) 1138.
[86] X. Tian, D. Li, Z. Chen, W. Zhou, Study on the fabrication accuracy of ceramic parts by direct stereolithography: Ceramic parts can be prepared using stereolithography by building composite parts from ceramic powder-loaded resins, followed by simultaneous polymer pyrolysis and ceramic sintering. This paper describes a systematic study into the influence of several parameters on the accuracy of such parts, Virtual and Physical Prototyping 7(3) (2012) 195-202.
[87] P. Ożóg, H. Elsayed, L. Grigolato, G. Savio, J. Kraxner, D. Galusek, E. Bernardo, Engineering of silicone-based blends for the masked stereolithography of biosilicate/carbon composite scaffolds, Journal of the European Ceramic Society 42(13) (2022) 6192-6198.
[88] E. Rosado, R. Moreno, Mullite-silica scaffolds obtained by stereolithography and reaction sintering, Open Ceramics 14 (2023) 100361.doi: https://doi.org/10.1016/j.oceram.2023.100361.
[89] Z.C. Eckel, C. Zhou, J.H. Martin, A.J. Jacobsen, W.B. Carter, T.A. Schaedler, Additive manufacturing of polymer-derived ceramics, Science 351(6268) (2016) 58-62.doi: https://doi.org/10.1126/science.aad2688.
[90] K.M. Arif, T. Murakami, Slant beam rotation UV scanning to eliminate stair-steps in stereolithography fabrications, The International Journal of Advanced Manufacturing Technology 41 (2009) 527-537.
[91] L.J. Hornbeck, Digital light processing update: status and future applications, Projection displays V, SPIE, 1999, pp. 158-170.
[92] J. Schmidt, A.A. Altun, M. Schwentenwein, P. Colombo, Complex mullite structures fabricated via digital light processing of a preceramic polysiloxane with active alumina fillers, Journal of the European Ceramic Society 39(4) (2019) 1336-1343.doi: https://doi.org/10.1016/j.jeurceramsoc.2018.11.038.
[93] A. Dasan, H. Elsayed, J. Kraxner, D. Galusek, P. Colombo, E. Bernardo, Engineering of silicone-based mixtures for the digital light processing of Åkermanite scaffolds, Journal of the European Ceramic Society 40(7) (2020) 2566-2572.
[94] Y.J. No, J.J. Li, H. Zreiqat, Doped calcium silicate ceramics: a new class of candidates for synthetic bone substitutes, Materials 10(2) (2017) 153.
[95] H. Elsayed, M. Picicco, A. Dasan, J. Kraxner, D. Galusek, E. Bernardo, Glass powders and reactive silicone binder: Application to digital light processing of bioactive glass-ceramic scaffolds, Ceramics International 46(16) (2020) 25299-25305.
[96] J. Wang, X. Dai, Y. Peng, M. Liu, F. Lu, X. Yang, Z. Gou, J. Ye, Digital light processing strength-strong ultra-thin bioceramic scaffolds for challengeable orbital bone regeneration and repair in Situ, Applied Materials Today 22 (2021) 100889.
[97] Z. He, C. Jiao, H. Zhang, D. Xie, M. Ge, Y. Yang, G. Wu, H. Liang, L. Shen, C. Wang, Fabrication of a zirconia/calcium silicate composite scaffold based on digital light processing, Ceramics International 48(18) (2022) 25923-25932.

[98] S. Maruo, O. Nakamura, S. Kawata, Three-dimensional microfabrication with two-photon-absorbed photopolymerization, Optics letters 22(2) (1997) 132-134.
[99] S. O'Halloran, A. Pandit, A. Heise, A. Kellett, Two-Photon Polymerization: Fundamentals, Materials, and Chemical Modification Strategies, Advanced Science 10(7) (2023) 2204072.
[100] X. Wang, F. Schmidt, D. Hanaor, P.H. Kamm, S. Li, A. Gurlo, Additive manufacturing of ceramics from preceramic polymers: A versatile stereolithographic approach assisted by thiol-ene click chemistry, Additive manufacturing 27 (2019) 80-90.
[101] E. Zanchetta, M. Cattaldo, G. Franchin, M. Schwentenwein, J. Homa, G. Brusatin, P. Colombo, Stereolithography of SiOC ceramic microcomponents, Advanced Materials 28(2) (2016) 370-376.doi: https://doi.org/10.1002/adma.201503470.
[102] A. Mazzoli, Selective laser sintering in biomedical engineering, Medical & biological engineering & computing 51 (2013) 245-256.
[103] T. Friedel, N. Travitzky, F. Niebling, M. Scheffler, P. Greil, Fabrication of polymer derived ceramic parts by selective laser curing, Journal of the European Ceramic Society 25(2-3) (2005) 193-197.doi: https://doi.org/10.1016/j.jeurceramsoc.2004.07.017.
[104] B. Dermeik, N. Travitzky, Laminated object manufacturing of ceramic-based materials, Advanced engineering materials 22(9) (2020) 2000256.
[105] H. Sieber, H. Friedrich, J. Zeschky, P. Greil, Light weight ceramic composites from laminated paper structures, 24th annual conference on composites, advanced ceramics, materials, and structures: B: ceramic engineering and science proceedings, Wiley Online Library, 2000, pp. 129-134.
[106] F. Wolff, H. Münstedt, Continuous direct melt foaming of a preceramic polymer using carbon dioxide: extrusion device and first results, Journal of materials science 46 (2011) 6162-6167.
[107] J. Cesarano, R. Segalman, P. Calvert, Robocasting provides MOULDLESS fabrication from slurry deposition, Ceramic industry 148(4) (1998) 94-96.
[108] M. Saadi, A. Maguire, N.T. Pottackal, M.S.H. Thakur, M.M. Ikram, A.J. Hart, P.M. Ajayan, M.M. Rahman, Direct ink writing: a 3D printing technology for diverse materials, Advanced Materials 34(28) (2022) 2108855.
[109] L. Wei, J. Li, S. Zhang, B. Li, Y. Liu, F. Wang, S. Dong, Fabrication of SiOC ceramic with cellular structure via UV-Assisted direct ink writing, Ceramics International 46(3) (2020) 3637-3643.
[110] A. Zocca, G. Franchin, H. Elsayed, E. Gioffredi, E. Bernardo, P. Colombo, Direct ink writing of a preceramic polymer and fillers to produce hardystonite (Ca2ZnSi2O7) bioceramic scaffolds, Journal of the American Ceramic Society 99(6) (2016) 1960-1967.
[111] L. Fiocco, H. Elsayed, D. Badocco, P. Pastore, D. Bellucci, V. Cannillo, R. Detsch, A. Boccaccini, E. Bernardo, Direct ink writing of silica-bonded calcite scaffolds from preceramic polymers and fillers, Biofabrication 9(2) (2017) 025012.doi: 10.1088/1758-5090/aa6c37.
[112] A. Dasan, H. Elsayed, J. Kraxner, D. Galusek, E. Bernardo, Hierarchically porous 3D-printed akermanite scaffolds from silicones and engineered fillers, Journal of the European Ceramic Society

39(14) (2019) 4445-4449.
[113] H. Elsayed, M. Picicco, A. Dasan, J. Kraxner, D. Galusek, E. Bernardo, Glass powders and reactive silicone binder: Interactions and application to additive manufacturing of bioactive glass-ceramic scaffolds, Ceramics International 45(11) (2019) 13740-13746.
[114] H. Elsayed, M. Secco, F. Zorzi, K. Schuhladen, R. Detsch, A.R. Boccaccini, E. Bernardo, Highly porous polymer-derived bioceramics based on a complex hardystonite solid solution, Materials 12(23) (2019) 3970.
[115] K. Huang, H. Elsayed, G. Franchin, P. Colombo, 3D printing of polymer-derived SiOC with hierarchical and tunable porosity, Additive Manufacturing 36 (2020) 101549.
[116] H. Elsayed, C. Gardin, L. Ferroni, B. Zavan, P. Colombo, E. Bernardo, Highly porous Sr/Mg-doped hardystonite bioceramics from preceramic polymers and reactive fillers: direct foaming and direct ink writing, Advanced Engineering Materials 21(6) (2019) 1800900.doi: https://doi.org/10.1002/adem.201800900.
[117] P. Zhang, Z. Wang, J. Li, X. Li, L. Cheng, From materials to devices using fused deposition modeling: A state-of-art review, Nanotechnology Reviews 9(1) (2020) 1594-1609.
[118] J. Gonzalez-Gutierrez, S. Cano, S. Schuschnigg, C. Kukla, J. Sapkota, C. Holzer, Additive manufacturing of metallic and ceramic components by the material extrusion of highly-filled polymers: A review and future perspectives, Materials 11(5) (2018) 840.doi: https://doi.org/10.3390/ma11050840.

Chapter 3- Effect of MgO sintering additive on mullite structures manufactured by fused deposition modeling (FDM) technology

Fateme Sarraf, Edoardo Abbatinali, Lovro Gorjan, Tutu Sebastian, Paolo Colombo, Sergey V. Churakov, Frank Clemens

Journal of the European Ceramic Society (2021), Volume 41, Issue 13, October 2021, Pages 6677-6686

DOI: https://doi.org/10.1016/j.jeurceramsoc.2021.06.012

- This study answers the first research question, "**How sintering additives affect the densification and mullite formation during the sintering process?**", by investigating the impact of MgO sintering additive on densification of polymer derived mullite ceramics. Three different amount of MgO (0, 0.5 and 1wt%) was added to a PCP-based ceramic feedstock containing a commercial methyl-silsesquioxane (SILRES MK), submicron alumina powder and EVA thermoplastic binder to develop PCP-based filaments for mullite ceramics. XRD analysis revealed that 0.5wt% MgO was sufficient for pure mullite at 1600°C with a dwell time of 2.5h, while 1wt% MgO was necessary to achieve dense microstructure after 5h. Flexural tests indicated that samples with 1wt% MgO had higher strength values, attributed to greater densification during sintering. The addition of MgO eliminated the influence of printing direction on mechanical strength. The presence of closed porosity in the fracture surface of sintered bars, resulting from degassing during crosslinking and pyrolysis of PCPs, explained the low Weibull modulus observed. The presence of scattered macro-pores in the sintered specimens with MgO was linked to limited diffusion of water molecules vapor through the EVA binder.

Effect of MgO sintering additive on mullite structures manufactured by fused deposition modeling (FDM) technology

Fateme Sarraf, Edoardo Abbatinali, Lovro Gorjan, Tutu Sebastian, Paolo Colombo, Sergey V. Churakov, Frank Clemens

Abstract

An optimized recipe for 3D printing of Mullite-based structures was used to investigate the effect of MgO sintering additive on the processing stages and final ceramic properties. To achieve dense 3:2 mullite, ceramic filaments were prepared based on an alumina powder, a methyl silicone resin, EVA elastomeric binder and MgO powder. Using 1wt% MgO and a dwell time of 5h at 1600°C, a dense mullite structure could be obtained from filaments with a diameter of 1.75 mm. Ceramic structures with and without sintering additive were printed in vertical and horizontal direction, to investigate the effect of printing direction on mechanical strength after sintering. Using four-point bending test, it was demonstrated that by using MgO, the printing orientation did not affect the mechanical strength significantly anymore. The low Weibull modulus could be explained by the closed porosity that emerge during the degassing of the preceramic polymer due to crosslinking.

Keywords: Fused deposition modeling (FDM), mullite, polymer derived ceramic (PDC), polysiloxane, sintering additive

3.1. Introduction

Mullite, e.g. a mixed oxide ceramic based on $3Al_2O_3 \cdot 2SiO_2$, is one of the most commonly used ceramic materials because of its remarkable thermal and mechanical properties [1, 2]. The use of mullite in heat protection systems relies on its low thermal conductivity and refractoriness. Moreover, mullite is proposed as a common option for tableware, construction and engineering ceramics, refractories, kiln furniture, substrates for catalytic converters and electronic devices, due to its relatively low thermal expansion coefficient, low creep at high temperatures and associated high thermal shock resistance [3-5]. Considering its low electric conductivity and dielectric constant, mullite can also be employed for electrical insulation applications, for instance, a substrate for electronic devices as well [6].

In the last decade, mullite was investigated additionally for optical, dielectric and structural components, produced using various synthesis and processing strategies. Mullite is a rarely found natural ceramic material, but often it is synthesized using alumina and silica-based raw materials by various methods, such as conventional powder metallurgy [7], atomic layer deposition (ALD) [8], sol-gel [9-12], co-precipitation [13], combustion [14], chemical vapor deposition (CVD) [15-17] and transient viscous sintering (TVS) [18,19].

Another way to synthesize mullite, by using preceramic polymers, has been investigated by Bernardo et al. in 2006. In this process, the silica that is produced from the decomposition of the preceramic polymer during the thermal heat treatment reacts with alumina powder at 1200–1500°C [20, 21]. The main difficulty in using preceramic polymers for the fabrication of relatively large components is the high mass loss and change in density associated with the polymer to ceramic conversion. This process has a high volume change leading to the formation of pores, blisters and cracks during the pyrolysis process. Using a passive or an active filler, the preceramic polymer content can be reduced, and as a result, the amount of released gaseous by-products and the global shrinkage can be significantly decreased. Passive fillers remain inert during the whole process and do not undergo phase transitions. Those passive fillers neither react with the ceramic residue of the preceramic polymer, nor with the gaseous products released during the pyrolysis step. On the contrary, active fillers interact by chemical reaction with the preceramic polymer and the gas atmosphere during thermal treatment, compensating for the shrinkage by volume expansion. Greil et al. pioneered this approach, investigating the processing of preceramic polymers containing different intermetallic and metal active fillers [22]. For the synthesis of mullite, active fillers based on metallic aluminum have been already

discussed in his paper, the use of alumina powder is an alternative approach investigated by other researchers [20, 23-27].

Fused deposition modeling (FDM) was introduced in the 1990s as an additive manufacturing method for ceramics to overcome the practical difficulties of producing ceramic structures with complex geometries and minimize the material waste in comparison to conventional shaping processes [28]. FDM/FFF printing of mullite structures using preceramic polymers has been already reported by Gorjan et al. in 2019, though, full mullite conversion and structure densification could not be achieved at 1550°C [26].

The Si^{4+} and Al^{3+} cations within the mullite lattice show very low bulk and grain-boundary diffusion coefficients. Accordingly, mullite has poor solid-state sinterability, and usually requires high temperatures for densification [29]. To overcome this obstacle, oxides, such as MgO, Y_2O_3 and La_2O_3, have been introduced as sintering aids, among which the MgO has shown the most promising results so far [30]. It has been reported that the sinterability of mullite ceramics can be improved by the formation of a liquid phase in the presence of MgO, which appears in a narrow temperature range, from 1410 to 1425°C [31]. The enhanced densification of doped mullite bodies via this mechanism has been also confirmed for industrial mullites. The amount of glassy phase significantly influences the sinterability of mullite, which decreases when the amount of glass phase is reduced [32].

In this paper, we investigated the effect of MgO sintering additive on thermoplastic processing, sinterability, mechanical and microstructural characteristics of filaments and FDM/FFF printed structures derived from preceramic polymer- γ-alumina mixtures, to achieve full mullite transformation and densification. For the first time, a commercial FDM printer has been used to investigate the effect of the printing orientation on the mechanical properties for FDM/FFF printed mullite structures with and without sintering additives, using four-point bending test.

3.2. Material and methods

3.2.1. Material

The 3:2 mullite ($3Al_2O_3.2SiO_2$) was produced using a micron-sized alumina powder (PURALOX SCFa-140 UF5, Sasol Performance Chemicals Ltd) and a methyl silicone resin (Silres MK, Wacker Chemie AG). The Silres MK has a silica yield of approximately 82wt.% when heated in air at temperatures > ~1000°C. In addition, magnesium oxide (MgO, Fluka™) was added as a sintering additive. According to the literature [32, 33], 0, 0.5 and 1wt.% of MgO

were investigated. An ethylene-vinyl acetate copolymer resin (Elvax 420, Dupont), with a melting point of 73°C, was employed as a thermoplastic binder for FDM/FFF printing.

The three feedstock formulations used in this study are listed in Table 1. A constant powder content of 40 vol.% was used. Due to the thermoplastic properties of the silicone resin, which has a glass transition temperature in the range of 50-60°C, the preceramic polymer was treated as a binder with a high ash content after pyrolysis. The powder content of Al_2O_3 and MgO was fixed to a low volume content of 13.8 vol.%.

Table 1. Formulations for ceramic components in the feedstock (i.e. filaments).

Feedstock	UF5 (wt.%)	Silres MK (wt.%)	MgO content in feedstock (wt.%)	MgO content in sintered part (wt.%)
F1	32.47	25.76	0.00	0
FM05	32.34	25.66	0.27	0.5
FM1	32.22	25.57	0.54	1

3.2.2. Processing

Thermoplastic feedstocks were prepared by mixing all the components in a torque rheometer (Rheomix 600, HAAKE™ PolyLab™ OS, Thermo Fisher Scientific, Germany). Before mixing, the alumina and magnesia powder were dried for 12h at 110°C. The mixing was performed for 1h at 120°C and 10 rpm using roller rotors. Thermoplastic filaments were fabricated by extrusion through a die with a diameter of 1.8 mm. For the filament fabrication, a capillary rheometer (Rosand RH7, NETZSCH-Gerätebau GmbH, Germany) with a piston speed of 10 mm/min and temperature of 90°C was used.

The obtained filaments were used for freeform shaping with a commercial FDM/FFF printer (CraftBot2, Craftunique LTD, Hungary). In an FDM printer, the filaments are guided through a roll and a gear wheel that pulls the filament from the spool and pushes it into the heated extrusion nozzle (hot end) with a constant feeding rate. The structure is printed layer by layer on a support according to a 3D model saved as an stl-file. In the heated extrusion nozzle, the tip of the filament is melted while the solid part of the filament (outside the hot end) acts as a piston to push the melted part out of the printer head. The printing parameters, optimized by Gorjan et al. in 2019, have been used [26]. The extruder temperature, printing speed, printing angle, nozzle diameter and layer height were set to 170°C, 7mm/s, 45°-90°, 0.8mm and 0.475mm, respectively.

Thermal processing was carried out in two steps: I) thermal debinding and pre-sintering followed by II) sintering of the filaments and printed samples. Both thermal steps were conducted in a static air atmosphere. For debinding and pre-sintering, a box furnace (Pyrotec PC 12, Michel Keramikbedarf, Switzerland) was used. The filament and printed samples were placed on top of a γ-alumina powder bed covered with a thin layer of carbon black (to avoid sticking to the alumina powder bed) and heated at 1K/min to 140°C, then at 0.2K/min to 230°C; with an 8h dwell time at 230°C. After heating up to 375°C at a rate of 0.3K/min, the temperature was held at 375°C for 10h. This was followed by an increase in temperature at the same heating rate to 500°C, then it was raised to 1000°C at 3K/min followed by a dwelling time of 2h at the same temperature. After debinding at 500°C, the samples were too brittle to handle, and thus pre-sintering up to 1000°C was required. Sintering of the filaments was carried out in an electrically heated furnace (LHT 03/17 D, Nabertherm GmbH) at 3K/min to 1600°C with two different dwell times: 2.5 and 5h. Based on the results of the firing of the filaments, only a dwell time of 5 h was used for sintering of the 3D printed samples.

3.2.3. Characterization

Alumina and magnesium oxide powders were analyzed by the gas adsorption method (BET, SA 3100, Beckman Coulter, USA) to determine the specific surface area, and laser diffraction (LS 13 320 XR, Beckman Coulter, USA) to measure the particle size distribution. For the particle size analysis, the powders were dispersed in distilled water and ultrasonicated for 10 minutes to break agglomerates.

The d_{BET} is an average diameter calculated from the theoretical density and the measured specific surface area (SSA), assuming that the particles are spherical and monodisperse [34, 35]. The d_{BET} can be calculated using Equation (1):

$$d_{BET} = \frac{6}{SSA \times \rho} \quad (1)$$

The agglomeration factor (d_{50}/d_{BET}) describes the ratio between the measured median particle size by the particle size analyzer and the calculated value obtained from BET (primary particles size). This value can be used to estimate the content of binder that is immobilized in the agglomerates and does not contribute to the plasticization of the feedstock [34, 35].

To study the microstructure of sintered filaments, the fracture surface of four-point bending test samples, as well as of printed and sintered parts, scanning electron microscopy (SEM, VEGA

3, TESCAN, Czech Republic) was employed. For lower magnifications, an optical stereo microscope (SteREO Discovery.V20, Carl Zeiss AG, Switzerland) was used.

X-ray diffraction analysis (XRD, X'Pert PRO MPD, Malvern Panalytical Ltd, Germany) was carried out between10-80 degrees at room temperature with a copper anode to evaluate the phase assemblage after sintering of the filaments. The XRD patterns were analyzed using the software (HighScore, Version 4.8, Malvern Panalytical Ltd, Germany).

The pressure during filament fabrication was measured and compared with the viscosity of the feedstocks, measured by a rotational rheometer (MCR 302, Anton Paar, Austria) with a plate on plate configuration at 90°C with a maximal shear rate limited to 10 1/s to avoid draining of the gap.

To investigate the shrinkage and densification of the sintered filaments and specimens, the weight and geometrical size were measured by balance and caliper. Therefore, bulk density- defined as the total mass of a body divided by the geometrical volume- was calculated for 10 samples for each printing configuration.

To evaluate the effect of the printing direction on the mechanical strength of the sintered mullite samples, rectangular specimens were fabricated and four-point flexural strength test was carried out using a universal testing machine (XforceP S/N 760560, ZwickRoell GmbH, Germany). It is worthwhile to mention that only the edges of the specimens were polished (DIN EN 843-1). It is well-known that the roughness of the first printed layer (in contact with the printing bed) is significantly lower in comparison to the top layer (final layer of the printed structure). Therefore, the specimens were turned for the four-point bending tests to observe compression mode on the final printed layer.

3.3. Results and discussion

3.3.1. Materials characterization

The γ-Al_2O_3 (UF5) and MgO ceramic powders were characterized and the results are summarized in Table 2 and Fig. 1.

Table 2. Properties of ceramic components.

		UF5 ($\gamma - Al_2O_3$)	MgO
Particle size distribution	**D_{10} (μm)**	1.11	1.03
	D_{50} (μm)	5.45	5.49
	D_{90} (μm)	13.04	14.90
Specific surface area	**SSA (m^2/g)**	146.1	30.0
	d_{BET} (μm)	0.01	0.04
Agglomeration factor	**d_{50}/d_{BET}**	545	137.2
Density	**(g/cm^3)**	3.95	3.6

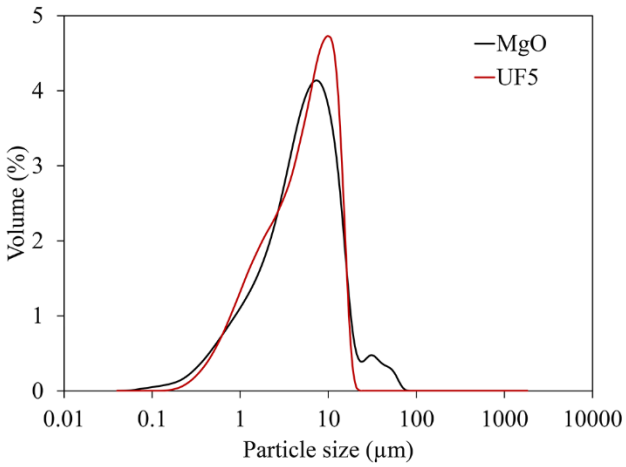

Fig.1. Particle size distribution of MgO and Alumina (UF5) powder measured by laser diffraction technique.

As can be seen in Table 2, UF5 has a much higher specific surface area. According to the particle size measurement (d_{50}), both powders have a similar particle size distribution (Fig. 1). However, the primary particle size d_{BET}, calculated from the SSA, is 4 times lower for γ-Al_2O_3. This results in a 4 times higher agglomeration factor for the γ-Al_2O_3 powder.

Typically, powder agglomerates break during the high-shear kneading process. If the agglomerates do not break during the compounding step, the internal porous structure will trap some binder. Subsequently, the immobilized binder will not be able to participate efficiently as a plasticizer and only a low ceramic filler content within the thermoplastic polymer can be achieved. Fig. 1 demonstrates the presence of some large agglomerates in the MgO powder (> 20 µm) that could not be destroyed by sonication. While the UF5 presents an asymmetric particle size distribution, with a maximum particle size of ~20 µm.

3.3.2. Fabrication of ceramic-based thermoplastic filaments

Ceramic-based thermoplastic filaments were extruded to be used for the FDM/FFF 3D printing process. The filaments, containing three different amounts of MgO, were flexible enough for spooling and feeding into a commercial FDM printer. An example of a spooled filament is shown in Fig. 2. A minimal bending radius of 8 mm could be achieved before fracture.

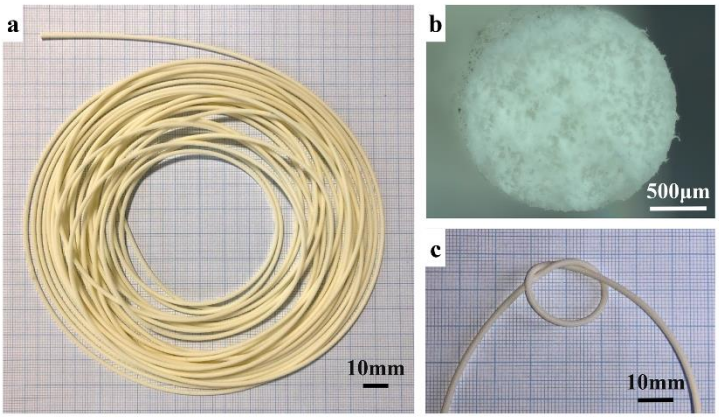

Fig. 2. A spooled filament made from FM1 after extrusion (a) and a cross section of the green filament (b). Flexibility of the filament is demonstrated by tying a knot without filament fracturing (c).

The pressure versus time relations during filament fabrication for the three different feedstocks (0, 0.5 and 1wt.% of MgO) are shown in Fig. 3. The pressure increase, due to the addition of the sintering additive, was not significant. Therefore, it could be assumed that constant printing parameters for all filaments could be used. However, pressure peaks observed during the filament fabrication (diameter of 1.75 mm) for the F1 composition revealed that agglomerates were still present. Unexpected (see Fig. 1) coarse agglomerates seemed to be formed during the mixing process. Interestingly, building agglomerates could be reduced when introducing MgO, as inferred by the smaller number and magnitude of the pressure peaks in Fig. 3.

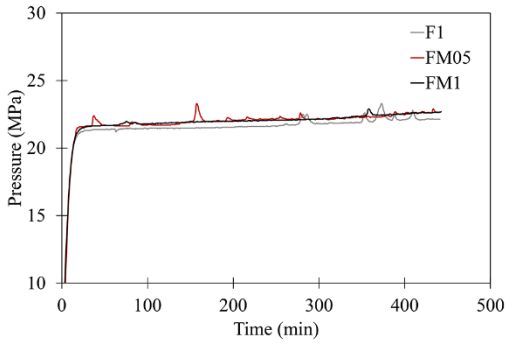

Fig. 3 Pressure versus time plot during the filament extrusion process of the three different feedstocks. The feedstocks were extruded in a capillary rheometer at 90°C, with a fixed extrusion speed (10 mm/min).

In order to prove that the slight increase of the pressure, required during the filament extrusion, was a consequence of viscosity behavior, rotation rheometer experiments were performed using a plate on plate configuration (Fig. 4). As expected, the rheological measurements indicated a slight increase in filament viscosity after introducing the MgO sintering aid powder into the feedstock formulation, and all the feedstocks showed a shear thinning behavior.

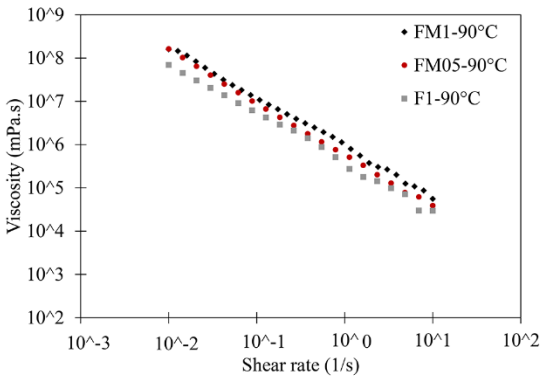

Fig. 4. Viscosity of F1 (0wt.% MgO), FM05 (0.5wt.% MgO) and FM1 (1wt.% MgO) feedstocks, as a function of shear rate at 90 °C, measured by rotational viscosimeter with plate on plate configuration.

3.3.3. Sintering behavior of the thermoplastic filaments

Thermoplastic filaments with different MgO concentrations were sintered in order to investigate the mullite formation and sinterability (e.g. densification). Based on the results of Gorjan et al. [26], the sintering behavior of the filaments was investigated at 1600°C for 2.5h and 5h dwell time in air atmosphere. The microstructures of all sintered filaments are shown in Fig. 5.

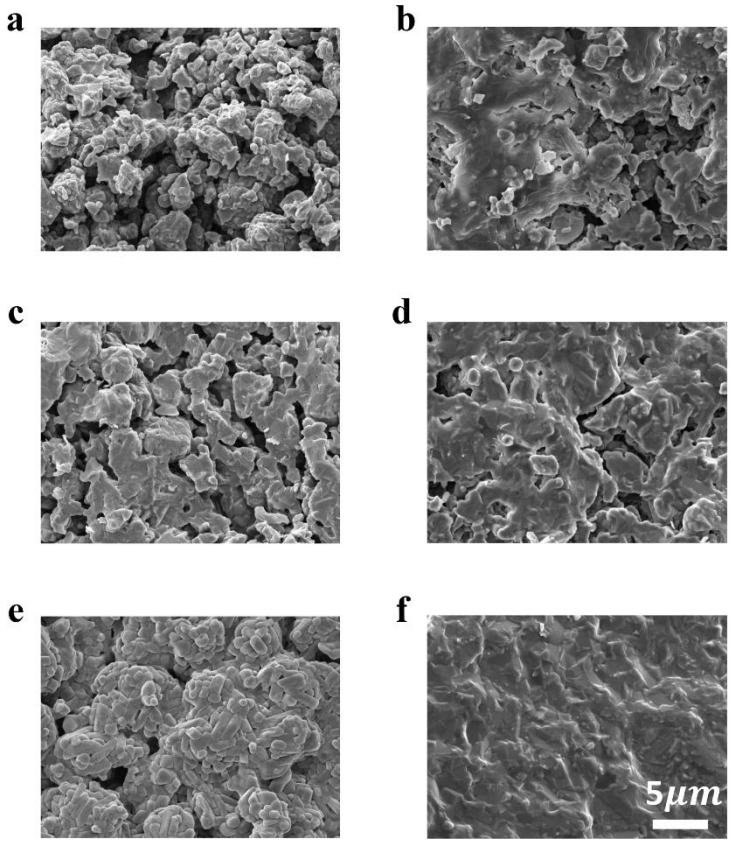

Fig. 5. SEM images of filaments after sintering in air, at 1,600°C for 2.5 (left) and 5 h (right). From the top there are: (a&b) F1, (c&d) FM05 and (e&f) FM1.

A dense mullite structure could be obtained by adding MgO and a dwell time of 5h at 1600°C, as shown in Fig. 5. The calculated shrinkage of the filament diameter, shown in Fig. 6, confirmed the densification process shown by the SEM analysis.

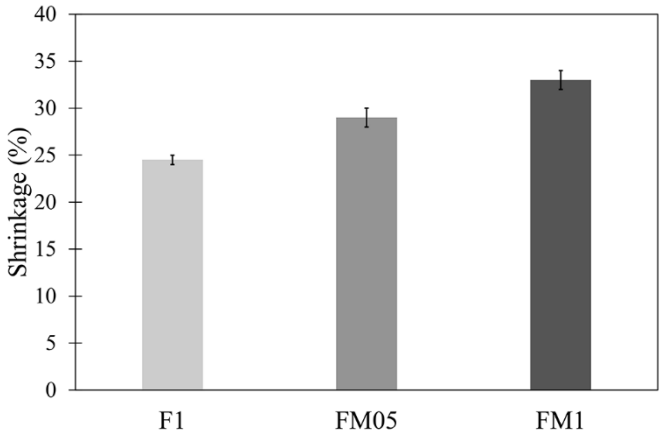

Fig. 6. Mean diameter shrinkage of F1, FM05 and FM1 filaments (d= 1.75mm) after heat-treatment at 1600°C for 5 h of dwell time, in air atmosphere.

Mullite formation during the sintering was monitored by XRD analysis (see Fig. 7). Free γ-Al_2O_3 could still be observed after 5h at 1600°C for the filament without MgO. Adding a small amount of MgO (0.5wt.%), full conversion of mullite could be achieved even after a 2.5h dwell time. Based on the results, it can be concluded that the MgO sintering additive enables full conversion of the SiO_2 and Al_2O_3 into mullite [37].

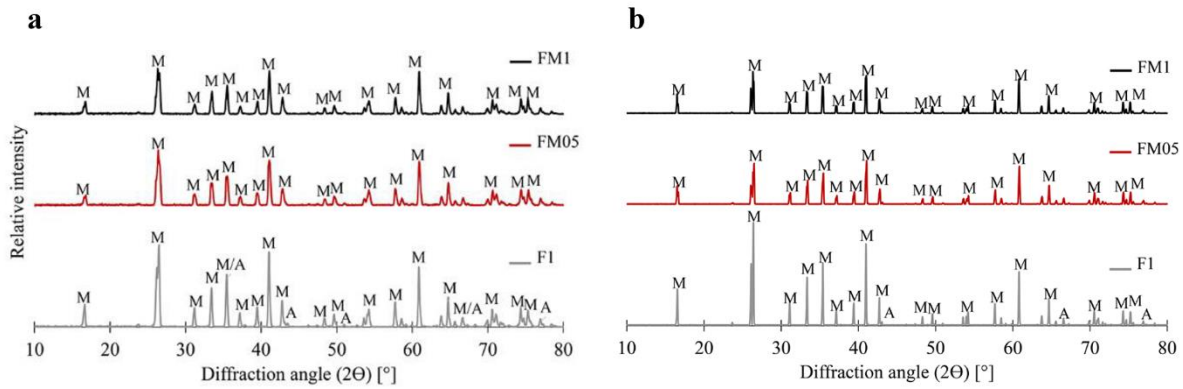

Fig. 7. XRD results comparison between F1 (without MgO), FM05 (0.5wt.% MgO) and FM1 (1wt.% MgO) after sintering at 1600°C for (a) 2.5h and (b) 5h.

3.3.4. Shrinkage and mechanical properties of 3D printed mullite specimens

To investigate the mechanical properties of the sintered FDM/FFF printed mullite material, rectangular specimens printed in vertical and horizontal orientations were fabricated and tested

in a four-point bending configuration. Since 1wt.% of MgO (FM1) was necessary to obtain dense microstructure, ceramic specimens for four-point bending test were printed with an infill of 100% only for the F1 and FM1 formulations (Fig. 8).

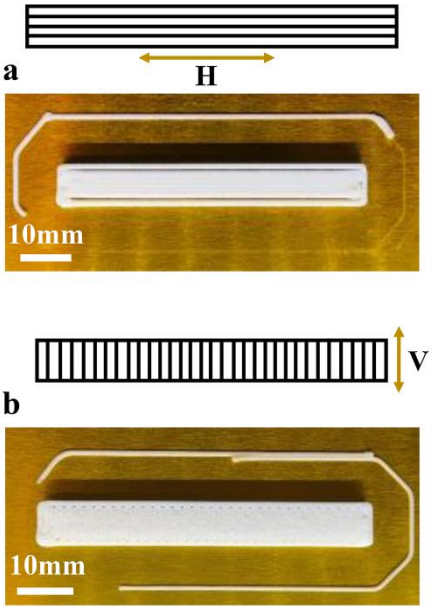

Fig. 8. Printed specimens for mechanical testing. (a) horizontal layout (H) and (b) vertical layout (V). The specimens were cut and polished after printing. Specimen size: 60 mm in length (L), 4.8 mm in width (W) and 3.8 mm in height (H) after printing.

The sintered specimens for mechanical testing are shown in Fig. 9-a. Using the measured geometrical values and the weight of the printed and sintered specimens (1600°C-5h), their density was calculated (Fig. 9-b). It can be concluded that vertically printed specimens had a slightly higher green density compared to the horizontally printed ones. However, this effect was neglected after the sintering due to the higher shrinkage and we reached a similar density for both printing orientations.

Based on Fig. 9-b, a density of 1.44 and 2.27 g/cm^3 was estimated for the F1 and FM1 sintered specimens, respectively. Since pure mullite has a density of 3.1 g/cm^3, highly porous microstructure for the sintered specimens is expected, according to this result. Based on the data, relative density values of 47 % and 73 % were calculated for the F1 and FM1 specimens, respectively.

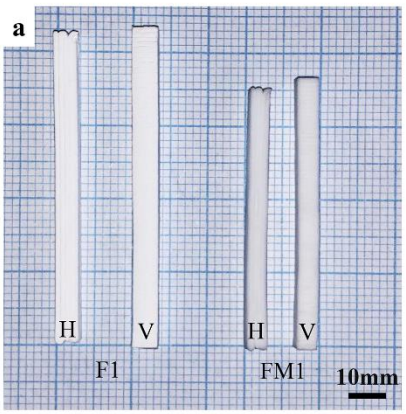

b

	Density (g/cm³)		Relative density (%)	Volume shrinkage (%)
	Green	Sintered		
F1H	1.12±0.01	1.48±0.02	48	57
F1V	1.24±0.03	1.44±0.02	47	51
FM1H	1.15±0.02	2.27±0.07	73	71
FM1V	1.20±0.03	2.21±0.08	71	69

Fig. 9. Specimens for mechanical tests after sintering (1600°C-5h). (a) F1 and FM1, horizontal (H) and vertical (V) layout, (b) Density and volume shrinkage data calculated for green and sintered printed specimens.

The flexural strength was investigated by four-point bending test, and the Weibull distribution was calculated for all four different specimen configurations: horizontally (H) and vertically (V) printed specimens, with or without MgO.

Obviously, the specimens containing 1wt.% MgO had higher bending strength compared to those without MgO (Fig. 10). For the specimens without MgO (F1), the mechanical strength between the vertical and horizontal orientation changed significantly, whereas by using 1wt.% of MgO (FM1), the confidence interval of the horizontal and vertical printed specimens overlapped, and therefore no significant difference could be observed. In general, the mechanical properties of the specimens printed in the vertical orientation were lower than in horizontal orientation. This data can confirm the lower shrinkage and relative density values reported in Fig. 9-b.

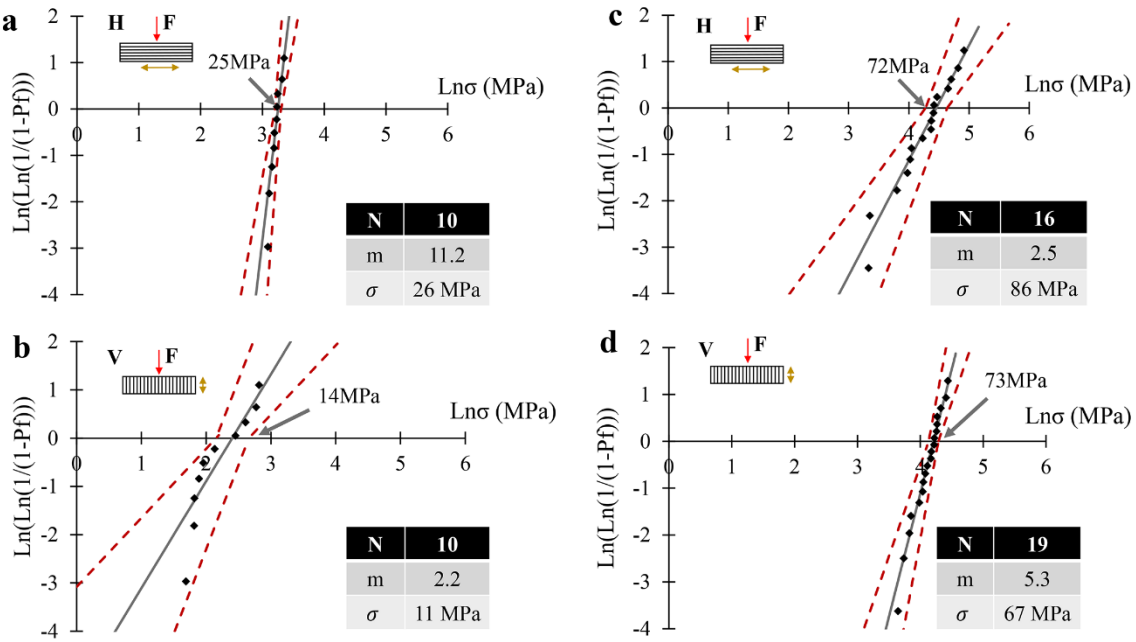

Fig. 10. Weibull distribution of F1 specimens with (a) horizontal and (b) vertical layout and of FM1 specimens with (c) horizontal and (d) vertical layout. N, m and σ represent the number of samples, the Weibull modulus and the average flexural strength value, respectively.

3.3.5. Fractography analysis of FM1 specimens

For fractography analysis, FM1 specimens with the highest mechanical strength were selected, as shown in Fig. 11. The macroporosity was still present in the sintered samples independent of the printing orientations (Fig. 11); however, such structural defects were not present in the green specimens (Fig. 11-a).

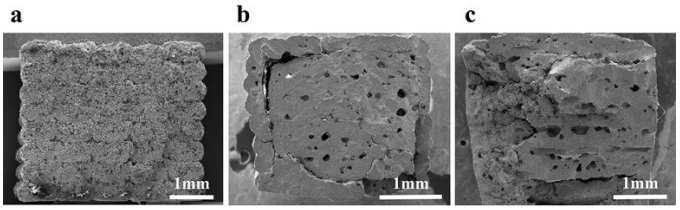

Fig. 11. Fracture surface of (a) green and sintered FM1 specimens (1wt.% MgO) for (b) horizontal and (c) vertical printing orientations.

The thermal debinding process was investigated by changing different parameters like lower heating rates and longer dwell times to avoid the formation of these pores; however, the phenomena of spherical pores formation could not be solved. Finally, we could prove that the formation of spherical pores happens below the onset temperature of the Silres MK (Fig. 12) that conflicts with the findings of Gorjan et al. in 2019 who investigated the degradation of pure

Silres MK and a feedstock based on Silres MK, γ-Al_2O_3 powder and Elvax420 [26]. Regardless of the material combination, an onset temperature of 170°C was identified for thermal degradation by TGA analysis.

We posit that the revealed pores below 170°C are due to the evaporation of water molecules generated by the thermal crosslinking reaction of Silres MK at low temperatures, leading to the condensation of reactive Si-OH groups and release of gas by-products. Indeed, this effect has been exploited for producing SiOC foams through the self-foaming of a similar silicone resin [38]. At temperatures above 73°C, Elvax 420 starts to melt and subsequently will have high plasticity. Therefore, the released gases during the crosslinking are enclosed and forms bubbles instead of cracks. This phenomenon leads to the presence of macro-pores in the microstructure of the final ceramic part. We also observed that the growth of the bubbles depended on the time and temperature the sample was exposed to heat (Fig. 12). Since the decomposition of the Elvax 420 binder starts at higher temperatures (>~240°C [26]), at which the silicone resin has already mostly undergone thermal crosslinking, we don't expect its decomposition gases to contribute significantly. In addition to the bubble formation, core-shell structure in the SEM image (Fig. 11-b) could be related to the debinding process. In fact, gas species formed during the thermal degradation of the polymeric binder and pyrolysis of the preceramic polymer will result in high internal stresses for the specimens and cause crack formation.

To investigate the formation of the spherical pores during the debinding process, lightweight sintering substrate with a honeycomb shape was printed.

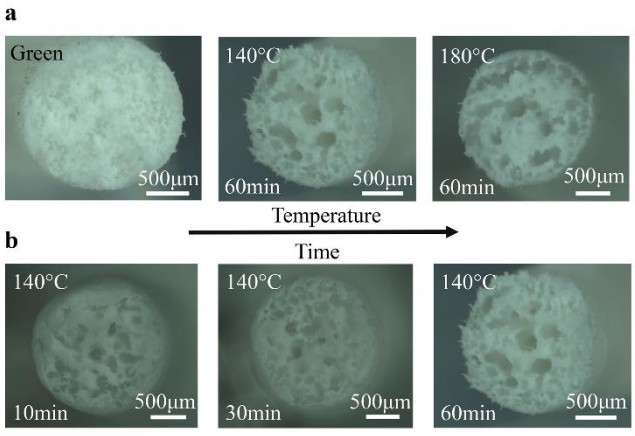

Fig. 12. Optical microscope image for a cross section of FM1 filament in (a) green state and after heat treatment at 140°C and 180°C for 60 minutes, (b) after heat treatment at 140°C for 10, 30 and 60 minutes.

3.3.6. FDM printing of honeycomb structures

A light weight sintering substrates based on a honeycomb structure with a thin bottom layer was printed and sintered (Fig. 13). After the thermal process, the samples retained the shape. As expected, high shrinkage of 37 % and 30 % could be observed for the diameter and the height, respectively.

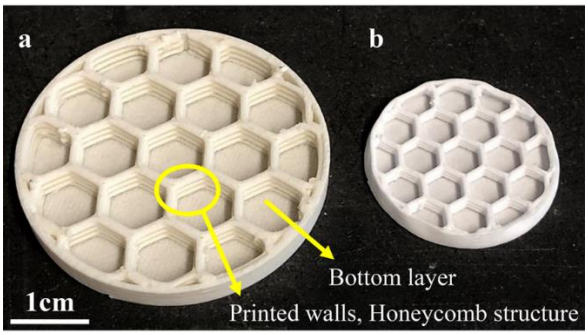

Fig. 13. (a) Green mullite-based lightweight honeycomb substrate with a bottom layer, printed using the FM1 filament, (b) sintered honeycomb substrate at 1600°C for 5h. Size after printing: 50 x 10 mm.

To investigate the microstructure of the mullite-based substrate, the structure was broken by hand and the fracture surface was analyzed. Fig. 14 shows SEM images of a region connecting the bottom layer and the honeycomb wall. As can be seen, the different printed threads and layers were well diffused. However, macro-pores could be detected in the whole structure, attributable to the evaporation of water molecules as explained above. Nevertheless, the pore size was much smaller than the observed ones in individual filaments or flexural test specimens (see Fig. 11 and 12), and only in some areas with larger wall thickness pores with larger diameter could be detected. Summarizing the observed pore structure present in the lightweight honeycomb substrate and the flexural test specimens, we posit that the wall thickness of the structure will affect the size of the spherical pores. Thus, diffusion of the water molecules through the EVA binder is possible; however, printing of structures with large wall thicknesses should be avoided.

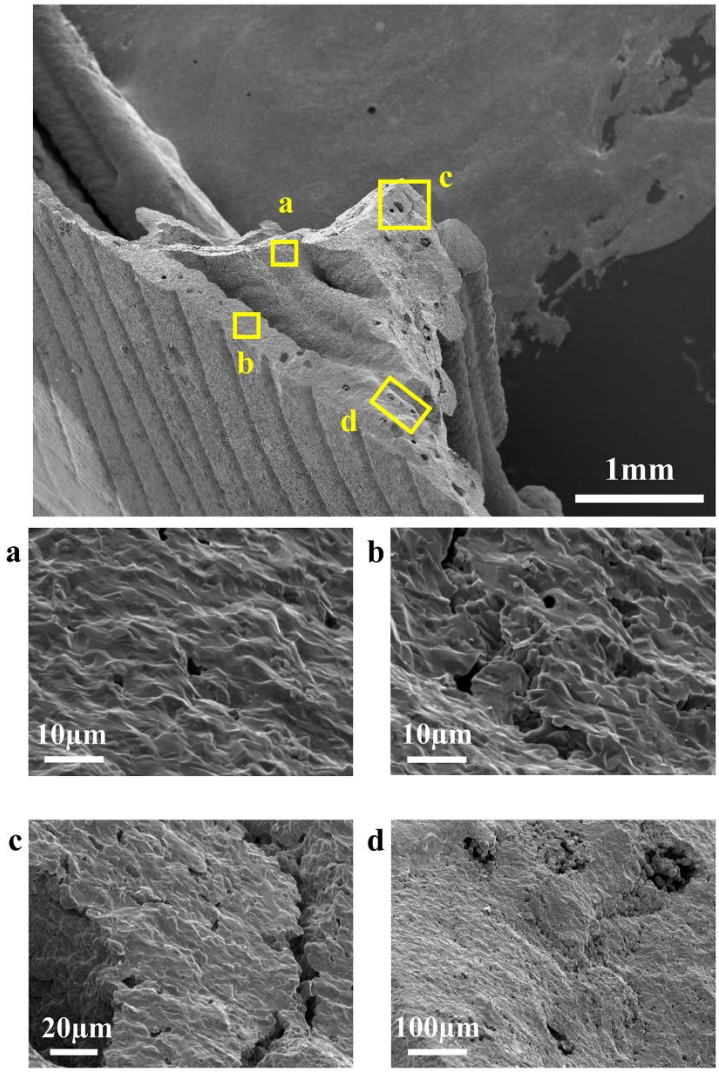

Fig. 14. SEM images of a cross section of the sintered honeycomb substrate, showing the microstructure of both the bottom layer and the honeycomb walls (images taken at different locations).

3.4. Conclusion

In this work, preceramic polymer-based filaments were developed for FDM printing using a combination of a silicone resin and an alumina powder as active filler. Ethylene vinyl acetate was added as thermoplastic binder to promote the plasticity of the material during extrusion through a hot nozzle.

MgO powder was used as a sintering additive to promote the sinterability and densification of the mullite structures, by forming a liquid phase. Using XRD analysis for the samples with different MgO contents, we demonstrated that only a small amount of MgO (0.5wt.%) was sufficient to obtain pure mullite after sintering at 1600°C even with a relatively short dwell time

of 2.5h. However, 1wt.% of MgO was required to achieve a dense microstructure after sintering at 1600°C for 5h.

Although printed samples in horizontal orientation showed a higher green density than the vertical orientation, this effect was neglected after sintering due to higher volume shrinkage. As a result, same sintered density for both orientations was achieved.

Four-point flexural tests were conducted on the specimens with and without 1wt.% MgO additive to investigate the mechanical properties of the samples printed in the horizontal and vertical orientation. Considering the average flexural strength, we can conclude that the samples with 1wt.% MgO had higher values, due to the significant higher densification (e.g. shrinkage) during sintering. Considering the fracture surface of the sintered specimens with 1wt.% MgO, the low relative density values of the specimens could be explained by the presence of the scattered macro-pores. The formation of pores is attributable to the evaporation of water molecules produced by crosslinking reactions of the Si-OH groups present in the silicon resin. This pores are formed because of the limited diffusion of water molecules through the EVA binder component. Based on these results, we can assume that printing of preceramic-based structures with large wall thickness should be avoided.

Acknowledgement

This work was supported by the Swiss National Science Foundation (SNSF) [grant number 200021_184691 / 1].

References

[1] T. Sato, M. Ishizuka, M. Shimada, Sintering and characterization of mullite—Alumina composites, Ceramics international, 12 (1986) 61-65. https://doi.org/10.1016/0272-8842(86)90018-0.

[2] H. Schneider, J. Schreuer, B. Hildmann, Structure and properties of mullite—a review, Journal of the European Ceramic Society, 28 (2008) 329-344. https://doi.org/10.1016/j.jeurceramsoc.2007.03.017.

[3] H. Schneider, E. Eberhard, Thermal expansion of mullite, Journal of the American Ceramic Society, 73 (1990) 2073-2076. https://doi.org/10.1111/j.1151-2916.1990.tb05270.x.

[4] M. Camerucci, G. Urretavizcaya, M. Castro, A. Cavalieri, Electrical properties and thermal expansion of cordierite and cordierite-mullite materials, Journal of the European Ceramic Society, 21 (2001) 2917-2923. https://doi.org/10.1016/S0955-2219(01)00219-9.

[5] H. Schneider, R.X. Fischer, J. Schreuer, Mullite: crystal structure and related properties, Journal of the American Ceramic Society, 98 (2015) 2948-2967. https://doi.org/10.1111/jace.13817.

[6] I.A. Aksay, D.M. Dabbs, M. Sarikaya, Mullite for structural, electronic, and optical applications, Journal of the American Ceramic Society, 74 (1991) 2343-2358. https://doi.org/10.1111/j.1151-2916.1991.tb06768.x.

[7] T. Huang, M.N. Rahaman, T.I. Mah, T.A. Parthasarathay, Anisotropic grain growth and microstructural evolution of dense mullite above 1550 C, Journal of the American Ceramic Society, 83 (2000) 204-210. https://doi.org/10.1111/j.1151-2916.2000.tb01171.x.

[8] K.P. Furlan, T. Krekeler, M. Ritter, R. Blick, G.A. Schneider, K. Nielsch, R. Zierold, R. Janßen, Low-temperature mullite formation in ternary oxide coatings deposited by ALD for high-temperature applications, Advanced Materials Interfaces, 4 (2017) 1700912. https://doi.org/10.1002/admi.201700912.

[9] M. Ismail, H. Tsunatori, Z. Nakai, Preparation of MgO-doped mullite by sol-gel method, powder characteristics and sintering, Journal of materials science, 25 (1990) 2619-2625. https://doi.org/10.1007/BF00638068.

[10] D. Amutharani, F. Gnanam, Low temperature pressureless sintering of sol-gel derived mullite, Materials Science and Engineering: A, 264 (1999) 254-261. https://doi.org/10.1016/S0921-5093(98)01094-6.

[11] M.S. Banu, F. Gnanam, Microstructure and mechanical properties of sol-gel derived mullite containing needle-like grains, Transactions of the Indian Ceramic Society, 61 (2002) 122-124. https://doi.org/10.1080/0371750X.2002.10800045.

[12] (Roy et al. 2015) J. Roy, S. Das, S. Maitra, Solgel-processed mullite coating—a review, International Journal of Applied Ceramic Technology, 12 (2015) E71-E77. https://doi.org/10.1111/ijac.12230.

[13] M. Sanad, M. Rashad, E. Abdel-Aal, M. El-Shahat, Synthesis and characterization of nanocrystalline mullite powders at low annealing temperature using a new technique, Journal of the European Ceramic Society, 32 (2012) 4249-4255. https://doi.org/10.1016/j.jeurceramsoc.2012.07.014.

[14] G.R. Chandran, K. Patil, G. Chandrappa, Combustion synthesis, characterization, sintering and microstructure of mullite-cordierite composites, Journal of materials science letters, 14 (1995) 548-551. https://doi.org/10.1007/BF00275372.

[15] R.P. Mulpuri, V.K. Sarin, Synthesis of mullite coatings by chemical vapor deposition, Journal of materials research, 11 (1996) 1315-1324. https://doi.org/10.1557/JMR.1996.0166.

[16] S. Basu, P. Hou, V. Sarin, Formation of mullite coatings on silicon-based ceramics by chemical vapor deposition, International Journal of Refractory Metals and Hard Materials, 16 (1998) 343-352. https://doi.org/10.1016/S0263-4368(98)00043-2.

[17] V. Sarin, R. Mulpuri, Chemical vapor deposition of mullite coatings, Google Patents, 1998.

[18] M.D. Sacks, N. Bozkurt, G.W. Scheiffele, Fabrication of mullite and mullite-matrix composites by transient viscous sintering of composite powders, Journal of the American Ceramic Society, 74 (1991) 2428-2437. https://doi.org/10.1111/j.1151-2916.1991.tb06780.x.

[19] M. Bartsch, B. Saruhan, M. Schmücker, H. Schneider, Novel low-temperature processing route of dense mullite ceramics by reaction sintering of amorphous SiO2-coated γ-Al2O3 particle nanocomposites, Journal of the American Ceramic Society, 82 (1999) 1388-1392. https://doi.org/10.1111/j.1151-2916.1999.tb01928.x.

[20] E. Bernardo, P. Colombo, E. Pippel, J. Woltersdorf, Novel mullite synthesis based on alumina nanoparticles and a preceramic polymer, Journal of the American Ceramic Society, 89 (2006) 1577-1583. https://doi.org/10.1111/j.1551-2916.2006.00963.x.

[21] F. Griggio, E. Bernardo, P. Colombo, G. Messing, Kinetic studies of mullite synthesis from alumina nanoparticles and a preceramic polymer, Journal of the American Ceramic Society, 91 (2008) 2529-2533. https://doi.org/10.1111/j.1551-2916.2008.02515.x.

[22] P. Greil, Active-filler-controlled pyrolysis of preceramic polymers, Journal of the American Ceramic Society, 78 (1995) 835-848. https://doi.org/10.1111/j.1151-2916.1995.tb08404.x.

[23] D. Suttor, H.J. Kleebe, G. Ziegler, Formation of mullite from filled siloxanes, Journal of the American Ceramic Society, 80 (1997) 2541-2548. https://doi.org/10.1111/j.1151-2916.1997.tb03156.x.

[24] R. Riedel, L. Toma, C. Fasel, G. Miehe, Polymer-derived mullite–SiC-based nanocomposites, Journal of the European Ceramic Society, 29 (2009) 3079-3090. https://doi.org/10.1016/j.jeurceramsoc.2009.05.016.

[25] G. Parcianello, Advanced ceramics from preceramic polymers and fillers, PhD thesis, University of Padua, (2012).

[26] L. Gorjan, R. Tonello, T. Sebastian, P. Colombo, F. Clemens, Fused deposition modeling of mullite structures from a preceramic polymer and γ-alumina, Journal of the European Ceramic Society, 39 (2019) 2463-2471. https://doi.org/10.1016/j.jeurceramsoc.2019.02.032.

[27] J. Schmidt, A.A. Altun, M. Schwentenwein, P. Colombo, Complex mullite structures fabricated via digital light processing of a preceramic polysiloxane with active alumina fillers, Journal of the European Ceramic Society, 39 (2019) 1336-1343. https://doi.org/10.1016/j.jeurceramsoc.2018.11.038.

[28] M.K. Agarwala, A. Bandyopadhyay, R. van Weeren, A. Safari, S.C. Danforth, N.A. Langrana, V.R. Jamalabad, P.J. Whalen, FDC, rapid fabrication of structural components, American Ceramic Society Bulletin, 75 (1996).

[29] Q. Ma, H. Tian, Fabrication and characterization of porous mullite ceramics from pyrolysis of alumina powders filled silicone resin, Journal of Wuhan University of Technology-Mater. Sci. Ed., 28 (2013) 1082-1084. https://doi.org/10.1007/s11595-013-0823-1.

[30] V. Viswabaskaran, F. Gnanam, M. Balasubramanian, Effect of MgO, Y2O3 and boehmite additives on the sintering behaviour of mullite formed from kaolinite-reactive alumina, Journal of Materials Processing Technology, 142 (2003) 275-281. https://doi.org/10.1016/S0924-0136(03)00577-6.

[31] L. Montanaro, C. Perrot, C. Esnouf, G. Thollet, G. Fantozzi, A. Negro, Sintering of industrial mullites in the presence of magnesia as a sintering aid, Journal of the American Ceramic Society, 83 (2000) 189-196. https://doi.org/10.1111/j.1151-2916.2000.tb01169.x.

[32] P.M.d. Souto, R.R. Menezes, R.H.G.A. Kiminami, Evaluation of the Influence of MgO and La2O3 on the Fast Sintering of Mullite, Materials Research, 18 (2015) 42-53. https://doi.org/10.1590/1516-1439.264814.

[33] L. Montanaro, J. Tulliani, C. Perrot, A. Negro, Sintering of industrial mullites, Journal of the European Ceramic Society, 17 (1997) 1715-1723. https://doi.org/10.1016/S0955-2219(97)00043-5.

[34] J. Heiber, F. Clemens, T. Graule, D. Huelsenberg, Fabrication of SiO {sub 2} glass fibres by thermoplastic extrusion, Glass Science and Technology (Frankfurt), 77 (2004).

[35] J. Heiber, F.J. Clemens, T. Graule, D. Hülsenberg, Influence of fibre diameter on the microstructure and the piezoelectric properties of PZT-fibres, Advances in Science and Technology, Trans Tech Publ, (2006) 2459-2463. https://doi.org/10.4028/www.scientific.net/AST.45.2459.

[36] Advanced technical ceramics - Mechanical properties of monolithic ceramics at room temperature - Part 1: Determination of flexural strength; German version EN 843-1:2006, DIN Deutsches Institut für Normung e. V.*DIN German Institute for Standardization, 08 (2008). https://dx.doi.org/10.31030/1457589.

[37] M. Ismail, H. Tsunatori, and Z. Nakai, Preparation of MgO-doped mullite by sol-gel method, powder characteristics and sintering, Journal of materials science, 25.5 (1990) 2619-2625. https://doi.org/10.1007/BF00638068.

[38] J. Zeschky, F. Goetz-Neunhoeffer, J. Neubauer, S.J. Lo, B. Kummer, M. Scheffler, P. Greil, Preceramic polymer derived cellular ceramics, Composites Science and Technology, 63 (2003) 2361-2370. https://doi.org/10.1016/S0266-3538(03)00269-0.

Chapter 4- Crosslinking and pyrolysis of a methyl-silsesquioxane: effect of heating rate and atmosphere

Fateme Sarraf, Amir Hadian, Frank Gfeller, Sergey V. Churakov, Frank Clemens

Final version ready for submission

- This study aims to answer the second research question, "**How to design the thermal post-printing process to control the ceramic yield of PCP materials for silicate based ceramic materials?**", by investigationg the crosslinking and pyrolysis behavior of SILRES MK using different atmospheres and heating rates. TG analysis revealed that SiO_2 yield after pyrolysis in air was influenced by the heating rate, where slower heating rates resulted in lower SiO_2 yield due to the longer time available for volatile species to evaporate and a higher fraction of cage-like POSS molecules escaping the structure. Thermal behavior of MK is important in the context of FDM printing, as a thermal debinding of organics with low heating rates and dwell times is necessary after printing to achieve defect-free ceramic objects. Mixing PCP-based mullite feedstocks below the crosslinking temperature of MK resulted in a SiO_2 deficiency during thermal debinding, while mixing at temperatures above the crosslinking temperature ensured a constant SiO_2 yield of 81% and prevented uncontrolled evaporation of POSS species. XRF results highlighted the importance of crosslinking the PCP-based feedstocks during the mixing step to ensure successful fabrication of polymer-derived ceramics in air atmosphere with a stable SiO_2 yield.

Crosslinking and pyrolysis of a methyl-silsesquioxane: effect of heating rate and atmosphere

Fateme Sarraf, Amir Hadian, Frank Gfeller, Sergey V. Churakov, Frank Clemens

Abstract

Poly-silsesquioxane preceramic polymers (PCPs) have been numerously used to produce SiO_2 or $Si_xO_yC_z$ ceramics through pyrolysis under different atmospheres. Using additive manufacturing (AM) techniques to produce complex polymer derived ceramic structures, a controlled thermal treatment is necessary to gradually remove processing additive (e.g. binders) needed for the shaping process and convert the PCP into a ceramic phase at elevated temperatures, avoiding the occurrence of failures (blisters, pores, and cracks). In this study, crosslinking and pyrolysis behavior of a commercial methyl-silsesquioxane, was examined using different heating rates under air, nitrogen, and argon up to 800°C. Thermogravimetry analysis (TG) revealed that yield of methyl-silsesquioxane after pyrolysis is only influenced under air atmosphere and was reduced to 69.1 and 75.0% using 0.3 and 0.6K/min heating rates, respectively. Furthermore, a stoichiometric mixture of SILRES® MK and γ-Al_2O_3 was prepared to produce a mullite composition with 60/ 40 wt% Al_2O_3/ SiO_2 ratio. The stoichiometric ratio of alumina to silica was altered using low heating rates and mullite ceramics with 61.70/37.70 wt% of Al_2O_3/ SiO_2 were obtained based on XRF analysis.

Keywords: Preceramic polymers, methyl-silsesquioxane, Polyoctahedral silsesquioxanes (POSS), Silicate, Fused deposition modeling

4.1. Introduction

Use of molecular precursors to produce ceramic structures was first introduced by the studies of Ainger and Herbert in 1960 [1]. Synthesis of SiC ceramics from polycarbosilane published by Yajima et al. in 1975 initiated a major advance in the field of polymer pyrolysis to produce polymer derived ceramics (PDCs) [2]. Since then, numerous research studies have been conducted on the fabrication of amorphous or nanocrystalline PDCs, particularly non-oxide ceramics such as SiC [3], Si_3N_4 [4], SiCN [5], SiOC [6]. While most of the publications focus on synthesis of non-oxide ceramics using an inert atmosphere, there are several reports on synthesizing silicate and oxynitride ceramics including mullite [7], wollastonite [8], zircon [9], cordierite [10], SiAlONs [11], and more [12]. Although a wide variety of materials has been synthesized using preceramic polymers, researcher have mainly focused on fabrication of coatings [13-15], thin structures [16], foams and porous structures [17-19]. The reason is that the intensive release of gaseous byproducts during crosslinking and pyrolysis and high shrinkage of the these polymers during transformation into ceramics can cause cracks, blisters, or bubbles when larger parts are processed [20].

To avoid crack formation by controlling the shrinkage during pyrolysis, Greil in 1995 introduced addition of non-volatile fillers, including metal and ceramic particles and reduced the shrinkage to a great extent [21]. To solve the issue of cracks, blisters and bubbles, Sarraf et al. developed a partially water soluble binder system to provide interconnected open porous network for the removal of gaseous products [22]. The presence of cracks initiated by gas release during pyrolysis is also influenced by the heating rate. Therefore, applying a suitable heating program for pyrolysis of the preceramic polymer (PCP) with relatively low heating rates (e.g. 2K/min or less) is of great importance for larger parts (around a few mm^3) as gradual release of gases during ceramization step is favorable [23].

For shaping complex PDC parts, different additive manufacturing (AM) methods including UV-assisted AM, laser assisted and extrusion based AM methods have been used; Processes like stereolithography [24, 25], digital light processing (DLP) [26] [27], selective laser sintering [28, 29], direct ink writing (DIW) [30, 31] and material extrusion based additive manufacturing (MEX-AM) [16]. Among the used AM methods, material extrusion based additive manufacturing (MEX-AM), previously called fused deposition modeling (FDM), fused filament fabrication (FFF) or fused deposition of ceramics (FDC), has been used for shaping pure preceramic polymers or their mixtures with fillers because they often show thermoplastic properties before crosslinking and have low processing temperatures that make it desirable for

MEX-AM [16, 32-36]. Mei et al. in 2019 successfully fabricated SiOC honeycomb structures using a commercial methyl-silsesquioxane resin, known as SILRES MK, with zinc acetylacetonate hydrate serving as the crosslinking catalyst under an argon atmosphere [35]. Carbon fibers were incorporated as the reinforcing component, while PLA was utilized as the thermoplastic binder to create a printable filament. Additionally, Silres MK was directly printed using a screw extruder, by melting the powder to flow through a nozzle and print complex structures. The samples were printed at 210°C, followed by a crosslinking step at 150°C for 2 hours. Amorphous SiOC structures were obtained by heating samples up to 1100°C under argon atmosphere. Gorjan et al. in 2019 combined SILRES MK resin and an ethylene vinyl acetate polymer to achieve the plasticity needed for the MEX-AM process [16]. Adding an alumina source with a stoichiometric ratio of 3:2 between Al_2O_3 and SiO_2, a 3:2 mullite phase was reached after sintering at 1550°C in air. Hollow struts made of SiOC were produced by Kulkarni et al. in 2020 through the pyrolysis of impregnated 3D-printed PLA structures with a liquid polysiloxane [34]. The pyrolysis process involved heating the printed structures up to 1200°C with a heating rate of 10K/min under a nitrogen atmosphere. Three-dimensional β-SiC ceramics were fabricated by Zhao et al. in 2021 using a polycarbosilane precursor [32]. To achieve sufficient thermoplastic behavior for printing, a polypropylene binder was utilized. After printing the feedstock below 300°C, samples went through an oxidative crosslinking at 200°C, using a heating rate of 2K/min. Subsequently, the samples were pyrolyzed for 2h at 1200°C under an argon atmosphere. XRD analysis of the final structures, exhibited the formation of β-SiC ceramics with an amorphous SiO_xC_y content. Furthermore, Chawich et al. in 2022 conducted a study where SiCN and SiC cellular ceramic structures were produced using PolyVinylSilazane (PVZ) and AllylHydridoPolyCarboSilane (AHPCS) in combination with DiCumyl Peroxide (DCP) as a crosslinking agent [33]. Initially, PLA molds were created using a filament printer. Subsequently, these printed molds were subjected to a dip coating process, where they were coated six times with mixtures of PVZ/DCP or AHPCS/DCP. The impregnated molds were then pyrolyzed at 1000°C for 2 hours, with a heating rate of 2K/min under nitrogen and argon atmosphere to obtain amorphous SiCN and SiC ceramics, respectively.

The study from Tian et al. in 2012 demonstrated that pore size and porosity of polymer derived foams can be tailored by changing the heating rate below crosslinking temperature [37]. To obtain SiOC ceramics, a commercial silicone resin was crosslinked by heating up to 250°C with different heating rates (0.25-3K/min) in air and pyrolyzed up to 1200°C with a heating rate of 5K/min in Ar atmosphere. Total porosity of the foam increased below heating rate of 1K/min with a maximum of 88.2% with a heating rate of 0.5K/min. Colombo et al. in 2010 reported

that the composition and microstructure of the ceramic are influenced by thermal treatment parameters like heating rate, dwell temperatures, and dwell times [23]. This aspect is of significant importance as precise stoichiometric ratios of oxides, particularly in the synthesis of polymer derived silicate ceramics, are crucial based on the studies by Bernardo et al. in 2006 [38] and Gorjan et al. in 2019 [16].

Although synthesis and fabrication of various PDCs powders and parts have been investigated under different atmospheres using various thermal programs, there is no literature on comparing the pyrolysis behavior under air and inert atmospheres and the effect of the heating rate on crosslinking and pyrolysis behavior to the best of our knowledge. Therefore, in this study, we investigated the effect of thermal treatment conditions on the yielded SiO_2 of a commercial methyl-silsesquioxane preceramic polymer under three different atmospheres (air, nitrogen and argon) up to 800°C. Looking at the crosslinking and pyrolysis of PCP, complementary techniques such as thermogravimetric analysis (TG), gas chromatography-mass spectrometry (GC-MS) and fourier transformed infrared spectroscopy (FT-IR) were employed. Subsequently, the effect of the SiO_2 yield on composition stoichiometry of a silicate system was studied. The formed mullite phase was investigated using X-ray fluorescence (XRF) and X-ray diffraction (XRD) analyses, based on the yielded SiO_2 content achieved by different debinding and pyrolysis conditions and a constant amount of alumina.

4.2. Material and methods

4.2.1. Materials

A commercial polysilsesquioxane resin powder, SILRES® MK (abbreviated MK , Wacker–Chemie GmbH, Germany), containing methyl groups, was used. According to the manufacturer, approximately 82 wt% SiO_2 content after pyrolysis at 1000°C in air was expected. MK contains functional OH groups that enables it to undergo thermal crosslinking via polycondensation reactions [39, 40].

In order to achieve a SiO_2-rich mullite phase, 40 vol% of powder consisting of 30.4 wt% of alumina powder (γ-Al_2O_3-PURALOX SCFa-140 UF3, Sasol Performance Chemicals Ltd) and 24.1 wt% of MK were mixed with 60 vol% of thermoplastic binder. The thermoplastic binder contained 50 vol% polyvinyl alcohol (PVA, Sigma-Aldrich) and 50 vol% ethylene vinyl acetate copolymers (Elvax, DuPont, International SARL). To improve the sinterability of the mullite phase, 1 wt% of magnesium oxide (MgO, Fluka™) was added to the mixture. The mixture

composition is described in more detail elsewhere [22]. Initially the binder components were melted in the the chamber of a torque rheometer equipped with roller-rotors mixing elements (Rheomix 600, HAAKE™ PolyLab™ OS, Thermo Fisher Scientific, Germany). Then, dry powders were gradually added to the mixing chamber. MK starts thermal crosslinking at temperatures above 160°C [41]; therefore, two different batches were mixed at 160°C and 190°C and torque versus time plots were recorded for comparison. In this way, the effect of crosslinking prior to heat-treatment on the yield of the SiO_2 and the obtained mullite stoichiometry using different heating rates could be investigated. Mixed feedstocks at 160°C and 190°C were extruded at 150°C and 160°C, respectively, in the form of rods with a capillary rheometer (Rosand RH10, NETZSCH-Gerätebau GmbH, Germany). Binder removal occurred in two steps including solvent and thermal debinding; First PVA was removed by immersing the rods in a water bath [22] followed by wick debinding of the remained binder at 210°C for 48h in a box furnace (Pyrotec PC 12, Michel Keramikbedarf, Switzerland). Then, rods were heated up to 800°C to remove all the binder and paralyze MK with two different heating rates (0.6 and 20K/min). Finally, sintering was carried out at 1700°C for 5 hours in a furnace equipped with $MoSi_2$ heating elements (LHT 03/17 D, Nabertherm GmbH) to ensure the full transformation to mullite. To compare, rods were thermally debound, pyrolyzed and sintered without a wick debinding step.

4.2.2. Characterization

To investigate the effect of the heating rate and the atmosphere on the yield of SiO_2, MK was heated to 800°C in different atmospheres. Thermal analysis of MK was performed using a constant amount of powder heat-treated under air, argon (Ar) and nitrogen (N_2) atmosphere by DTA/TGA instrument (STA 449 F3 Jupiter, Netzsch GmbH, Germany) with a constant gas flow of 70 ml/min and different heating rates, namely 0.3, 0.6, 2, 5, 10 and 20K/min.

To characterize the exhaust gases from the pyrolysis of MK, a transfer line at 250°C was used to carry the pyrolysis products of MK heated to 800°C with a rate of 20K/min to a combined gas chromatograph and mass spectrometer (GC 7890 B-MS5977 B, Agilent, USA), called GC-MS instrument. Two configurations were used for these studies. First, gaseous species were collected in 20°C intervals and frozen in a cryogenic trap at temperature of -150°C before the inlet of the GC column. At the end of the TG analysis, the cryogenic trap was heated and the GC-MS analysis was performed. The gaseous species were separated by a fused silica capillary column (HP 5ms UI, Agilent, USA) coated with (5%-phenyl)-methylpolysiloxane stationary phase under a programming temperature condition; 35°C (2 min hold) – (10 K/ min) – 300°C

(20 min hold). Gas species with $33<M_w<550$ were identified with the MS unit. In the second configuration, the pyrolysis products were transferred directly to the MS using a bypass line to investigate the actual temperature of released gaseous species. The NIST mass spectral search program was used to analyze the data.

To understand the bond characteristics of MK resin, as received, after crosslinking and pyrolysis, Fourier-transformed infrared spectroscopy (FT-IR) spectroscopy measurements were performed at room temperature with Tensor 27 (Bruker, country) equipped with a diamond attenuated total reflectance (ATR). Optical transmission data were collected from 600 to 1800 cm^{-1} with a resolution of 4 cm^{-1} and with 32 scans.

Using a rotational rheometer (MCR 302, Anton Paar, Austria), the rheological behavior of pure MK powder was investigated at the mixing temperature of the feedstocks (160 and 190°C) to confirm if crosslinking of MK already happened in these temperatures. Measurements were performed with a plate-plate system at a constant shear rate of $1s^{-1}$.

X-ray diffraction (XRD) analysis of sintered mullite powders was performed using a PANalytical EMPYREAN diffractometer (Institute of Geological Sciences, University of Bern) equipped with a Cu X-ray source (45 kV/40 mA) and a 1 Der detector. Fixed divergence slit of 0.25° and 0.02 radian soller slits were used. Measurements were carried out betweem 2Θ of 5-90° with a step size of 0.0167°/step at 120 s/step. Lattice parameters were derived from Pawley refinements to accurately extract peak maxima by treating the data independently of the structural model. The software TOPAS-Academic V6 was used for all refinements.

Using X-Ray Fluorescence (XRF), chemical mass analysis of mullite powders were obtained to quantify each oxide content. Fused beads were prepared from a 1:10 sample:flux mixture. The flux used was "Claisse Borate Flux" from Malvern PANalytical with 66.67% $Li_2B_4O_7$, 32.87% $LiBO_2$ and 0.5% LiI. The PANalytical Zetium wavelength dispersive XRF spectrometer (Department of Geosciences, University of Fribourg) was used for bulk chemical analysis. The instrument calibration is based on the PANalytical WROXY software application. The XRF analytical procedure employing WROXI software was established using sets of PANanalytical materials based on 200 international Certified Reference Materials (CRM's).

4.3. Results and discussion

4.3.1. Thermogravimetry analysis of MK

At the beginning of this study, we investigated the SiO_2 yield of the MK preceramic polymer by simultaneous thermal analysis (STA) using different heating rates and atmospheres. As can

be seen in Fig. 1, MK yielded the same amount of SiO_2 after heating up to 800°C using different heating rates under nitrogen and argon atmosphere. A constant yield of 82.0 wt% was obtained which confirms the reported yield by the manufacturer. The observations are in good agreement with the reported values by Ma et al., where they studied the pyrolysis of VTES (vinyltriethoxysilane)/ TEOS (tetraethoxysilane) system with different heating rates under argon atmosphere to achieve SiOC aerogels, obtaining a stable SiOC yield [42].

Pyrolysis under air atmosphere, however, resulted in an unexpectedly higher mass loss when a heating rate below 2K/min was used. A SiO_2 residue of 69.1 wt% and 75.0 wt% was achieved using 0.3 and 0.6K/min heating rates, respectively. The occurrence of such low yield means that the lower the heating rate, the higher the chance to evaporate unlinked low molecular weight symmetric species before any crosslinking (polycondensation reactions) occurs. Tian et al. [37] observed an effect of heating rate up to crosslinking temperature (250°C) in air atmosphere and were able to fabricate preceramic foams with different pore sizes and porosity. Although they did not investigate the change of mass loss with heating rate, it was shown that by decreasing the heating rate from 3 to 0.5 K/min, higher porosity and higher pore sizes were achieved due to the higher release of volatiles.

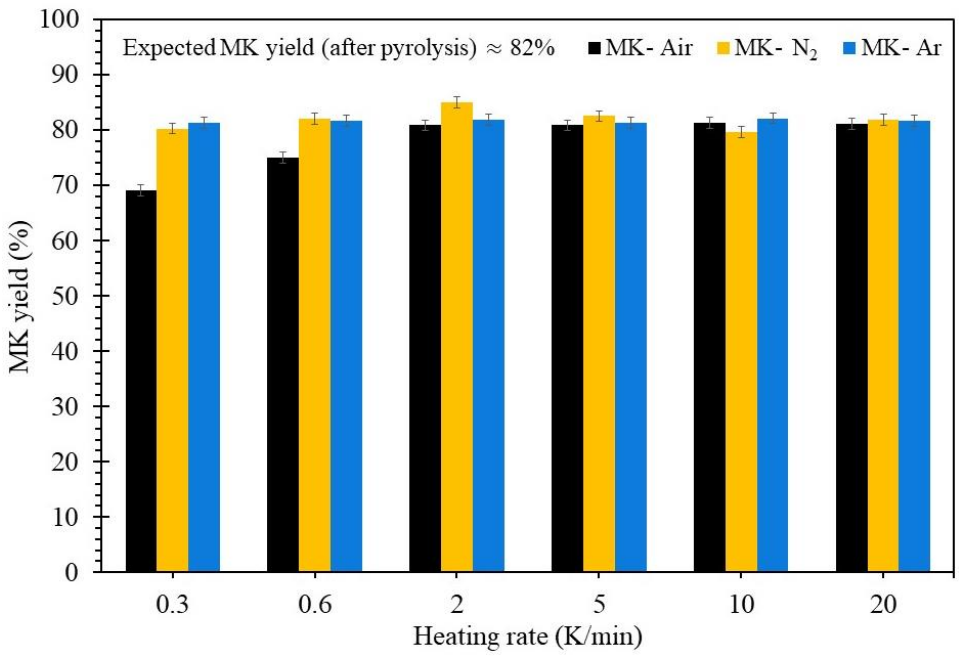

Fig. 1. Yield of MK preceramic polymer heated to 800°C with heating rates, between 0.3 and 20K/min, under three different atmospheres (air, N_2, Ar).

To make silicate ceramics by PCP route, typically debinding and sintering in air is used;

therefore, a non-stoichiometric composition of the silicate ceramic can be expected using low heating rates or dwell times at critical temperatures during the thermal debinding, typically used in MEX-AM process.

To explore this phenomenon further, additional investigations were conducted into the pyrolysis of MK in air atmosphere. As shown in Fig. 2, the thermal evolution of MK occurs in two steps corresponding to its crosslinking (polycondensation reactions) and pyrolysis (ceramization). For comparison, only two heating rates, namely 0.6 and 20K/min, were chosen to demonstrate the dependence of the SiO_2 yield on the heating rate after heat treatment up to 800°C. Crosslinking with 0.6K/min occurred at a temperature range between 100°C and 250°C, whereas for a heating rate of 20K/min, the crosslinking continued up to higher temperatures (100-305°C). A second mass loss appeared in the range of 310-440°C and 400-590°C for the heating rate of 0.6 K/min and 20K/min, respectively. In steps 1 and 2, the MK sample heat treated with a rate of 0.6K/min, released 2.2 and 3.8 % more volatiles in comparison to the heat treatment with 20k/min, respectively.

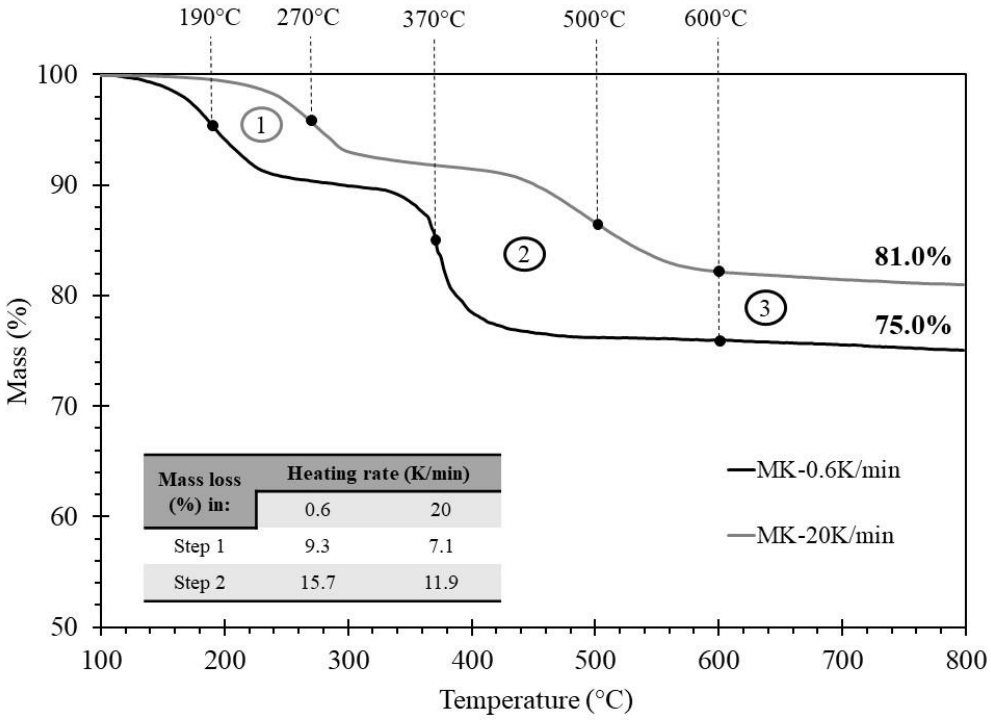

Fig. 2. TG analysis of MK heated up to 800°C with a heating rate of 0.6 K/min and 20K/min under air.

4.3.2. GC-MS analysis of MK up to 800°C

To investigate the gaseous species released during the crosslinking and pyrolysis steps and determine the underlying causes for the unstable SiO_2 yield during PCP processing in air atmosphere, gas chromatography/mass spectrometry (GC-MS) equipment was used. The MK was heated up to 800°C and the gases were collected between 100 to 800°C. Cryo-trap setup was used to collect the gas species during thermal treatment. As shown in GC-MS analysis in Fig. 3a, two sets of peaks could be detected at low (i.e. 1-5 minutes) and high (i.e. 12-20 minutes) retention times. The peaks appearing at lower retention times belonged to low molecular weight gas species with higher polarity. Due to the application of a non-polar stationary phase in GC, these high polarity species were released earlier. In Table 1, the identified gas molecules associated with lower retention times included mainly carbon dioxide (CO_2), acetaldehyde (C_2H_4O), ethanol (C_2H_6O) and acetone (C_3H_6O). The peaks appeared at high retention times corresponded to the POSS (Polyhedral Oligomeric Silsesquioxane) molecules with a general chemical formula of $(RSiO_{1.5})_n$ (where n=4, 6, 8, 10, and 12, and in most cases 8) [43]. Our setup was unable to detect species with molecular weights below 32 (to avoid oxygen background in the chromatogram); therefore, release of other species such as hydrogen, methane, and water that is mentioned in the literature [41] [44], could not be identified in our experiments.

In addition to the GC-MS analysis using a cryo-trap, a bypass was used to detect the temperature ranges at which selected gas species are evolving. Specific m/z values of 15, 18, 31, 44 and 521 corresponding to methane, water, ethanol, carbon dioxide and octamethyl-T8 ($C_8H_{24}O_{12}Si_8$, a POSS molecule with Mw=536) were selected to monitor the crosslinking and the conversion step to amorphous SiO_2 ceramic with a heating rate of 20K/min up to 600°C (Fig. 3b). Based on Fig. 3b, release of methane, water, ethanol, carbon dioxide and POSS was observed during the first step of mass loss up to 300°C. In the second step, the removal of mainly water and carbon dioxide were continued.

According to Lonescu et al., crosslinking due to polycondensation reactions occurred between 170 and 370°C under argon atmosphere [44]. In our experiments, however, this step finished earlier as we used air instead of argon atmosphere, which can be explained by additional thermal oxidation processes. Moreover, release of POSS molecules was reported in both steps. On the contrary, based on our findings, it is apparent that the evaporation of low molecular POSS primarily occurs during the crosslinking process when exposed to air atmosphere. Looking at the mass loss in Fig. 2, we can conclude that if the time of the second step increases due to a

lower heating rate, volatile species have more time to disappear and this will result in a higher mass loss.

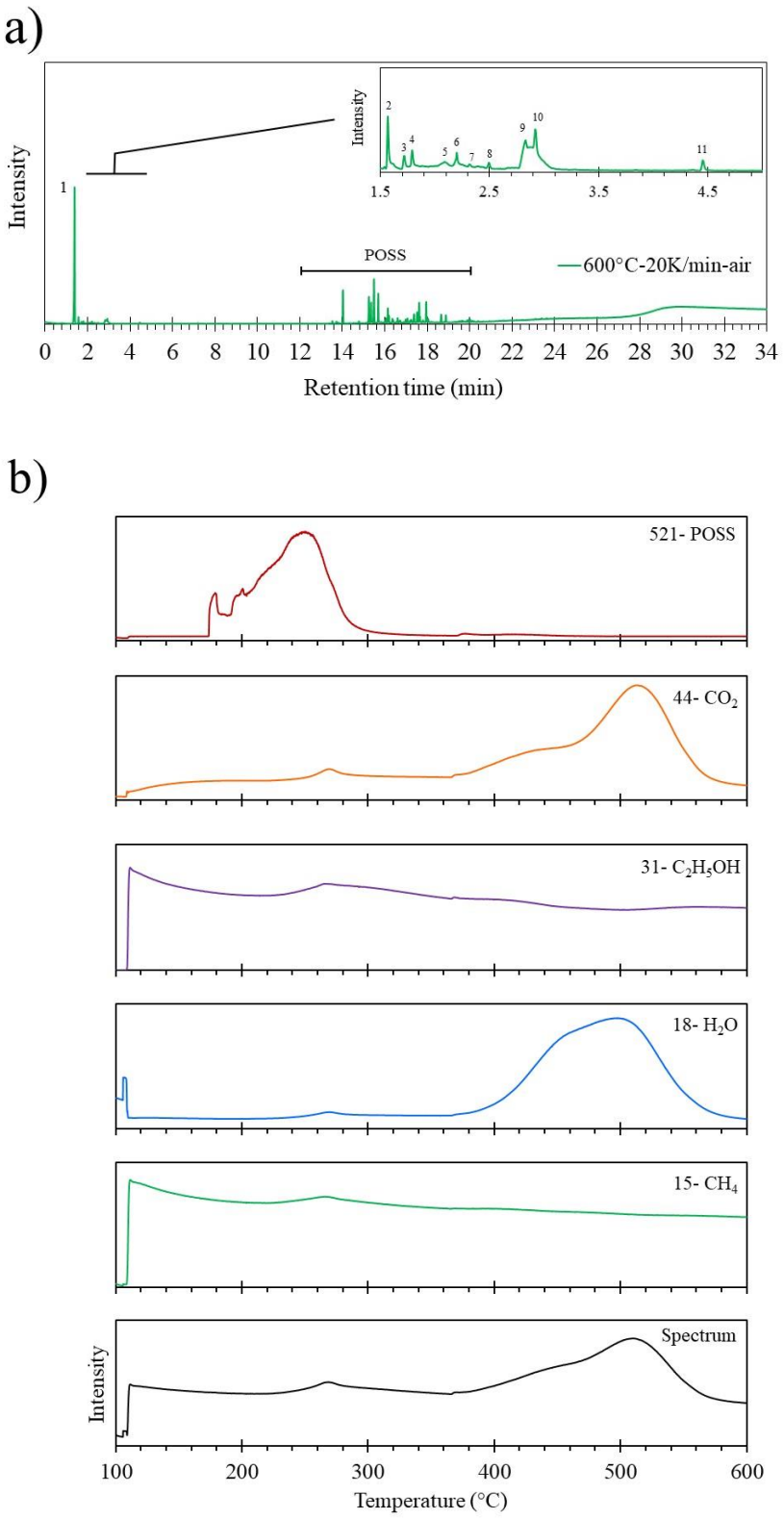

Fig. 3. a) GC-MS chromatograms from MK heated with a rate of 20K/min up to 800°, b) bypass measurement of MK up to 600°C with a heating rate of 20K/min for specific m/z gas molecules.

Table 1. Identified peaks with retention time between 1 and 5 minutes.

Peak No.	1	2	3,5	4	6,7	8	9	10	11
Compound	CO_2	C_2H_4O	C_2H_6O	C_3H_6O	$C_6H_8N_2O_8$	-	$C_4H_{10}O_3$	C_6H_6	C_7H_8
Mw	44	44	46	58	236	?	106	78	92

A schematic chemical structure of MK resin including Si-O-Si cages along with hydroxyl (–OH), methoxy (–CH_3O) and $SiCH_3O$ groups is presented in Fig. 4a. As highlighted in this figure, water, ethanol and POSS molecules can potentially be released from the chemical structure. The $SiCH_3O$ groups are responsible for the SiO_2 yield of MK after pyrolysis in air. The POSS molecules containing Si-O-Si bonds can be present in unstable form of cages or crosslinked dense networks as shown in Fig. 4b. By heating MK, these bonds split, the cages collapse, and dense Si–O–Si network structures start to appear [45]. Based on our results, we assume that using a lower heating rate, the volatile Si-O-Si cage structures have more time to evaporate before crosslinking is completed which will result in a higher mass loss.

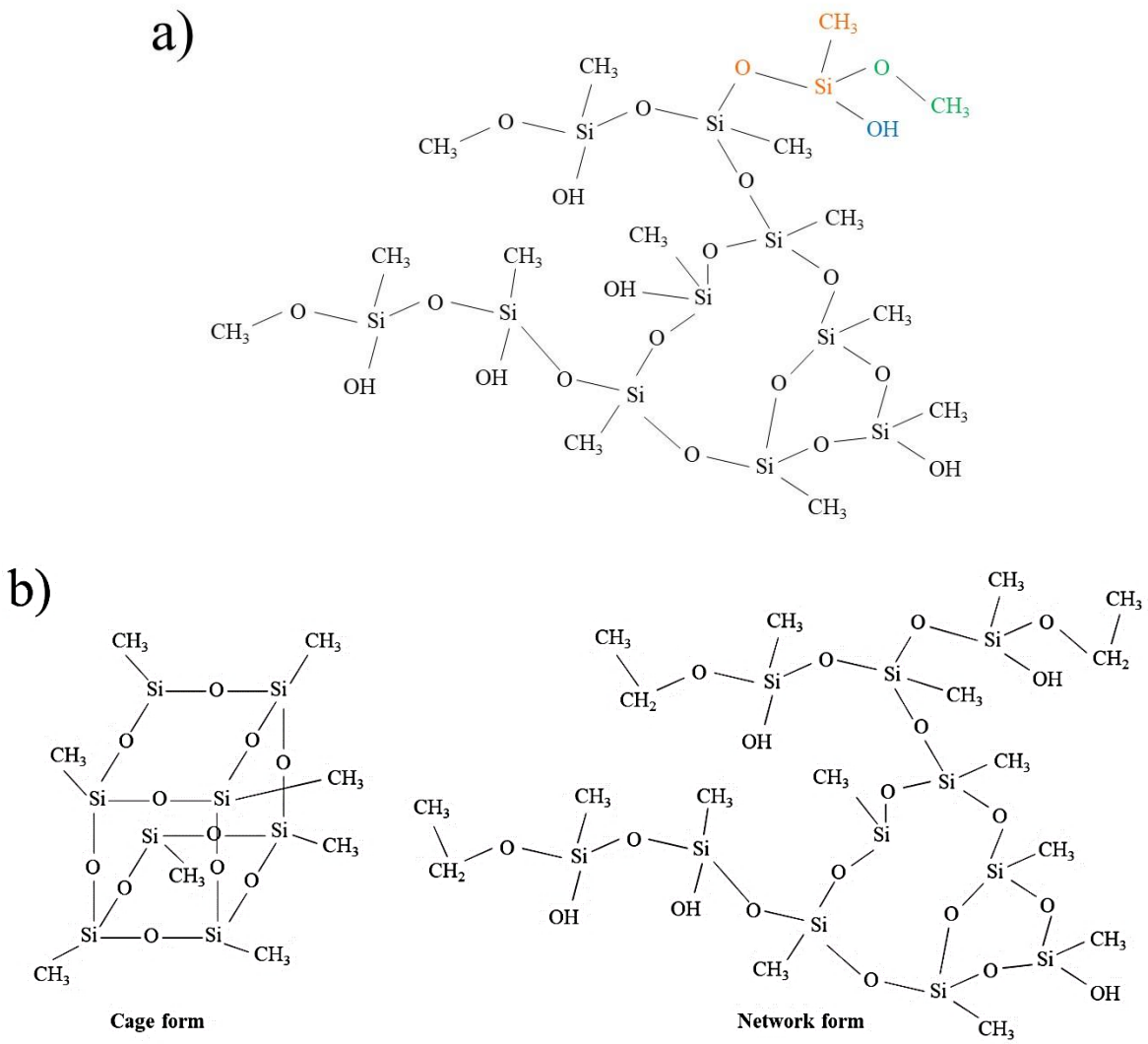

Fig. 4. a) schematic molecular structure of MK resin indicating different species removed by heating up to 800°C, b) Methyl-silsesquioxane (abbreviated MSQ, R=CH_3) in form of cage (T8 structure) and network (based on [46]).

4.3.3. FTIR of selected MK samples

Based on the GC-MS analysis of pure MK up to 800°C in air atmosphere, release of POSS molecules was detected. In order to understand the transition from volatile POSS with Si-O-Si cage structures to stable Si-O-Si network, which determines the SiO_2 yield after pyrolysis, the characteristic bonds of MK were analyzed by FTIR at different stages of heat treatment, using heating rates of 0.6 and 20K/min. To investigate the right temperatures for this study, DTG plots from TG analyses in Fig. 2 were utilized, and the temperature corresponding to the DTG peak at each step of mass evolution was selected for both heating rates (0.6 and 20K/min). Two DTG peaks are expected for each heating rate which indicate the maximum mass loss rate during crosslinking and pyrolysis steps. Accordingly, 190 and 270°C as representatives of crosslinking (step 1) and 370 and 500°C as representatives of the pyrolysis (step 2) were chosen

for heating rates of 0.6 and 20K/min, respectively, to be further investigated. Also, a sample at 600°C was analyzed for both heating rates after pyrolysis. Selected samples are presented in Table 2.

Table 2. Selected samples for FTIR analysis.

	Before heat treatment	Step 1 (Crosslinking)		Step 2 (Pyrolysis)		Finished pyrolysis	
Sample code (TXHY)	Raw MK	T190H0.6	T270H20	T370H0.6	T500H20	T600H0.6	T600H20
Temperature (T)- [°C]	-	190	270	370	500	600	600
Heating rate (H)- [K/min]	-	0.6	20	0.6	20	0.6	20
Mass loss (%)	-	4.6	4.3	14.5	13.4	24.1	17.8

X is the mixing temperature in °C

Y is the heating rate for the thermal debinding in K/min)

FTIR analysis of raw MK can be seen in Fig. 5a. Si–CH_3, O-Si-CH_3 , Si–O–C, δ-CH_3 and Si–O–Si transmission bands were identified as characteristic signals of polymethylsilsesquioxes in the polymeric state [41, 47]. A combination of Si-O-Si bonds in form of cages (ν_{cage} = 1095cm^{-1}) and network (ν_{net} = 1010, 1060 cm^{-1}) existed in raw MK before crosslinking step [45, 48]. Samples T190H0.6 and T270H20 were used to investigate the atomic bonds after crosslinking and same transmission bands were observed for both samples as in raw MK (Fig. 5a). Raising the temperature to 370°C and 500°C with heating rates of 0.6 and 20K/min respectively, noticeable changes in the transmission bands of T370H0.6 and T500H20 were detected (Fig. 5b). As can be seen in regions I and II, Si–CH_3 bonds still existed in sample T370H0.6; furthermore, a second peak around 795cm^{-1} attributed to two different bonds, namely Si-C and Si-O-Si [49, 50]. In comparison, for sample T500H20 only the peak at 795 cm^{-1} was observed. Additionally, there was no evidence of Si–CH_3 bonds after pyrolysis (T=600°C) regardless of heating rate and only the peak at 795 cm^{-1} persisted. Also, C=O bond, already formed at 370 and 500°C, was present in both samples. After the pyrolysis, broad peaks in the range of 960-1125 cm^{-1}, interestingly shifted in different directions. In sample T600H0.6, Si-O-Si bond in form of cages seemed to be more prevalent. However, Si-O-C network bond appeared as the dominant feature in sample T600H20.

As shown in Fig. 5a, a combination of Si-O-Si bonds in form of cages and network existed in raw MK. In addition, detected Si-CH_3 bonds in FTIR analysis of raw MK indicated the presence of unstable low molecular POSS species in form of cages inside the polymer [48]. Both Si-O-Si bond types could still be detected in samples T190H0.6 and T270H20 which showed transformation to a dense Si-O-Si network was not yet completed after crosslinking. Looking at sample T500H20 in Fig. 5b, a significant amount of Si-O-Si network was already formed at 500°C as Si-SH_3 Bonds disappeared. In contrast, due to remained Si-CH_3 Bonds in sample T370H0.6, we assume that evaporation of POSS species continues up to 600°C using heating rate of 0.6K/min. The wide peak around 785-810 cm^{-1} appeared in both samples is linked to the combined effect of the Si-C and Si-O vibrations bonds formed during the pyrolysis step. The CH_3 bond, which corresponds to the outgassing of ethanol, vanished in both samples T370H0.6 and T500H20 which means no more release of ethanol is expected. C=O bond was formed at 1622 cm^{-1} in both samples indicating the release of carbon dioxide. This finding is in a good agreement with the GC-MS bypass analysis (Fig. 3b). Based on the observations in Fig. 5c, we conclude that POSS species in cage form are partially released during the crosslinking step and the remained fraction is stabilized as network Si-O-Si bonds using a heating rate of 20K/min.

By the FTIR results, it can be assumed that heating with a rate of 0.6K/min in air atmosphere resulted in an excessive release of cage POSS species happens during the crosslinking as volatile unstable molecules have more chance to evaporate before stabilizing as network which is consistent with a lower yield for MK-0.6K/min in Fig. 2.

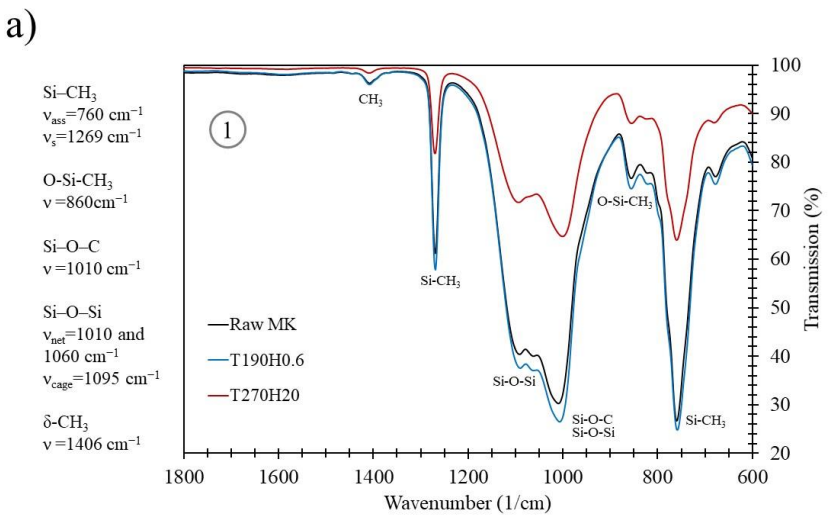

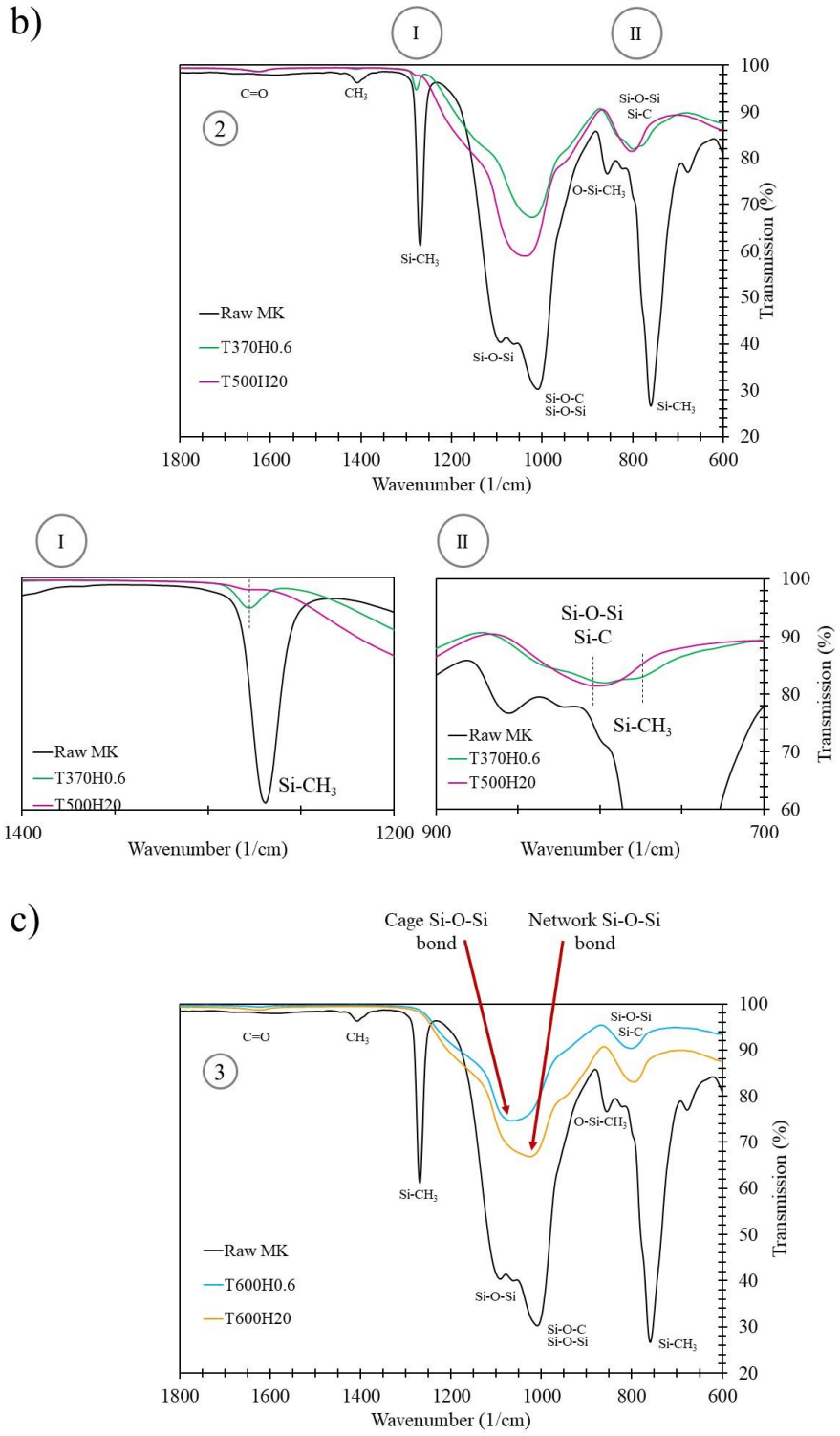

Fig. 5. FTIR analysis of raw MK compared with a sample after heat treatment at a) 190 and 270°C, b) 370 and 500°C, and c) 600°C with a heating rate of 0.6 and 20K/min, respectively.

4.3.4. Processing of polymer derived mullite ceramics

The results obtained from GC-MS and FTIR analysis on MK resin shows when the material is subjected to a low heating rate of 0.6K/min in air, the structure of the resin retains volatile Si-O-Si bonds resulted in a lower amount of SiO_2.

To prove the effect of this phenomenon on the processing of polymer derived mulilite ceramic, a SiO_2-rich mullite ceramic was investigated using material extrusion based additive manufacturing (MEX-AM) method, because a slow debinding process is needed to remove organic binder (e.g. thermoplastics) during their thermal treatment. Typically, low heating rates (below 1K/min) and appropriate dwell times are common to ensure the stability of printed structures up to sintering step. Fig. S1 (appendices) provides an example of a debinding program for MEX-AM of PDCs. Consequently, the fabrication of silicate ceramics that require precise stoichiometric ratios can be challenging.

In order to determine the effect of the heating rate on SiO_2-rich mullite ceramic, a composition of 40 wt% $SiO_2$and 60 wt% Al_2O_3 was investigated. Mullite feedstocks were mixed at two different temperatures, namely 160°C and 190°C. Torque data over time were recorded for both feedstocks (Fig. 6a,b). By mixing at 160°C, the torque slightly increased and a torque of ~13Nm was achieved after 50 minutes (Fig. 6a). At a mixing temperature of 190°C, the behavior of the sample was distinct. Initially, the torque steadily rose to approximately 16 Nm within 60 minutes. Subsequently, the torque gradually diminished and stabilized around 14 Nm after 80 minutes (Fig. 6b).

It was assumed that the increase in torque was caused by the thermal crosslinking of MK; therefore, the viscosity of MK resin was measured under constant shear rate of 1 1/s by parallel plate configuration at 160 and 190°C (Fig. 6c). MK showed a stable viscosity at 160°C over a period of 20 minutes. Viscosity at 190°C, however, started increasing already after 5 minutes. These measurements confirm the findings of Harshe et al., who observed a similar absence of crosslinking up to 160°C without using a crosslinking agent [41]. However, when the temperature was increased to 190°C, thermal crosslinking of the MK resin could be observed (Fig. 6b and Fig. 6c). Based on the last part of the torque analysis during mixing process, it can be assumed that the crosslinked pieces inside the feedstock were disrupted due to the shear forces applied in the mixing chamber which resulted in a decrease and final plateau in the mixing torque.

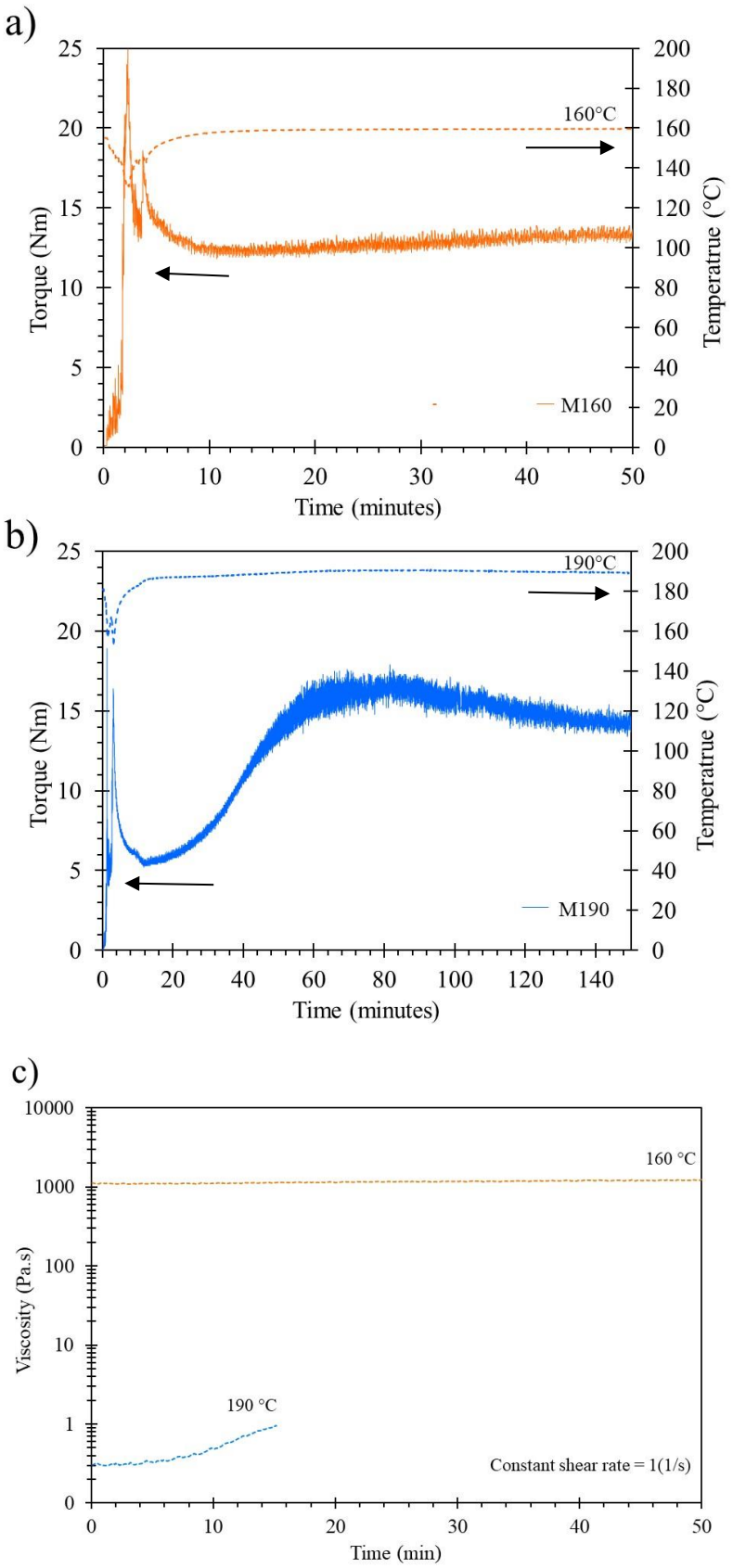

Fig. 6. a,b) Torque versus time plot for sample mixed at 160 and 190°C, labeled as M160 and M190, respectively, c) viscosity versus time plot for pure MK powder at a constant shear rate of 1(1/s).

4.3.5. XRF and XRD analysis of sintered mullite ceramics

After mixing the composition of 60/ 40 wt% Al_2O_3/ SiO_2 with thermoplastic binder at two different temperatures, filaments were extruded, debound and sintered at 1700°C for 5h. Based on TG results, an Al_2O_3/SiO_2 ratio of 1.52 was expected with a rate of 20K/min. For the lower heating rate (0.6 k/min), a ratio of 1.64 was expected according to Fig. 2.

As shown in Fig. 6, it is possible to thermally crosslink MK during the mixing process. To investigate this effect, five different samples were investigated (Table 3). Four samples were mixed at 160°C and 190°C and pyrolyzed up to 800°C with a heating rate of 0.6K/min, among which two were wick debound at 210°C prior to pyrolysis as reported elsewhere [22]. In addition, a sample mixed at 190°C and pyrolyzed up to 800°C with a heating rate 20K/min was analyzed, serving as a reference for comparison.

The elemental composition of Al_2O_3, SiO_2 and MgO was investigated using XRF analysis. The calculated Al_2O_3, SiO_2 and MgO contents for each sample are presented in Table 3. Notably, the samples mixed at 190°C consistently exhibited an Al_2O_3/SiO_2 ratio of 1.50, regardless of the heating rate employed during pyrolysis and the implementation of a wick debinding step. On the other hand, the samples mixed at 160°C displayed a higher Al_2O_3/SiO_2 ratio, ranging from 1.62 to 1.64. XRF result of sample mixed at 190°C and heat treated with a rate of 20K/min aligns well with the findings obtained from TG and FTIR analyses (Fig. 2 and Fig. 5). By using the fast heating rate, a mass loss of 81 wt% can be confirmed which will result in the expected Al_2O_3/SiO_2 ratio of 1.5. On the other hand, the samples mixed at 190°C and 160°C with a heating rate of 0.6K/min exhibited a completely different behavior. When mixed at 190°C, the MK undergoes full crosslinking. This leads to a higher fraction of stabilized POSS molecules that transform into Si-O-Si network bonds, resulting in the observed Al_2O_3/SiO_2 ratio of 1.5. When mixing at 160°C and heat treating with a rate of 0.6K/min, the release of unstable POSS molecules occurs before crosslinking takes place which reduces the yield of SiO_2. Even if a wick debinding step at 210°C is implemented, the evaporation of volatile POSS molecules cannot be prevented, as a high fraction of molecules are already gradually eliminated below 210°C. Based on these findings, it can be concluded that crosslinking of the preceramic polymer during the mixing step is necessary to preserve a higher SiO_2 yield for thermoplastic processing like MEX-AM.

Table 3. XRF analysis of prepared mullite feedstocks after sintering at 1700°C for 5h.

Sample MXX*HYY**	Al_2O_3 (wt%) (2σ= ±0.2)	SiO_2 (wt%) (2σ= ±0.15)	MgO (wt%) (2σ= ±0.05)	Al_2O_3/SiO_2	Sum
M160H0.6	61.70	37.70	0.51	1.64	99.91
M160H0.6W (Wick debound)	61.38	37.96	0.52	1.62	99.87
M190H0.6	59.77	39.76	0.30	1.50	99.83
M190H0.6W (Wick debound)	59.54	39.93	0.42	1.49	99.89
M190H20	59.60	39.69	0.57	1.50	99.86

* XX is the mixing temperature in °C

** YY is the heating rate for the thermal debinding

Additionally, samples M160H0.6 and M190H0.6 were analyzed by XRD. As can be seen in Fig. 7a,b, conversion to mullite phase has been achieved. Also, an amorphous content between 2θ of 15° and 30° is visible. Successful dispersion of highly active alumina particles within the PCP matrix led to the prevention of cristobalite impurity. Similar behavior has been reported by other researchers [51, 52]. However, using XRD analysis, no difference in the amorphous content could be detected between the two samples after sintering at 1700°C for 5h (Fig. 7c). Fig. S2 (appendices) presents the microstructure of a sintered mullite, mixed at 160°C and heated with a rate of 0.6 K/min, indicating the presence of mullite needles and the amorphous phase.

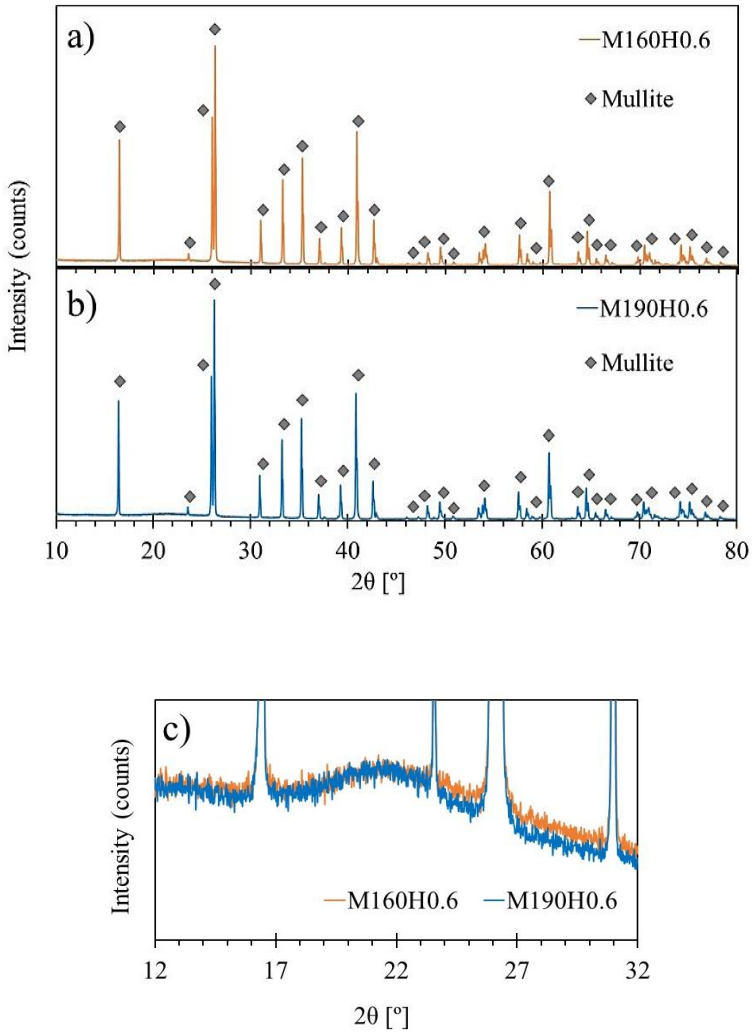

Fig. 7. XRD result of sintered mullite, mixed at a) 160°C and b) 190°C with a heating rate of 0.6, c) amorphous phase in both samples.

4.4. Conclusions

In this study, thermal behavior of a commercial methyl-silsesquioxane (SILRES MK) was studied up to 800°C under air and inert atmospheres. Based on TG analysis of pure MK resin, heating rate is a crucial factor to determine the SiO_2 yield of the preceramic polymer after pyrolysis under air atmosphere. Heating slowly (below 2K/min) in air reduces the SiO_2 yield as volatile species have longer time to evaporate below the crosslinking temperature and a higher fraction of POSS molecules with cage structures will escape the structure. In thermoplastic processes like MEX-AM, low heating rates and dwell times are mandatory to remove binder without cracks, blisters and bobbles. Therefore, the instability of POSS

molecules will significantly affect the fabrication of polymer derived oxide ceramics (e.g. silicate ceramics).

Mixing thermoplastic feedstocks at 160°C (below crosslinking temperature of

MK) resulted in a SiO_2 deficiency during thermal debiding. Interestingly, mixing the feedstock at 190°C (above crosslinking temperature of MK), provided a constant yield of 81 wt% and uncontrolled evaporation of POSS species could be avoided.

Acknowledgments

This work was supported by the Swiss National Science Foundation (SNSF) [grant number 200021_184691/1]. Authors would like to thank Beatrice Fischer for their help with the FTIR measurements.

References

[1] F. Ainger, J. Herbert, The preparation of phosphorus-nitrogen compounds as non-porous solids, Special Ceramics 168 (1960) 81.

[2] S. Yajima, K. Okamura, J. Hayashi, Structural analysis in continuous silicon carbide fiber of high tensile strength, Chemistry Letters 4(12) (1975) 1209-1212.doi: https://doi.org/10.1246/cl.1975.1209.

[3] R.M. Laine, F. Babonneau, Preceramic polymer routes to silicon carbide, Chemistry of materials 5(3) (1993) 260-279.

[4] G.T. Burns, G. Chandra, Pyrolysis of preceramic polymers in ammonia: preparation of silicon nitride powders, Journal of the American Ceramic Society 72(2) (1989) 333-337.doi: https://doi.org/10.1111/j.1151-2916.1989.tb06129.x.

[5] G. Feiertag, W. Ehrfeld, H. Freimuth, H. Kolle, H. Lehr, M. Schmidt, M. Sigalas, C. Soukoulis, G. Kiriakidis, T. Pedersen, Fabrication of photonic crystals by deep x-ray lithography, Applied Physics Letters 71(11) (1997) 1441-1443.doi: https://doi.org/10.1063/1.120431.

[6] P. Colombo, M. Modesti, Silicon oxycarbide ceramic foams from a preceramic polymer, Journal of the American Ceramic Society 82(3) (1999) 573-578.doi: https://doi.org/10.1111/j.1151-2916.1999.tb01803.x.

[7] Y.W. Kim, H.D. Kim, C.B. Park, Processing of microcellular mullite, Journal of the American Ceramic Society 88(12) (2005) 3311-3315.doi: https://doi.org/10.1111/j.1551-2916.2005.00597.x.

[8] E. Bernardo, E. Tomasella, P. Colombo, Development of multiphase bioceramics from a filler-containing preceramic polymer, Ceramics International 35(4) (2009) 1415-1421.doi: https://doi.org/10.1016/j.ceramint.2008.07.003.

[9] G. Parcianello, E. Bernardo, P. Colombo, Low temperature synthesis of zircon from silicone resins and oxide nano-sized particles, Journal of the European Ceramic Society 32(11) (2012) 2819-2824.doi:

https://doi.org/10.1016/j.jeurceramsoc.2011.11.028.
[10] I.-H. Song, M.-J. Kim, H.-D. Kim, Y.-W. Kim, Processing of microcellular cordierite ceramics from a preceramic polymer, Scripta Materialia 54(8) (2006) 1521-1525.doi: https://doi.org/10.1016/j.scriptamat.2005.12.039.
[11] E. Bernardo, P. Colombo, S. Hampshire, SiAlON-based ceramics from filled preceramic polymers, Journal of the American Ceramic Society 89(12) (2006) 3839-3842.doi: https://doi.org/10.1111/j.1551-2916.2006.01287.x.
[12] E. Bernardo, L. Fiocco, G. Parcianello, E. Storti, P. Colombo, Advanced Ceramics from Preceramic Polymers Modified at the Nano-Scale: A Review, Materials, 2014, pp. 1927-1956.
[13] Y.D. Blum, R.M. Platz, E.J. Crawford, Glass Strengthening by Polymer-Derived Ceramic Coatings, Journal of the American Ceramic Society 73(1) (1990) 170-172.doi: https://doi.org/10.1111/j.1151-2916.1990.tb05116.x.
[14] J.D. Torrey, R.K. Bordia, Processing of polymer-derived ceramic composite coatings on steel, Journal of the American Ceramic Society 91(1) (2008) 41-45.doi: https://doi.org/10.1111/j.1551-2916.2007.02019.x.
[15] C.H. Park, Y.J. Joo, J.K. Chung, Y.H. Han, C.J. Kim, Morphology control of a silicon nitride thick film derived from polysilazane precursor using UV curing and IR heat treatment, Advances in Applied Ceramics 116(7) (2017) 376-382.doi: https://doi.org/10.1080/17436753.2017.1339490.
[16] L. Gorjan, R. Tonello, T. Sebastian, P. Colombo, F. Clemens, Fused deposition modeling of mullite structures from a preceramic polymer and γ-alumina, Journal of the European Ceramic Society 39(7) (2019) 2463-2471.doi: https://doi.org/10.1016/j.jeurceramsoc.2019.02.032.
[17] T. Takahashi, H. Münstedt, M. Modesti, P. Colombo, Oxidation resistant ceramic foam from a silicone preceramic polymer/polyurethane blend, Journal of the European Ceramic Society 21(16) (2001) 2821-2828.doi: https://doi.org/10.1016/S0955-2219(01)00220-5.
[18] J. Zeschky, T. Höfner, C. Arnold, R. Weißmann, D. Bahloul-Hourlier, M. Scheffler, P. Greil, Polysilsesquioxane derived ceramic foams with gradient porosity, Acta Materialia 53(4) (2005) 927-937.doi: https://doi.org/10.1016/j.actamat.2004.10.039.
[19] C. Vakifahmetoglu, D. Zeydanli, P. Colombo, Porous polymer derived ceramics, Materials Science and Engineering: R: Reports 106 (2016) 1-30.doi: https://doi.org/10.1016/j.mser.2016.05.001.
[20] F. Sarraf, E. Abbatinali, L. Gorjan, T. Sebastian, P. Colombo, S.V. Churakov, F. Clemens, Effect of MgO sintering additive on mullite structures manufactured by fused deposition modeling (FDM) technology, Journal of the European Ceramic Society 41(13) (2021) 6677-6686.doi: https://doi.org/10.1016/j.jeurceramsoc.2021.06.012.
[21] P. Greil, Active-filler-controlled pyrolysis of preceramic polymers, Journal of the American Ceramic Society 78(4) (1995) 835-848.doi: https://doi.org/10.1111/j.1151-2916.1995.tb08404.x.
[22] F. Sarraf, A. Hadian, S.V. Churakov, F. Clemens, EVA-PVA binder system for polymer derived mullite made by material extrusion based additive manufacturing, Journal of the European Ceramic

Society 43(2) (2023) 530-541.doi: https://doi.org/10.1016/j.jeurceramsoc.2022.10.009.
[23] P. Colombo, G. Mera, R. Riedel, G.D. Sorarù, Polymer-Derived Ceramics: 40 Years of Research and Innovation in Advanced Ceramics, Journal of the American Ceramic Society (2010) no-no.doi: https://doi.org/10.1111/j.1551-2916.2010.03876.x.
[24] E. Rosado, R. Moreno, Mullite-silica scaffolds obtained by stereolithography and reaction sintering, Open Ceramics 14 (2023) 100361.doi: https://doi.org/10.1016/j.oceram.2023.100361.
[25] J. Essmeister, A.A. Altun, M. Staudacher, T. Lube, M. Schwentenwein, T. Konegger, Stereolithography-based additive manufacturing of polymer-derived SiOC/SiC ceramic composites, Journal of the European Ceramic Society 42(13) (2022) 5343-5354.doi: https://doi.org/10.1016/j.jeurceramsoc.2022.06.021.
[26] M. Wang, C. Xie, R. He, G. Ding, K. Zhang, G. Wang, D. Fang, Polymer-derived silicon nitride ceramics by digital light processing based additive manufacturing, Journal of the American Ceramic Society 102(9) (2019) 5117-5126.doi: https://doi.org/10.1111/jace.16389.
[27] J. Schmidt, A.A. Altun, M. Schwentenwein, P. Colombo, Complex mullite structures fabricated via digital light processing of a preceramic polysiloxane with active alumina fillers, Journal of the European Ceramic Society 39(4) (2019) 1336-1343.doi: https://doi.org/10.1016/j.jeurceramsoc.2018.11.038.
[28] M. Pelanconi, P. Colombo, A. Ortona, Additive manufacturing of silicon carbide by selective laser sintering of PA12 powders and polymer infiltration and pyrolysis, Journal of the European Ceramic Society 41(10) (2021) 5056-5065.doi: https://doi.org/10.1016/j.jeurceramsoc.2021.04.014.
[29] N. Kamboj, M. Aghayan, C.S. Rodrigo-Vazquez, M.A. Rodríguez, I. Hussainova, Novel silicon-wollastonite based scaffolds for bone tissue engineering produced by selective laser melting, Ceramics International 45(18) (2019) 24691-24701.doi: https://doi.org/10.1016/j.ceramint.2019.08.208.
[30] J.W. Kemp, A.A. Diaz, E.C. Malek, B.P. Croom, Z.D. Apostolov, S.R. Kalidindi, B.G. Compton, L.M. Rueschhoff, Direct ink writing of ZrB2-SiC chopped fiber ceramic composites, Additive Manufacturing 44 (2021) 102049.doi: https://doi.org/10.1016/j.addma.2021.102049.
[31] K. Huang, H. Elsayed, G. Franchin, P. Colombo, Embedded direct ink writing of freeform ceramic components, Applied Materials Today 23 (2021) 101005.doi: https://doi.org/10.1016/j.apmt.2021.101005.
[32] L. Zhao, X. Wang, H. Xiong, K. Zhou, D. Zhang, Optimized preceramic polymer for 3D structured ceramics via fused deposition modeling, Journal of the European Ceramic Society 41(10) (2021) 5066-5074.
[33] G. El Chawich, J. El Hayek, V. Rouessac, D. Cot, B. Rebière, R. Habchi, H. Garay, M. Bechelany, M. Zakhour, P. Miele, C. Salameh, Design and Manufacturing of Si-Based Non-Oxide Cellular Ceramic Structures through Indirect 3D Printing, Materials, 2022.
[34] A. Kulkarni, G.D. Sorarù, J.M. Pearce, Polymer-derived SiOC replica of material extrusion-based 3-D printed plastics, Additive Manufacturing 32 (2020) 100988.doi: https://doi.org/10.1016/j.addma.2019.100988.

[35] H. Mei, Y. Yan, L. Feng, K.G. Dassios, H. Zhang, L. Cheng, First printing of continuous fibers into ceramics, Journal of the American Ceramic Society 102(6) (2019) 3244-3255.doi: https://doi.org/10.1111/jace.16234.
[36] A. Kulkarni, J. Pearce, Y. Yang, A. Motta, G.D. Sorarù, SiOC (N) cellular structures with dense struts by integrating fused filament fabrication 3D printing with polymer-derived ceramics, Advanced Engineering Materials 23(12) (2021) 2100535.doi: https://doi.org/10.1002/adem.202100535.
[37] H. Tian, Q.-s. Ma, Effects of heating rate on the structure and properties of SiOC ceramic foams derived from silicone resin, Ceramics International 38(3) (2012) 2101-2104.doi: https://doi.org/10.1016/j.ceramint.2011.10.048.
[38] E. Bernardo, P. Colombo, E. Pippel, J. Woltersdorf, Novel mullite synthesis based on alumina nanoparticles and a preceramic polymer, Journal of the American Ceramic Society 89(5) (2006) 1577-1583.doi: https://doi.org/10.1111/j.1551-2916.2006.00963.x.
[39] E. Bernardo, P. Colombo, E. Dainese, G. Lucchetta, P.F. Bariani, Novel 3D wollastonite-based scaffolds from preceramic polymers containing micro-and nano-sized reactive particles, Advanced Engineering Materials 14(4) (2012) 269-274.doi: https://doi.org/10.1002/adem.201100241.
[40] G. Parcianello, E. Bernardo, P. Colombo, Cordierite ceramics from silicone resins containing nano-sized oxide particle fillers, Ceramics International 39(8) (2013) 8893-8899.doi: https://doi.org/10.1016/j.ceramint.2013.04.083.
[41] R. Harshe, C. Balan, R. Riedel, Amorphous Si(Al)OC ceramic from polysiloxanes: bulk ceramic processing, crystallization behavior and applications, Journal of the European Ceramic Society 24(12) (2004) 3471-3482.doi: https://doi.org/10.1016/j.jeurceramsoc.2003.10.016.
[42] J. Ma, F. Ye, S. Lin, B. Zhang, H. Yang, J. Ding, C. Yang, Q. Liu, Large size and low density SiOC aerogel monolith prepared from triethoxyvinylsilane/tetraethoxysilane, Ceramics International 43(7) (2017) 5774-5780.doi: https://doi.org/10.1016/j.ceramint.2017.01.124.
[43] S. Tsuge, H. Ohtani, C. Watanabe, Pyrolysis-GC/MS data book of synthetic polymers: pyrograms, thermograms and MS of pyrolyzates, Elsevier2011.
[44] E. Ionescu, C. Linck, C. Fasel, M. Müller, H.J. Kleebe, R. Riedel, Polymer-derived SiOC/ZrO2 ceramic nanocomposites with excellent high-temperature stability, Journal of the American Ceramic Society 93(1) (2010) 241-250.doi: https://doi.org/10.1111/j.1551-2916.2009.03395.x.
[45] F. Vivier, D. Santamaria, D. Pellerej, P. Buonfico, M. Sangermano, A kinetic analysis of a thermal curing reaction of a silicon resin in solid state, Characterization of Minerals, Metals, and Materials 2014 (2014) 63-72.
[46] K. Kanamori, Monolithic silsesquioxane materials with well-defined pore structure, Journal of Materials Research 29(23) (2014) 2773-2786.
[47] K. Papakollu, N. Moharana, K.H. Kumar, S. Lauterbach, H.-J. Kleebe, E. Ionescu, R. Kumar, Synthesis and temperature-dependent evolution of the phase composition in palladium-containing silicon oxycarbide ceramics, Journal of the European Ceramic Society 42(12) (2022) 4825-4834.doi:

https://doi.org/10.1016/j.jeurceramsoc.2022.05.032.
[48] W.-C. Liu, C.-C. Yang, W.-C. Chen, B.-T. Dai, M.-S. Tsai, The structural transformation and properties of spin-on poly (silsesquioxane) films by thermal curing, Journal of Non-Crystalline Solids 311(3) (2002) 233-240.doi: https://doi.org/10.1016/S0022-3093(02)01373-X.
[49] E. Radovanovic, M. Gozzi, M. Gonçalves, I. Yoshida, Silicon oxycarbide glasses from silicone networks, Journal of non-crystalline solids 248(1) (1999) 37-48.doi: https://doi.org/10.1016/S0022-3093(99)00101-5.
[50] A. Tamayo, R. Peña-Alonso, F. Rubio, J. Rubio, J. Oteo, Synthesis and characterization of boron silicon oxycarbide glass fibers, Journal of non-crystalline solids 358(2) (2012) 155-162.doi: https://doi.org/10.1016/j.jnoncrysol.2011.09.002.
[51] D. Suttor, H.J. Kleebe, G. Ziegler, Formation of mullite from filled siloxanes, Journal of the American Ceramic Society 80(10) (1997) 2541-2548.
[52] E. Bernardo, P. Colombo, E. Manias, SiOC glass modified by montmorillonite clay, Ceramics International 32(6) (2006) 679-686.

Appendices

S1: Debinding program for solvent debound filaments as temperature versus time plot

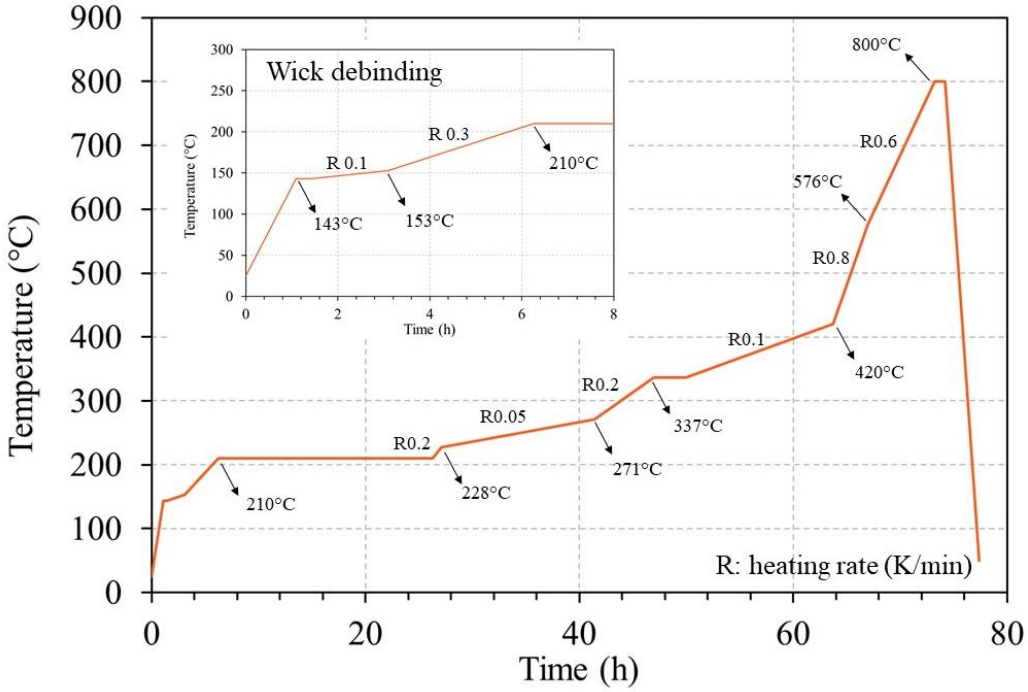

Fig. S1. Debinding program for a solvent debound filament.

S2: Microstructure of sintered polymer derived mullite mixed at 160°C and heated with a rate of 0.6 K/min

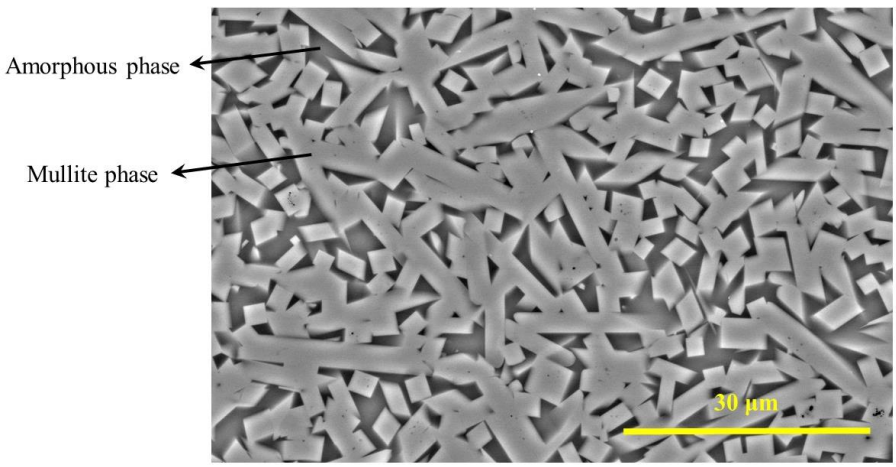

Fig. S2. SEM image of a cross section of the sintered mullite, mixed at 160°C and heated with a rate of 0.6 K/min.

Chapter 5- EVA-PVA binder system for polymer derived mullite made by material extrusion based additive manufacturing

Fateme Sarraf, Amir Hadian, Sergey V. Churakov, Frank Clemens

Accepted (peer-reviewed), Journal of the European Ceramic Society (2023), Volume 43, Issue 2, February 2023, Pages 530-541

DOI: https://doi.org/10.1016/j.jeurceramsoc.2022.10.009

- This study addresses the third research question, "**How to optimize FDM process to fabricate dense large PDCs structures?**", focusing on the fabrication of dense polymer-derived mullite ceramic structures using FDM technique. The use of a binder system consisting of a mixture of ethylene vinyl acetate (EVA) and polyvinyl alcohol (PVA) was explored to address challenges related to gas evolution and pore formation during the crosslinking process of PCPs. Rectangular bars were successfully printed from PVA containing ceramic feedstocks using a screw based FDM printer. The organic binder removal of the bars involved solvent debinding of the PVA, wick debinding, and full thermal debinding of the remaining EVA binder. The positive influence of vinyl acetate (VA) content in EVA binder on solvent and thermal debinding was highlighted. The kinetics of organic binder removal were studied to design the debinding program. Fracture surface analysis indicated that the binder composition of E460 with 50% PVA content performed the best after sintering and dense cross-sections without structural defects were achieved.

EVA-PVA binder system for polymer derived mullite made by material extrusion based additive manufacturing

Fateme Sarraf, Amir Hadian, Sergey V. Churakov, Frank Clemens

Abstract

Low processing temperature of preceramic polymers (PCPs) makes them attractive for material extrusion based additive manufacturing (MEX-AM), earlier called fused deposition modeling (FDM). Fabrication of bulk polymer derived ceramics is challenging due to gas evolution during crosslinking leading to pores and cracks in final product. Mixture of ethylene vinyl acetate (EVA) and polyvinyl alcohol (PVA) was successfully used to generate open porosity before crosslinking step. For 3D printing, a pellet extruder was used and a PVA binder content of 50 vol% was essential for succcessful solvent debinding process in water. The effect of PVA content and different EVA grades on printability and debinding behavior was studied. EVA with a lower melt flow index (MFI) showed better compatibility with PVA additive in terms of mixing and printing. EVA with higher vinyl acetate content seems to be more favorable for later thermal debinding processes because of its higher gas permeability.

Keywords

Material extrusion (MEX) additive manufacturing, Mullite, Polyvinyl alcohol, Ethylene vinyl acetate, FDM/FFF.

5.1. Introduction

Polymer derived ceramics (PDCs), introduced in the early 1960s, are obtained as a result of pyrolysis of preceramic polymers (PCPs), usually in non-oxidative atmospheres [1, 2]. Organosilicon precursors with a Si backbone and O, C, N, B or H atoms [3], known as Si-based preceramic polymers, have remained a hot topic since then and there have been a lot of studies on synthesis of oxide and non-oxide ceramics like mullite [4], wollastonite [5], cordierite [6], SiAlON [7, 8], SiOC [9, 10], SiC [11] and so on. These polymeric compounds release gas byproducts while crosslinking followed by pyrolysis at higher temperatures to obtain an amorphous ceramic residue [12]. Fabrication of PDC structures have been demonstrated by various additive manufacturing techniques such as direct ink writing (DIW) [13, 14], stereolithography [15], digital light processing (DLP) [16, 17], selective laser sintering [18], material extrusion based additive manufacturing (MEX-AM) [19, 20], etc [21]. Although DIW is a good candidate for printing simple geometries, fabrication of more complex geometries, overhangs, bridging or achieving high resolution is still a big challenge even by tailoring the rheological properties of the ink. DLP method is limited to the fabrication of thin and small structures [16, 17] and with SLS only a low relative density of 90% for SiC ceramics could be achieved after 7 times polymer infiltration and pyrolysis (PIP) post-treatment [18]. Using MEX-AM method, closed porosity appeared in sintered parts [22].

Among various SiO_2 sources investigated to produce mullite, PCPs bring some advantages. Pyrolysis under air atmosphere can form fine silica powder that is highly reactive and can enhance the sintering kinetics to form silicate phases, like mullite [23]. Although the pure phase can be achieved by sol-gel route as well, thermoplastic nature of preceramic polymers provides the opportunity to use various plastic forming methods such as injection molding [24], extrusion [25, 26], fused deposition modeling (FDM) [11, 22], tape casting [27], fiber electrospinning [28], etc. Preceramic polymers can be also used as a substitute for the binder component that makes the thermal debinding less critical [29]. Obtained ceramics from PCPs are incredibly resistant to oxidation and creep as they reduce or eliminate the need for sintering additives [30, 31]. Despite all the advantages of PCPs, obtaining dense ceramics using these polymers is still a challenge due to their large shrinkage and release of gaseous products (leading to high mass loss). Different studies have successfully addressed the shrinkage issue and solved it using inert or active fillers in order to control the dimensional changes throughout pyrolysis [32, 33]. However, intensive gas release due to crosslinking (polycondensation reactions) of preceramic polymers is still limiting the thickness of fabricated parts [22], especially if thermoplastic

ceramic processing route is used. Using thermoplastic ceramic processing, the crosslinking of the added preceramic polymer already starts below the decomposition temperature of the thermoplastic binder additives. Due to the low gas permeability of the other thermoplastic binder components, the gaseous species generated by crosslinking form spherical closed pores that cannot be removed after sintering process [2, 4].

Addition of thermoplastic polymeric components to ceramic powders is essential for thermoplastic shaping to ensure flowability. However, removal of volatile components after shaping can be challenging. In general, thermal debinding is one of the main steps to obtain ceramics through thermoplastic ceramic processing. A well-established common solution is to create interconnected pore channels by solvent debinding of one of binder components. Water soluble binder additives such as PEG (Polyethylene glycol), PVA (Polyvinyl alcohol), Agar, etc., are considered as sufficient and environmentally friendly options, and using an efficient amount of in-soluble backbone binder facilitates the solvent debinding process without risk of structural collapse [34-36]. Extraction of water-soluble binder leads to formation of an interconnected porous network from the surface to the center, which creates pathways for the escape of gaseous products generated during thermal decomposition of other binder components. Thus, cracks and blisters that appear as a result of an accumulation of decomposition gases due to low gas permeability through the structure, can be avoided. PVA is a common option for industrial applications due to its high chemical resistance, water solubility, non-toxicity and biodegradability. This linear polymer is the product of partial or full hydroxylation of polymerized vinyl acetate, and it is well known that lower hydrolysis degree improves the water-solubility of the synthesized PVA [37].

In material extrusion based additive manufacturing (MEX-AM), also known as fused deposition modeling technology, PVA filaments are already commercially available as a soluble support material. In comparison to other AM processes, MEX-AM is a simple shaping technology for ceramics with low investment costs, to produce ceramic and ceramic composite components [38-40]. Hadian et al. [41] demonstrated that 12 cm tall zirconia vase structures can be printed and sintered successfully using fused filament fabrication (FFF) method. Fabrication of ceramic parts using FDM printers requires a stiff filament, which resists the gears pressure and feeds the process continuously. On the other hand, filaments need to be flexible enough for spooling and running a print [42, 43].

As an alternative to thermoplastic ceramic filament, pellets or granulates can be employed for MEX-AM process [44]. A screw extruder printing head helps if the development of stiff but flexible thermoplastic ceramic filament is not successful. In some cases, the ceramic filaments

are too brittle to be printed continuously. Thermoplastic ceramic pellets are already used for other shaping processes like extrusion and injection molding, so pellet extrusion printers are becoming more popular in the ceramics industry.

In this research study, we present an improved material extrusion based additive manufacturing process of PDCs based on thermoplastic shaping approach, which allows us to avoid undesired closed pores formed during the crosslinking process of the preceramic polymer. Water-soluble PVA binder component is introduced to the thermoplastic binder system to generate an interconnected pore structure at room temperature to allow for the transport of gasses generated during crosslinking of the PCP. Printability, solvent, wick and thermal debinding along with sintering were studied by combining PVA binder with three different ethylene vinyl acetate copolymers (backbone binder) to finally achieve dense mullite ceramic parts.

5.2. Material and methods

5.2.1. Materials

To produce $3Al_2O_3$-$2SiO_2$ (3:2 mullite), alumina powder (γ-Al_2O_3) (PURALOX SCFa-140 UF3, Sasol Performance Chemicals Ltd) and polysiloxane polymer (SILRES MK, Wacker Chemie AG) were used. 1 wt% of magnesium oxide (MgO, Fluka™) was added as sintering additive. The composition is described in more detail somewhere else [5]. Polyvinyl alcohol (PVA, Sigma-Aldrich) was used as a water-soluble thermoplastic binder component and three grades of ethylene vinyl acetate copolymers (EVA) (Elvax, DuPont, International SARL) with different vinyl acetate (VA) content and melt flow index (MFI) were used to tailor the rheology, printability and debinding behavior. It is known that higher VA content provides higher softness, more flexibility and lowers the melting point of EVA polymers. On the other hand, low MFI corresponding to long polymer chains correlates with higher toughness and increases the melting point. The different thermoplastic binder components used in this study are listed in Table 1.

Table 1. EVA and PVA thermoplastics used as binder components for the PCP-based ceramic feedstocks.

Binder trade name	Melting point (°C)	Vinyl acetate (%)	Melt flow index (g/10 min)*	Abbreviation for feedstock label	Elastic modulus (MPa)
Elvax 420	73	18	150	E420	42
Elvax 460	88	18	2.5	E460	52
Elvax 760	100	9.3	2	E760	140
PVA	-	-	-	P	-

* at 190°C/ 2.16 kg

In Table 2, the feedstock composition used in this study having a constant ceramic loading of 40 vol%, with respect to the γ-Al_2O_3, MgO and SILRES MK powders, are listed.

Table 2. Feedstocks compositions.

Feedstock	PVA content (vol%)	UF3 (wt%)	SILRES MK (wt%)	EVA content (wt%)	PVA content (wt%)
E*X**-60P	60	30.0	23.8	15.1	30.7
EX-50P	50	30.4	24.1	19.1	25.9
EX-40P	40	30.8	24.4	23.3	21.0

* E: indication for EVA polymer

** X: Different Elvax grade

5.2.2. Processing

Initially, PVA and EVA polymers were mixed in a torque rheometer equipped with roller-rotors (Rheomix 600, HAAKE™ PolyLab™ OS, Thermo Fisher Scientific, Germany) at 190°C for 20 minutes to achieve a homogeneous mixture. Dried SILRES MK, Al_2O_3 and MgO powders were added and mixed until a torque equilibrium was reached. Extruded filaments with a diameter of 1.8 mm, fabricated by capillary rheometer (Rosand RH10, NETZSCH-Gerätebau GmbH, Germany) at 160°C were brittle due to strong bonding between hydroxyl groups in PVA. As a result, they were chopped into small pellets to be used in a pellet printer.

A screw based FDM pellet printer (Tumaker Voladora NX+) was used to print all the feedstocks. Horizontal bar structures with length, width and height of 60, 4.8 and 3.8 mm were printed, respectively. The pellets were fed into the screw extruder using a fed hopper. The screw extruder consists of a feeding, compression and melting zone. In the compression zone, the

pellets start to melt and due to the compression, the air is pass through the feeding zone. At the tip of the melting zone, a nozzle is fixed. For the screw section and the nozzle, temperatures of 180 and 210°C were used, respectively. The bed temperature, printing speed, nozzle diameter and layer height were set to 95°C, 8 mm/s, 0.8 mm and 0.5 mm, respectively. In Fig. 1, a schematic overview of the processing steps from mixing of the raw materials, extrusion and printing followed by solvent debinding, thermal debinding and sintering is summarized.

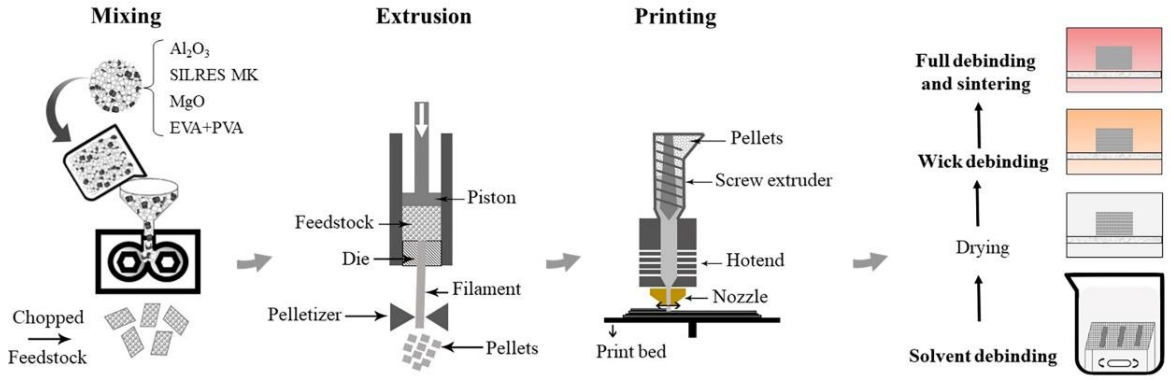

Fig. 1. Schematic overview of the processing steps from mixing until sintering for the fabrication of mullite ceramic using preceramic polymers.

A mullite ceramic was obtained by post-processing of the printed structure in several steps (Fig. 1). First, PVA was dissolved in deionized water (DI water at room temperature) as a solvent debinding step lasting for 3 and 6 days. Afterward, the samples were dried at room temperature under controlled humidity (10% RH) in a climate chamber (MKF 115, Binder, Germany). The dried samples were later placed in a box furnace (Pyrotec PC 12, Michel Keramikbedarf, Switzerland) for wick debinding under static air atmosphere. For this debinding step, the samples were placed in an alumina powder bed at 210°C for 48 h (Fig. 2a). For final debinding and sintering, the samples were removed from the powder bed, cleaned and placed in a high temperature furnace (LHT 03/17 D, Nabertherm GmbH). Heating profile (Fig. 2b) for the final debinding step was optimized by using model free kinetics analysis as reported by Hadian et al. [18]. Sintering program reported by Sarraf et al. was used [5]; therefore, the debound printed parts were heated up to 1600°C for 5h.

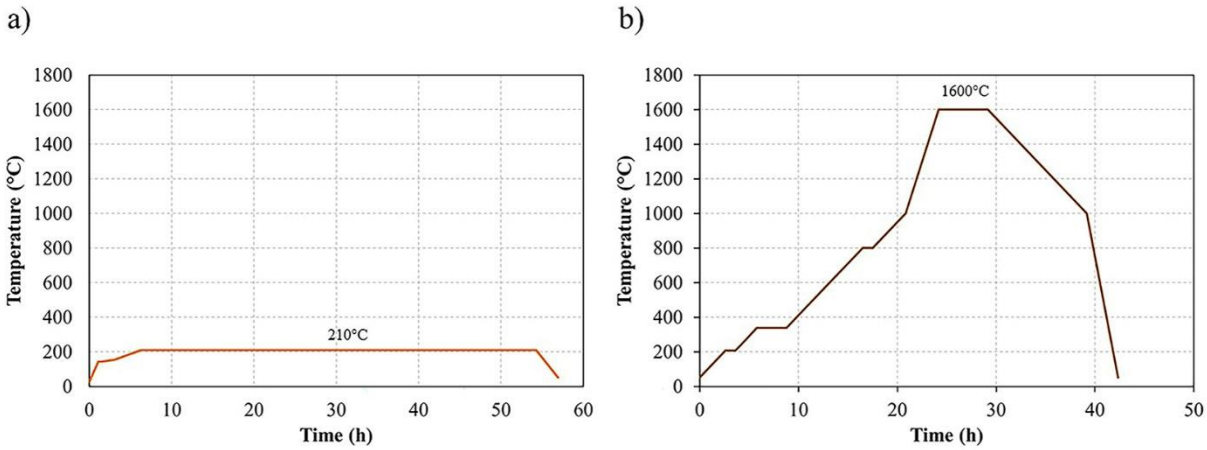

Fig. 2. Heating profile of (a) wick debinding, (b) thermal debinding and sintering used after solvent debinding of specimens.

5.2.3. Characterization

To study the rheological behavior of the feedstocks at printing temperature (210°C), a micro compounder (HAAKE™ MiniLab 3, ThermoFisher Scientific, Germany) was used. As shown by Hadian et al, the flow path of the feedstock inside the MiniLab can be changed using a bypass valve [45]. By running the instrument in circulation mode, the rheological data can be extracted using two pressure sensors placed inside a slit geometry. Subsequently, rheological measurements were performed in a range of rotation speeds from 100 to 10 rpm in five steps. Apparent viscosity as a function of shear rate was calculated for all the different feedstock compositions.

Pore formation at low temperatures (140, 180 and 220°C) was investigated. Higher temperatures were not investigated because wicking step was done at 210°C. To study the effect of solvent debinding on pore formation, green and solvent debound filaments were placed in an oven (Memmert GmbH+Co KG, Germany). The cross-section of the heat-treated filaments was investigated by optical microscope (SteREO Discovery.V20, Carl Zeiss AG, Switzerland).

Thermal analysis of the pure polymers and filaments (in green, solvent debound and partially debound state) was performed by DSC/TGA instrument (STA 449 F3 Jupiter, Netzsch GmbH, Germany) with 70 ml/min air flow and heating rate of 5K/min. In order to optimize the thermal debinding program, kinetic data (Friedman method) was analyzed by the Netzsch kinetics Neo software (Netzsch, Germany) using TG measurements with four different heating rates (2, 5, 10, and 20 k/min) up to 700 °C . Using kinetic analysis, a debinding program with a constant mass-loss rate was designed.

In addition, the cross-section of printed bars was investigated by optical microscope after each post-processing step to identify macro failures. Scanning electron microscope (SEM, VEGA 3, TESCAN, Czech Republic) was employed to study the microstructure of polished cross-section after sintering.

X-ray diffraction analysis (XRD, X'Pert PRO MPD, Malvern Panalytical Ltd, Germany) was carried out between10−80 degrees at room temperature with a copper anode to evaluate the phase assemblage after sintering of the bars. The XRD patterns were analyzed using the software (HighScore, Version 4.8, Malvern Panalytical Ltd, Germany).

5.3. Results and discussion

5.3.1. Flow behavior characterization of the PCP-based feedstocks

In comparison to the material properties reported by Gorjan et al. [19], the filaments produced in our study by the capillary rheometer were too brittle. This can be explained by the low thermoplasticity of PVA at its melting temperature due to strong hydrogen bonding forces between the hydroxyl groups [46]. Therefore, instead of filament based extruder head, a pellet extruder was used in this study (Fig. 1). During the extrusion step for filament fabrication with a capillary rheometer, the pressure was recorded and the results for the different feedstock recipes are shown in Fig. 3. For the Elvax 420, pressure deviation and roughness on the surface of the filaments could be observed (Fig. 3a). During the filament extrusion, extensional stress (e.g. extensional viscosity) appears at the entry of the die and this stress can cause melt rupture. This phenomenon results in pressure fluctuations and a rough surface of the extrudates. In Fig. 3b, the feedstocks with Elvax 460 are presented and both pressure curves and filament surfaces are smoother. Elvax 420 and Elvax 460 have the same vinyl acetate content but the melt flow index of the Elvax 460 is lower which can be explained by longer chain length of the polymer. The higher the molecular weight, the higher the degree of entanglement between the chains. Shorter chains have more end groups and the increase in the so-called free volume and molecular mobility of chains will result in lower Young's modulus and strength. This can result in flow instabilities and melt rupture as shown in Fig. 3a. To prove this, Elvax 760 with low MFI and low vinyl acetate content was investigated (Fig. 3c). As expected, the feedstocks made with Elvax 760 result in smoother pressure curves and filament surfaces.

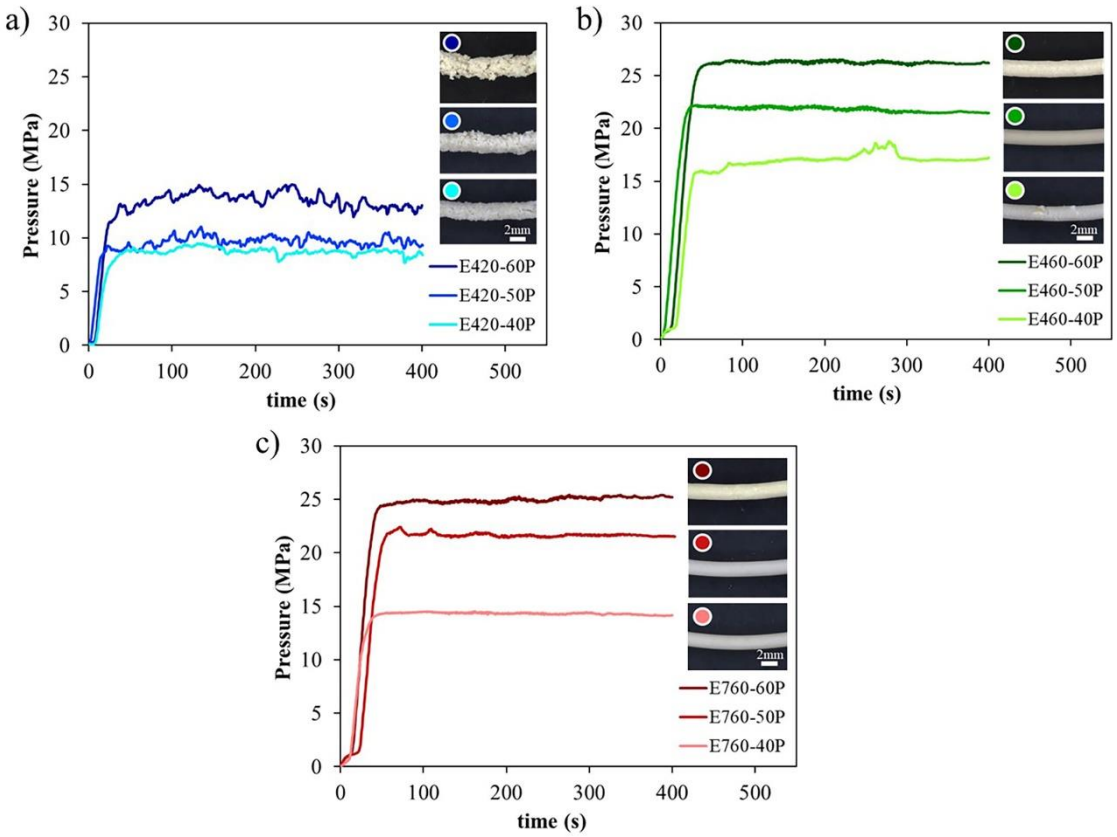

Fig. 3. Pressure versus time plots of extruded filaments with (a) E420, (b) E460 and (c) E760 containing 40, 50 and 60 vol% PVA. For the extrusion of the filaments, a temperature of 160°C and a die orifice of 1.8 mm was used.

Generally, the extrusion pressure increases with increasing the PVA content. The extrusion pressure for the feedstocks based on EVA with higher MFI (Elvax 420) is significantly lower. In Fig. 3a, it can be seen that the pressure increases with increasing the PVA content. As mentioned by Ku et al., PVA has a low thermoplasticity [46]. Decreasing the thermoplasticity of the feedstock will increase the extrusion pressure, which is observed for all three different EVA polymeric binders.

To avoid flow instabilities during rheological characterization of the feedstocks based on EVA 420, it was decided to use the MiniLab 3 equipment. As observed in the extrusion experiments (Fig. 3), a higher apparent viscosity was obtained by increasing the PVA content (Fig. 4), because of the lower thermoplasticity of PVA in comparison to EVA. Due to the high viscosity of E460-60P feedstock, the material was pushed out from the MiniLab (Fig. 4b); therefore, the rheological results are not reported. Typically, thermoplastic materials show shear-thinning behavior due to the entanglement of the polymer chains under shear stress. The shear-thinning

behavior can be quantitatively analyzed by using the Power law equation, e.g. Ostwald–de Waele relationship (1):

$$\sigma = \eta\gamma^n \quad (1)$$

σ: shear stress, η: apparent viscosity, γ: shear rate, n: power law index

A power law index below 1 indicates shear-thinning behavior. The lower the power law index, the higher the shear-thinning effect. As shown in Fig. 4d, an increase in PVA content results in a higher shear sensitivity and greater pseudoplastic behavior of the feedstocks.

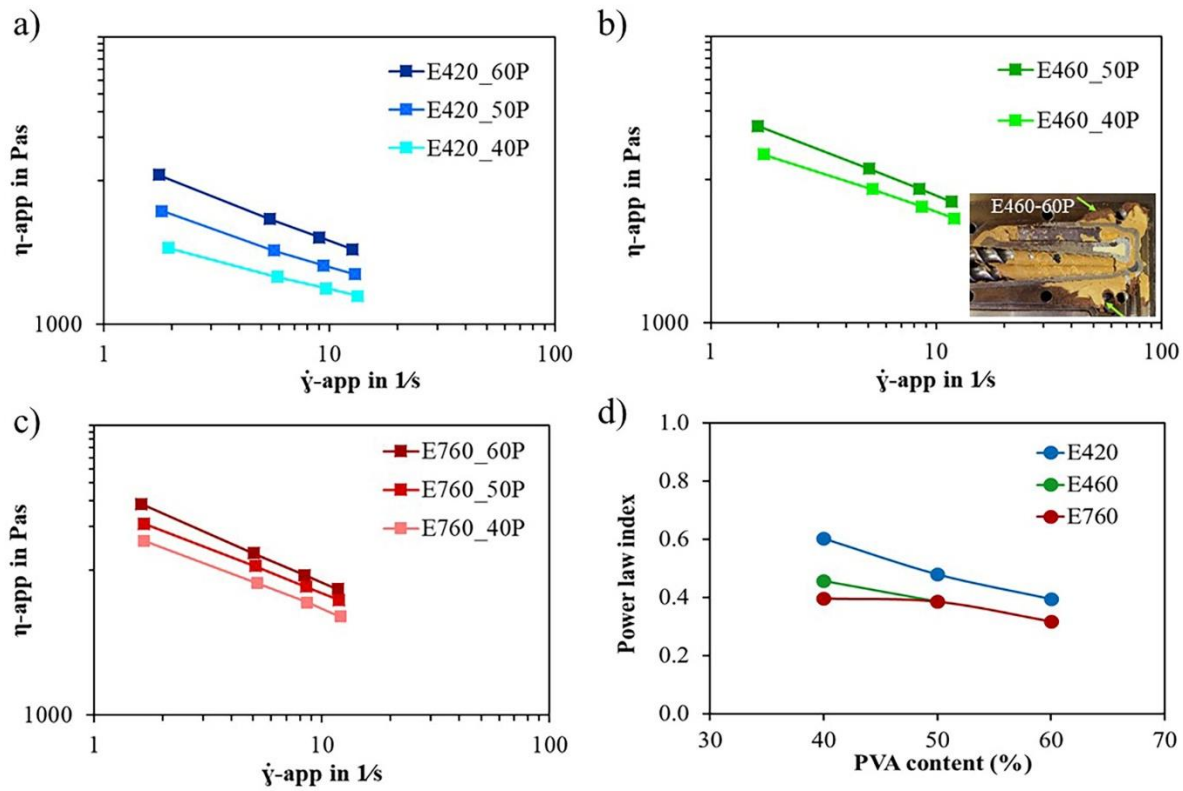

Fig. 4. Apparent viscosity versus shear rate plots for (a) E420, (b) E460 and (c) E760 with 40, 50 and 60vol% PVA. (d) Power law index calculated for all nine compositions. The analyses were performed at 210°C.

Heiber et al. reported that higher powder content in ceramic feedstocks results in lower power law index [47]. They explained that higher shear thinning effect occurs because the effective gap length in which the polymer can be sheared decreases. A lower gap length will result in higher internal shear stress and leads to a decrease in the viscosity and consequently, to a

convergence of the viscosity values at higher powder loading contents. It can be assumed that a similar effect will occur when mixing a polymer with low thermoplasticity, e.g. PVA, with EVA (high thermoplasticity).

5.3.2. Investigation of pore formation during crosslinking of the PCP-based feedstocks

To investigate the efficiency of the solvent debinding in order to avoid pore formation during crosslinking of preceramic polymers, E760-50P green and solvent debound filaments were heat treated at 140, 180 and 220°C for one hour. Fig. 5a shows that there is no evidence of pore formation up to 180°C and by increasing the temperature to 220°C, the pores start to appear, due to the gas evolution during the crosslinking of SILRES MK. However, by solvent debinding of the PVA binder additive, the pore formation can be avoided (Fig. 5b). Therefore, the obtained interconnected porous network after the PVA removal is sufficient to ensure the gas release during the crosslinking (polycondensation reactions) of the PCP.

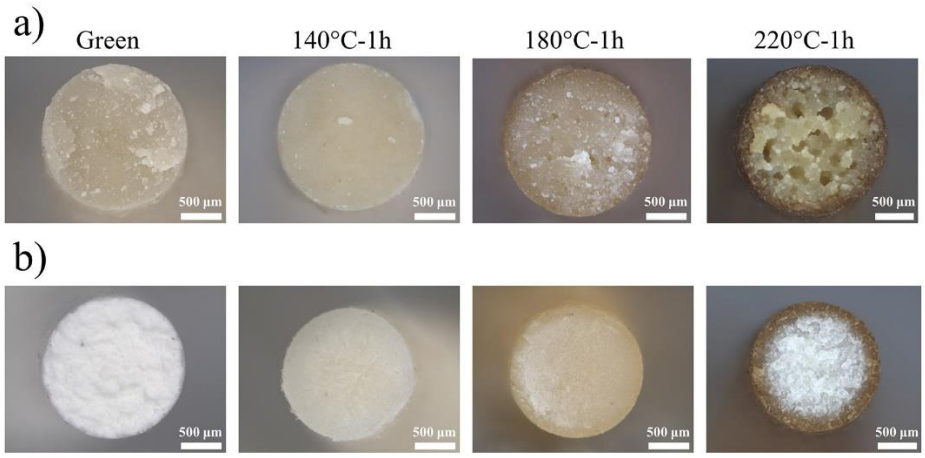

Fig. 5. Optical microscope analysis of Elvax 760-50P filament cross-sections after heat treatment at 140, 180 and 220°C for (a) green filament, (b) solvent debound filament (DI water for 6 days at 25°C).

5.3.3. Development of debinding program by kinetics analysis

Since the solvent debinding concept was successful in gas removal during crosslinking of the preceramic polymer (PCP), we further investigated the debinding process by model-free kinetics analysis. Solvent debound filaments of E760-50P were used to optimize further debinding steps. Constant mass-loss rate of 0.04 %/min was selected conservatively to optimize the debinding program for the solvent debound and wick debound ceramic parts.

Investigation of the debinding behavior for solvent debound PCP based ceramic filaments

Kinetic modeling of the solvent debound filaments presented in Fig. 6a, shows a drop in activation energy between 0.55 and 0.7 conversion values. This can be interpreted as an exothermic reaction [18]. This exothermic reaction is responsible for an overheating in the sample and subsequently higher mass loss rate can be expected. This phenomenon can result in formation of blisters and crack in the sample. To avoid these issues, a cooling step is needed at around 390°C for 5h (Fig. 6b). Accordingly, a multistep debinding approach was employed. First, a wick debinding step at 210°C was added. This is the temperature in Fig. 6b, at which the heating rate is decreasing due to higher binder mass loss.

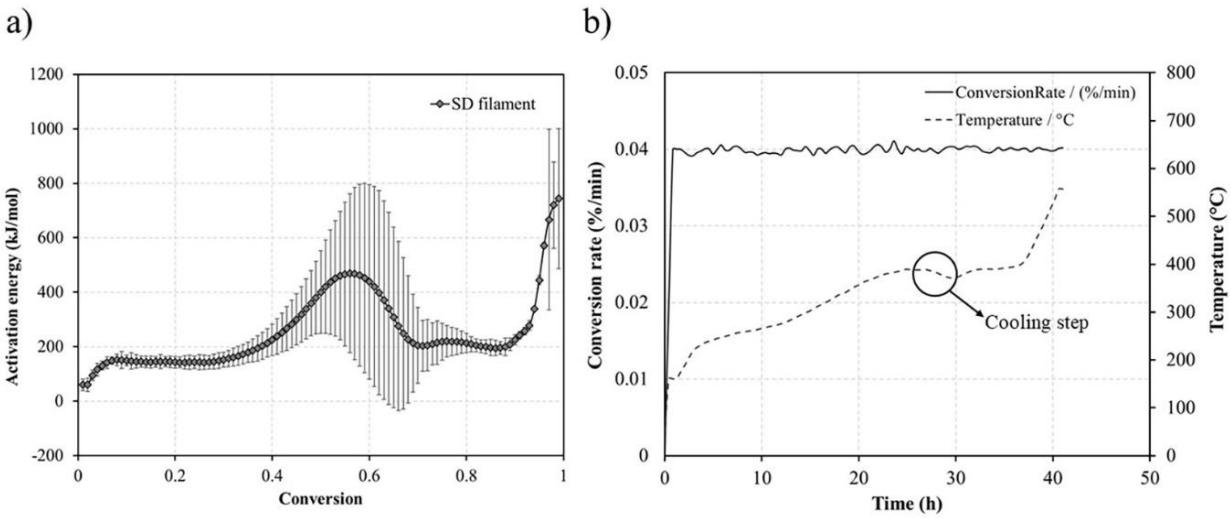

Fig. 6. (a) Kinetic modeling of the thermal debinding process for solvent debound E760-50P filament and (b) debinding program with a constant mass-loss rate of 0.04 %/min.

The wicking step represents an isothermal heat treatment for several hours aimed to remove binder of the printed and solvent debound parts retained by capillary forces. To set up the wicking program, solvent debound E760-50P filaments were heat treated at 210°C for 4, 8 and 48h. It can be seen in Fig. 7 that 4 and 8h dwell time at 210°C are not sufficient to remove the binder from the whole volume of filaments. It is obvious that during wicking debinding, mass is transported out of the sample through already gained pores by mainly capillary forces and pressure driven liquid transport; therefore, it can be expected that the wicking process for the printed bars will be longer in comparison to the filaments. Due to this reason, we decided to significantly increase the wicking time up to 48h (Fig. 7c). In Fig. 7d, the mass loss after wicking for 48h is shown. It can be seen that the mass loss calculated by free-model kinetics

and experimentally analyzed data differ by a factor of 4. As a result, we can conclude that isothermal debinding process cannot be modeled by free-model kinetics due to additional parameters like capillary forces, which have remarkable effect on the debinding process.

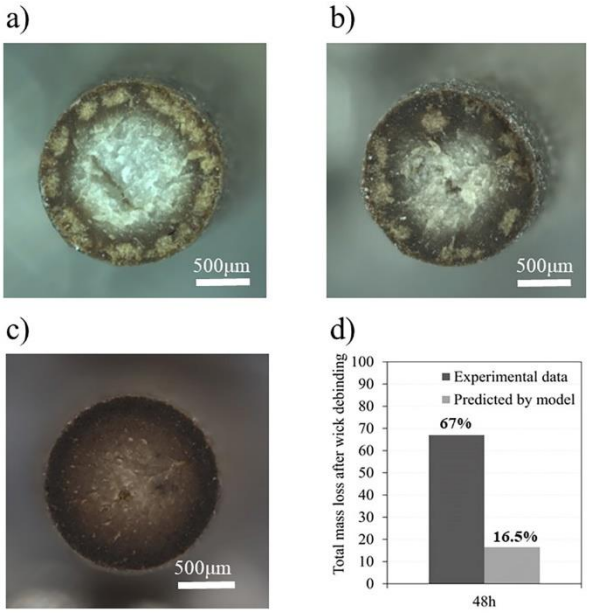

Fig. 7. Cross-section of E760-50P filaments after wick debinding at 210°C for (a) 4, (b) 8 and (c) 48h. Total mass loss weighed by balance (experimental data) and predicted using free-model kinetic simulated data after 48h dwell time.

After wick debinding, thermal debinding program was investigated again by model-free kinetics. As presented in Fig. 8a, activation energy is flattened and a full debinding program without a cooling step can be achieved with a constant conversion rate of 0.04 % per min.

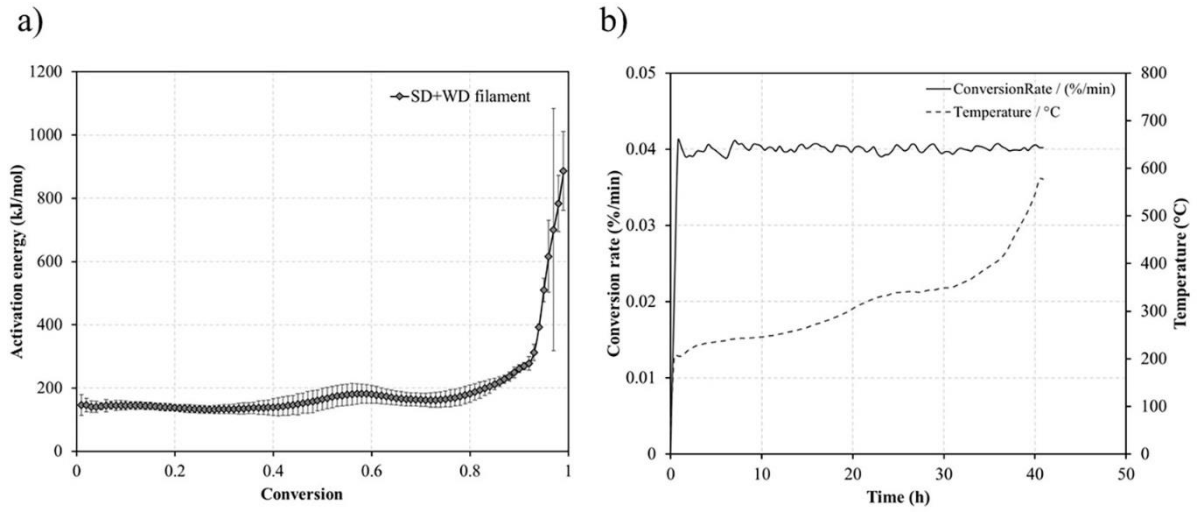

Fig. 8. (a) Kinetic modeling of the debinding process for solvent and wick debound filament E760-50P and (b) debinding program with a constant mass-loss rate of 0.04 %/min.

Investigation of the thermal evolution of PCP based ceramic filaments

In order to better understand the debinding steps in this system, thermogravimetric analysis (TG) was performed for the pure polymeric components and filaments after the printing, solvent debinding and wick debinding (Fig. 9). Decomposition and removal of volatile components can be divided into 3 different temperature zones. As can be seen in Fig. 9a, first mass loss in MK, starts in zone 1 due to polycondensation reactions during crosslinking of MK releasing water, ethanol and methanol [19]. This is followed by a second mass loss in zone 2 resulting from the polymer to ceramic conversion by removal of the organic fractions of MK. PVA also indicates an intense mass loss in zone 1 that relates to inclusion of oxygen and reduction of OH species in the polymer chains (water elimination) [48]. Second mass loss starts at around 400°C corresponding to a 2-step rapid oxidation indicated as zone 2. It is worthwhile to mention that PVA has an amorphous carbon residue of around 1.62% (pyrolisation product) in air atmosphere at temperatures below 600°C that will be oxidized and removed at 1000°C (see Fig. 9a). In the case of EVA, first mass loss happens due to deacetylation of EVA polymer and loss of acetic acid [49]. The second mass loss starts around 400°C (see zone 2) as EVA polymer continues the random chain scissoring of the remained polymer to form unsaturated vapors such as butene and ethylene and the crosslinked polyethylene structure breaks down into volatiles. Considering the TG and DTG curve of green filament, first mass loss that starts at 210°C, results from the overlap between crosslinking of Silres MK and water elimination in PVA indicated in zone 1. At temperatures between 300-380°C, a second drop appears in the green filament DTG curve as a result of the deacetylation of EVA. By increasing the temperature (zone 2), an overlap

of different reactions including pyrolysis of MK, oxidation of PVA and scissoring in remaining chains from EVA can be observed. Last trough in DTG curve (zone 3) is related to loss of remained molecules from EVA between 450 and 550°C. This forms a graphite like structure. The mentioned temperature range has shifted to higher temperatures as the diffusion of gases in the feedstock can be more difficult compared to pure polymer. According to the SD and WD-4h DTG curves, the mentioned trough for green filament in zone 1 is no longer visible due to extracting majority of PVA during the solvent debinding process. By increasing the temperature for SD filament (zone 2), the amount of mass loss is reduced due to dissolving the PVA in an earlier stage. The amount of mass loss for WD-4h filament is reduced even further. This can be explained by chain scissoring and removal of some EVA molecules during the WD-4h stage (dwell time of 4 hours). Moreover, the mentioned troughs are shifted to lower temperatures as the removal of PVA (creation of porous network) facilitated the release of decomposition gases.

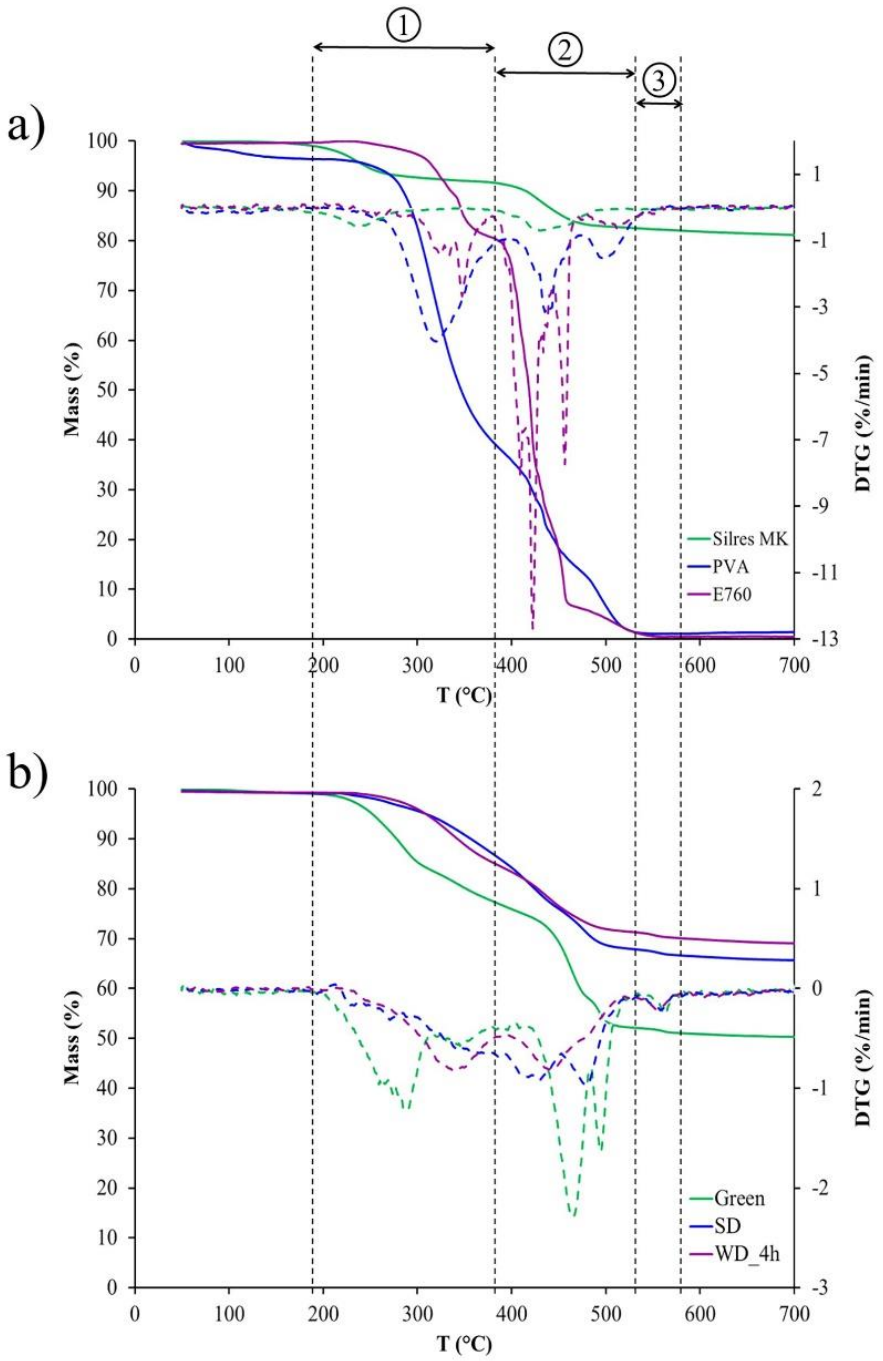

Fig. 9. (a) TG analysis of a) Silres MK, PVA and E760, b) filaments in green (G), solvent debound (SD) and wick debound (WD) indicated as TG (——) and DTG (- - - -) versus T (°C).

5.3.4. Printing of the PCP-based Feedstocks

As can be seen in Fig. 10a, 7-layer bar structures were printed in horizontal direction. Because of the flow instabilities, the feedstocks based on Elvax 420 were not further investigated. All feedstocks with 60 vol% PVA caused clogging in the printing nozzle and the fusion between the printed layers was not sufficient (Fig. 10c). We anticipate that the high amount of PVA

weakens the adhesion between the layers, due to the lower thermoplasticity. Therefore those feedstocks were not further investigated.

For the printing experiments, we focused on Elvax 460 and 760 binder compositions with 40 and 50 vol% PVA. All those feedstocks could be printed successfully with a sufficient fusion between the printed layers (Fig. 10b).

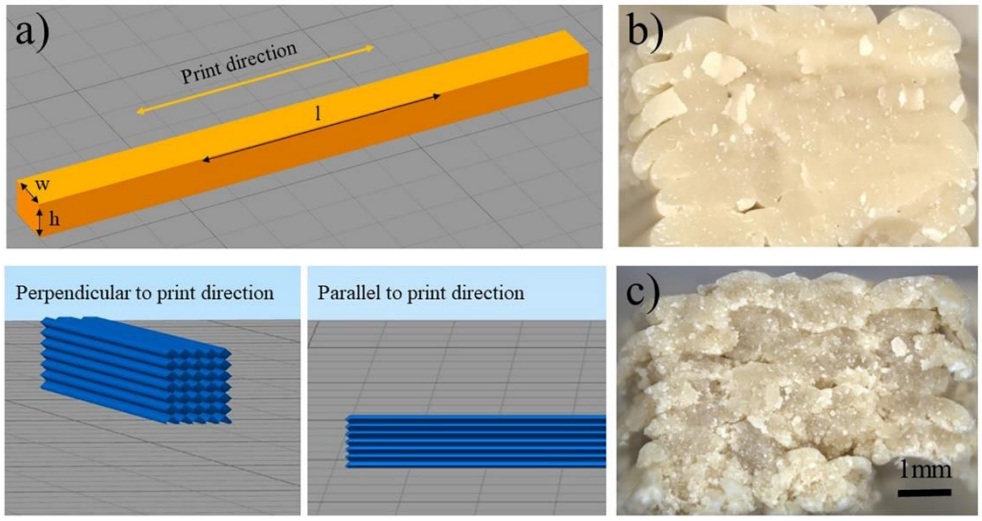

Fig. 10. (a) STL model of bar structure in Simplify3D software. (b) proper fusion between layers could be achieved with binder systems based on EVA mixed with 40 and 50 vol% PVA, (c) Introducing PVA content of 60 vol% inside the EVA binder system resulted in poor fusion between printed layers.

5.3.5. Debinding and sintering of printed PCP-based Feedstocks

Green printed structures went through a debinding and sintering process. Debinding of the printed structures was performed in three steps: 1) Solvent debinding to remove the PVA and generate an interconnected porous network, 2) Wick debinding in an alumina powder bed to extend the open porosity, and 3) Full thermal debinding without a powder bed to remove the organic binder completely and sinter the ceramic at 1600°C for 5h.

Solvent debinding of printed PCP-based Feedstocks

As can be seen in Fig. 11, green printed bars based on Elvax E460 with 40 and 50 vol% PVA were solvent debound in DI water for 3 and 6 days. By optical microscopy, a homogenous PVA removal after 3 days could be observed for E460-40 sample and 83% of the PVA could be removed (Fig. 11b,d). After 6 days, 90% of the PVA could be removed. Immersing E460-50P

samples in water for 3 days, provided a higher PVA removal of 88% that increased to 92% after 6 days.

Interestingly, as shown in Fig. 12, the samples based on E760-40P resulted in significantly lower PVA removal after 3 days (20%) and 6 days (42%). It could be observed that the PVA removal occurs from the edges to the center of the printed bars and a core-shell structure in the samples can be identified. The dissolving mechanism of water soluble binders (e.g. PEG and PVA) can be described in three general steps [50, 51]. In the initial stage (I), sample is immersed in water. Water diffuses in PVA cause swelling and gelation on the sample surface. Water further diffuses through the swelled gel and PVA starts to dissolve from the surface into bulk, generating fine pores. At the next Intermediate stage (II), water further penetrates inside the sample and more PVA is dissolved. III) Finally, pore size, pore distribution and volume continually increase while the water starts to reach the center of the sample. Eventually, a porous interconnected network is provided that ensures the transport pathway for gas to be released during the thermal debinding of backbone binder (EVA). By increasing the PVA to 50 vol% (E760-50P samples), the amount of PVA that could be removed was similar to the E460-50P samples. Therefore, 88% and 90% of PVA could be removed after 3 and 6 days, respectively.

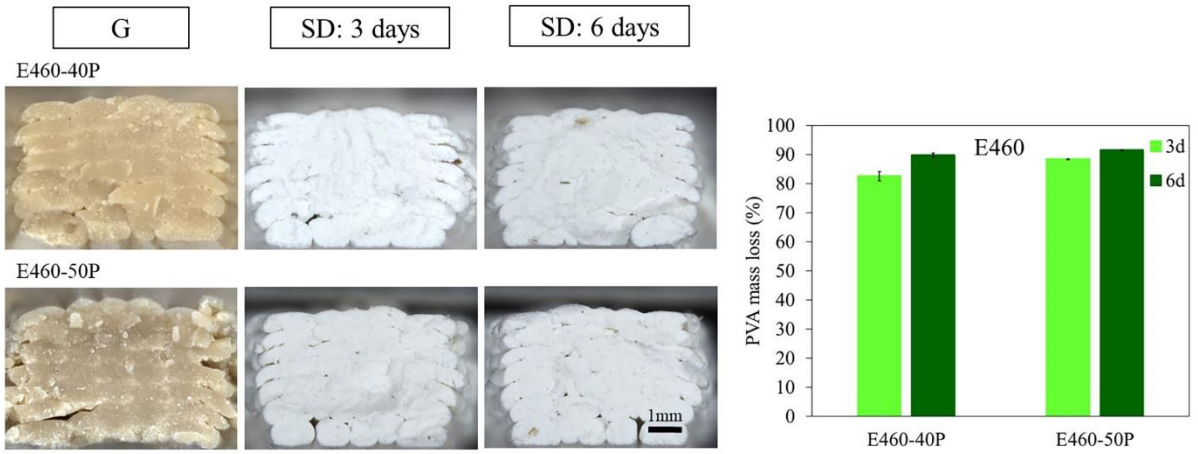

Fig. 11. Cross-section of green printed bars (G), Solvent debound bars for 3 (SD: 3 days) and 6 days (SD: 6 days) by optical microscope, from Elvax460 compositions. PVA mass loss (%) is reported for Elvax460 compositions after 3 and 6 days.

We conclude that PVA removal above 80% is necessary to avoid core-shell microstructure and to achieve a uniform solvent debound sample. As expected, a higher PVA content improves the

solvent debinding process. However, vinyl acetate content seems to affect the process, too; therefore, three days of solvent debinding seems insufficient for the E760-40P composition. Elvax460 has two-time higher vinyl acetate content compared to Elvax760. A higher vinyl acetate results in a lower elastic modulus (Table 1). Due to the higher elastic modulus for Elvax760, the printed structure is less flexible and hinders the swelling of the PVA. Therefore, PVA removal takes longer time. Initially, solvent debinding analysis for four different times (6 hours and 1, 3 and 6 days) were investigated. Considering the results, we focused on 3 and 6 days to investigate the solvent debinding process for the different PVA contents (appendices-Fig. S1).

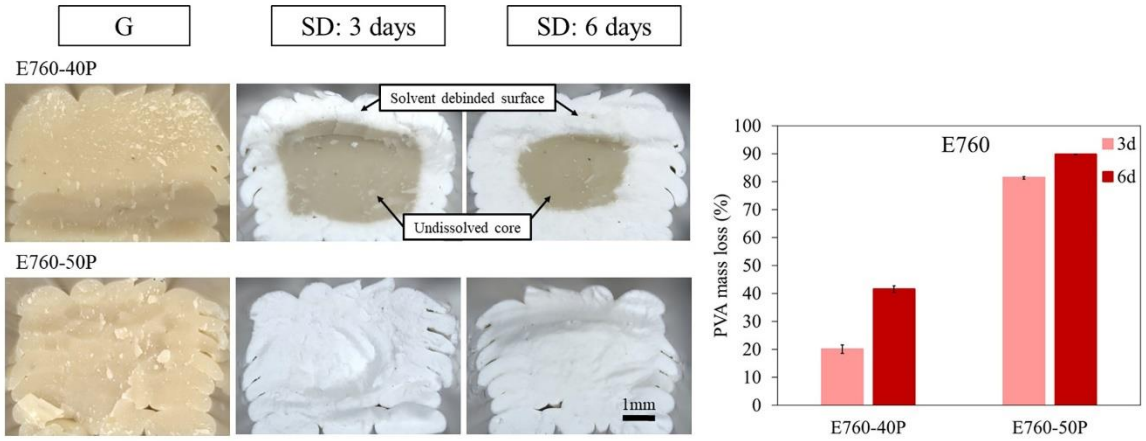

Fig. 12. Cross-section of green printed bars (G), Solvent debound bars for 3 (SD: 3 days) and 6 days (SD: 6 days) by optical microscope, from Elvax760 compositions. PVA mass loss (%) is reported for Elvax760 compositions after 3 and 6 days.

Wick debinding of the printed PCP-based Feedstocks

Due to the core formation of the E760-40P during solvent debinding, these samples were not further investigated. All other printed bars were further processed using wick debinding. By thermal treatment EVA and the rest of PVA binder will start to decompose in air atmosphere; therefore, the total binder mass loss is plotted in Fig. 13.

The E460-40P printed bars could not be homogeneously debound by wicking process. White parts (only solvent debound) still remained inside the samples and it can be assumed that the extent of the interconnected pore structure achieved by the solvent debinding process is not sufficient. A higher PVA content is needed to achieve desired volume of open pore channels for a successful wick debinding process, as shown by the microscopic analysis of the E460-50P samples. However, looking at the E760-50P samples, a lower vinyl acetate content of the EVA

will significantly reduce the wicking efficiency. This can be explained by higher gas permeability of the EVA polymers by increasing the vinyl acetate content [28]. Although wick debinding of filaments with E760-50P composition after 48h was successful (Fig. 7), a white core remains in the printed bar with higher wall thickness. It is anticipated that the white core can be removed by increasing the wicking time. We can conclude that EVA polymer with higher vinyl acetate content should be favored to develop thermoplastic binder for ceramic processing.

The brown color, which appeared after wick debinding, indicates the thermal-oxidative degradation of thermoplastic binders leaving carbon-saturated molecules, visible by the change in color. Solvent debinding step before thermal treatment provides a porous network as a pathway for the removal of volatile components during the wicking process. As shown in Fig. 13, 50 vol% PVA content in the Elvax 460 binder system results in a sufficient wicking process. Both, Elvax 460 and 760 binders with 50 vol% PVA, showed a similarly high binder removal after 3 and 6 days of solvent debinding. However, the samples show completely different wicking behavior. As already mentioned, the main difference between the two EVAs is the vinyl acetate content. The EVA 460 has two times higher vinyl acetate content, and therefore, a higher gas permeability can be expected [28]. We can conclude that a high gas permeability of the EVA binder is helpful to achieve faster debinding at low temperatures.

It is worthwhile to mention that up to 77% of the organics can be removed after solvent and wick debinding step using the Elvax 460 binder system with 50 vol% PVA.

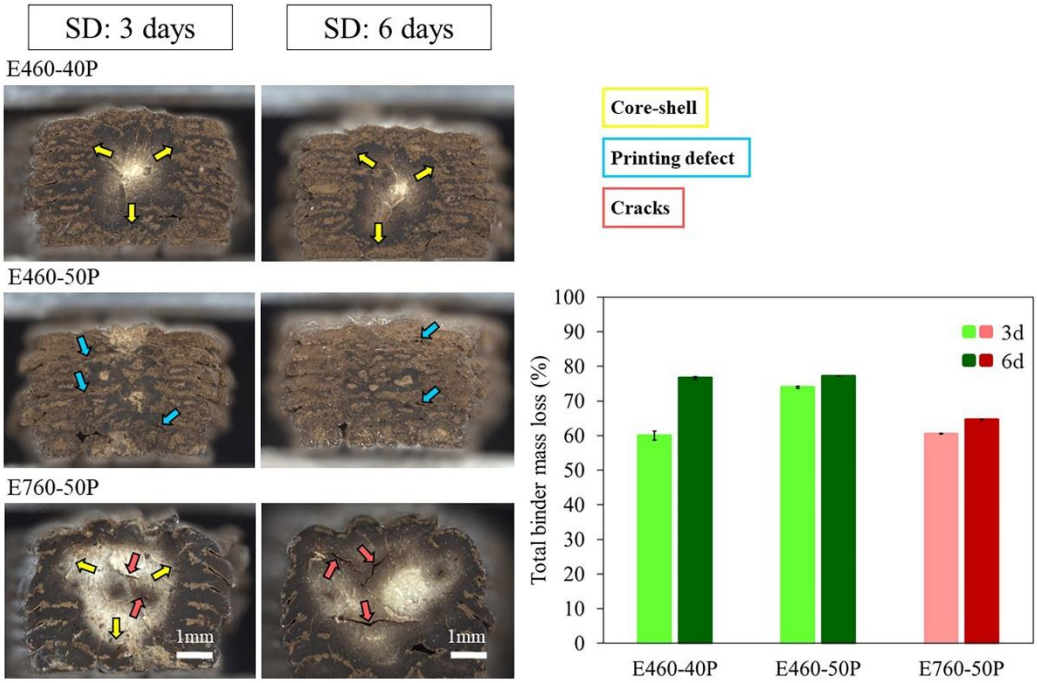

Fig. 13. Wick debinding of bars at 210°C for 48h, solvent debound for 3 and 6 days from different EVA-PVA binder compositions. Total binder mass loss (%) after solvent and wick debinding process is plotted for Elvax460 and Elvax760.

Full debinding and sintering of the printed PCP-based Feedstocks

Full debinding was performed up to 900°C followed by sintering at 1600°C for 5h. Fig. 14 presents cross-section of sintered samples, which shows horizontal cracks and pores inside the SEM pictures of sintered parts. Those defects remain from the printing process as can be already seen in Fig. 10b. In addition to these structural defects, core-shell structure was observed in sintered parts based on E460-40P subjected to solvent debinding for 3 days. The core-shell structure is highlighted with yellow arrows and a number (1). As can be seen in Fig. 13, this sample already showed an insufficient wick debinding and a low total mass loss. It can be expected that extended solvent debinding time would allow to prevent the formation of core shell defect due to the outgassing of the decomposed organic binders. By increasing the solvent debinding time up to 6 days, 17% higher total binder mass loss could be achieved and the structural artifacts by outgassing phenomena could be avoided, as shown inFig. 13. Independent of the solvent debinding time, sintered bars made of E460-50P binder system show only residual defects related to printing process (2). The numbers of structural defects during printing are significantly higher in comparison to Elvax 460-40P binder system due to the lower thermoplasticity of the PVA. For the sintered bars based on E760-50P, after solvent debinding for 3 days, the core-shell structure (1) and cracks (3) are visible in Fig. 14. By increasing the

solvent debinding time to 6 days, the core-shell structure is disappeared, however, debinding cracks (3) remained in the center of the sintered part. Elvax460 composition with 50% from each binder was considered as the optimum binder ratio as it lost a high percentage of PVA over 3 days. Nevertheless, the printing parameters may need to be optimized further. XRD analysis of E460-50P bar proved full mullitization after sintering (appendices- Fig. S2).

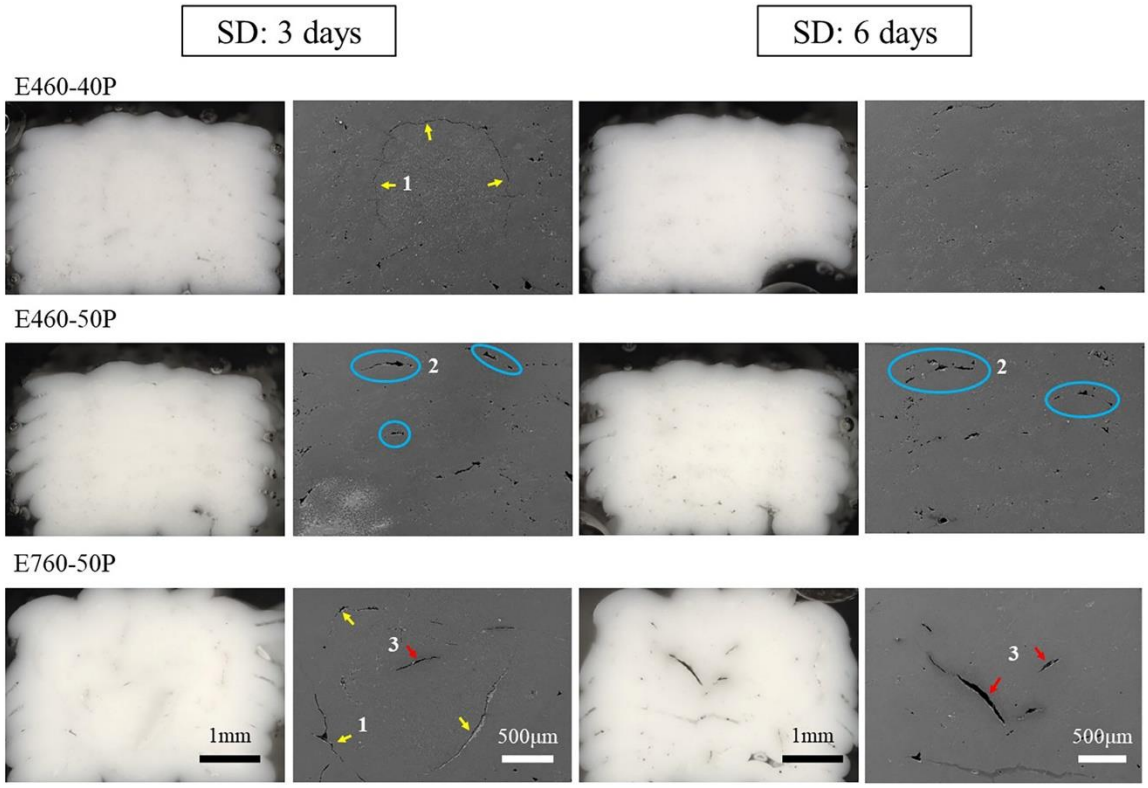

Fig. 14. Optical and scanning electron microscope images of sintered bars that were solvent debound for 3 and 6 days. Observed defects are labeled as (1) core-shell structure, (2) Printing defect and insufficient fusion between layers, and (3) crack in the center of sample.

5.4. Conclusion

Polymer derived mullite ceramic structures were printed by material extrusion based additive manufacturing (MEX-AM) technique, known also as fused deposition modeling. A mixture of EVA and PVA with a ratio of 40/60, 50/50 and 60/40 vol% were studied as the binder system. Rheological behavior of feedstocks with different compositions was investigated, it could be shown that increasing PVA content increases the feedstock viscosity due to its lower

thermoplasticity. Using three different EVA grades, it could be demonstrated that EVA with low molecular chain length (high MFI) results in flow instability and lead to melt rupture.
Bars with 40 and 50% PVA were successfully printed and solvent debound. A higher amount of PVA resulted in fusion problems between the layers and the orifice of the printing nozzle led to occlusion.
Removal of organic binders was performed in three steps. Initial solvent debinding in water at room temperature followed by wick debinding up to 210°C was used. Subsequently, full thermal debinding was performed to remove all volatile components before sintering. Solvent debinding step was necessary to achieve interconnected pore channels facilitating the escape of gaseous species during crosslinking of SILRES MK and removal of decomposition gases from backbone binder during wick debinding. The amount of vinyl acetate had a positive influence on the solvent debinding of PVA. As a result, EVA with higher VA content is more suitable for ceramic processing. As the PVA starts to form a swollen gel in contact with water, EVA with a higher amount of VA should not block the swelling phenomenon of PVA and penetration of water inside the sample will be easier, because EVA with higher VA content results in lower Young's modulus. To remove the remained organics after solvent debinding, model-free kinetics studies were performed in order to design the wick and full debinding programs for the samples with a constant mass loss rate (0.04%/min). Additional wick debinding was used to avoid a cooling step during thermal debinding. Interestingly samples with E460 binder system showed a higher mass loss, which can be explained by the higher gas permeability of EVA with higher vinyl acetate content.
Finally, an investigation on the fracture surface of bar structures after sintering revealed that samples based on E460 binder system with a PVA content of 50 vol% showed the best performance. However, printing parameters have to be adjusted to avoid printing defects. It can be assumed that for the E460-50P binder system only 3 days of solvent debinding is needed to remove almost 90% of the PVA binder.

Acknowledgements

This work was supported by the Swiss National Science Foundation (SNSF) [grant number 200021_184691/1].

References

[1] R. Sujith, S. Jothi, A. Zimmermann, F. Aldinger, R. Kumar, Mechanical behaviour of polymer derived ceramics–a review, International Materials Reviews, 66(6) (2021) 426-449. https://doi.org/10.1080/09506608.2020.1784616

[2] E. Bernardo, L. Fiocco, G. Parcianello, E. Storti, P. Colombo, Advanced ceramics from preceramic polymers modified at the nano-scale: A review, Materials, 7(3) (2014) 1927-1956. https://doi.org/10.3390/ma7031927

[3] P. Colombo, G. Mera, R. Riedel, G. D. Soraru, Polymer-derived ceramics: 40 years of research and innovation in advanced ceramics, J. Am. Ceram. Soc., 93(7) (2010) 1805-1837. https://doi.org/10.1111/j.1551-2916.2010.03876.x

[4] E. Bernardo, P. Colombo, E. Pippel, J. Woltersdorf, Novel mullite synthesis based on alumina nanoparticles and a preceramic polymer, J. Am. Ceram. Soc., 89(5) (2006) 1577-1583. https://doi.org/10.1111/j.1551-2916.2006.00963.x

[5] H. Elsayed, P. Colombo, Crack-free silicate bioceramics from preceramic polymers, Advances in Applied Ceramics, 115(4) (2016) 193-199. https://doi.org/10.1080/17436753.2015.1116663

[6] I. H. Song, M. J. Kim, H. D. Kim, Y. W. Kim, Processing of microcellular cordierite ceramics from a preceramic polymer, Scripta Materialia, 54(8) (2006) 1521-1525. https://doi.org/10.1016/j.scriptamat.2005.12.039

[7] G. Parcianello, E. Bernardo, P. Colombo, Z. Lenčéš, M. Vetrecín, P. Šajgalík, M. Kašiarová, Preceramic Polymer-Derived SiAlON as Sintering Aid for Silicon Nitride, J. Am. Ceram. Soc., 97(11) (2014) 3407-3412. https://doi.org/10.1111/jace.13134

[8] G. Parcianello, E. Bernardo, P. Colombo, Optimization of Phase Purity of β′-Sialon Ceramics Produced from Silazanes and Nano-Sized Alumina, J. Am. Ceram. Soc., 95(7) (2012). 148-2154. https://doi.org/10.1111/j.1551-2916.2012.05179.x

[9] G. Pierin, C. Grotta, P. Colombo, C. Mattevi, Direct Ink Writing of micrometric SiOC ceramic structures using a preceramic polymer, J. Eur. Ceram. Soc., 36(7) (2016) 1589-1594. https://doi.org/10.1016/j.jeurceramsoc.2016.01.047

[10] K. Huang, H. Elsayed, G. Franchin, P. Colombo, 3D printing of polymer-derived SiOC with hierarchical and tunable porosity, Addit. Manuf., 36 (2020) 101549. https://doi.org/10.1016/j.addma.2020.101549

[11] L. Zhao, X. Wang, H. Xiong, K. Zhou, D. Zhang, Optimized preceramic polymer for 3D structured ceramics via fused deposition modeling, J. Eur. Ceram. Soc., 41(10) (2021) 5066-5074. https://doi.org/10.1016/j.jeurceramsoc.2021.03.061

[12] Q. Wen, Z. Yu, R. Riedel, The fate and role of in situ formed carbon in polymer-derived ceramics, Progress in Materials Science, 109 (2020) 100623. https://doi.org/10.1016/j.pmatsci.2019.100623

[13] S. S. Hossain, I. W. Baek, H. J. Son, S. Park, C. J. Bae, 3D printing of porous low-temperature in-

situ mullite ceramic using waste rice husk ash-derived silica, J. Eur. Ceram. Soc., 42(5) (2022) 2408-2419. https://doi.org/10.1016/j.jeurceramsoc.2022.01.001

[14] K. Huang, H. Elsayed, G. Franchin, P. Colombo, Complex SiOC ceramics from 2D structures by 3D printing and origami, Addit. Manuf., 33 (2020) 101144. https://doi.org/10.1016/j.addma.2020.101144

[15] E. Zanchetta, M. Cattaldo, G. Franchin, M. Schwentenwein, J. Homa, G. Brusatin, P. Colombo, Stereolithography of SiOC ceramic microcomponents, Advanced Materials, 28(2) (2016) 370-376. https://doi.org/10.1002/adma.201503470

[16] C. He, X. Liu, C. Ma, X. Li, F. Hou, L. Yan, A. Guo, J. Liu, Digital light processing fabrication of mullite component derived from preceramic precusor using photosensitive hydroxysiloxane as the matrix and alumina nanoparticles as the filler, J. Eur. Ceram. Soc., 41(11) (2021) 5570-5577. https://doi.org/10.1016/j.jeurceramsoc.2021.04.051

[17] J. Schmidt, A. A. Altun, M. Schwentenwein, P. Colombo, Complex mullite structures fabricated via digital light processing of a preceramic polysiloxane with active alumina fillers, J. Eur. Ceram. Soc., 39(4) (2019) 1336-1343. https://doi.org/10.1016/j.jeurceramsoc.2018.11.038

[18] M. Pelanconi, P. Colombo, A. Ortona, Additive manufacturing of silicon carbide by selective laser sintering of PA12 powders and polymer infiltration and pyrolysis, J. Eur. Ceram. Soc., 41(10) (2021) 5056-5065. https://doi.org/10.1016/j.jeurceramsoc.2021.04.014

[19] L. Gorjan, R. Tonello, T. Sebastian, P. Colombo, F. Clemens, Fused deposition modeling of mullite structures from a preceramic polymer and γ-alumina, J. Eur. Ceram. Soc., 39(7) (2019) 2463-2471. https://doi.org/10.1016/j.jeurceramsoc.2019.02.032

[20] A. Kulkarni, J. Pearce, Y. Yang, A. Motta, G. D. Sorarù, SiOC (N) cellular structures with dense struts by integrating fused filament fabrication 3D printing with polymer-derived ceramics, Advanced Engineering Materials, 23(12) (2021) 2100535. https://doi.org/10.1002/adem.202100535

[21] P. Colombo, J. Schmidt, G. Franchin, A. Zocca, J. Günster, Additive manufacturing techniques for fabricating complex ceramic components from preceramic polymers, Am. Ceram. Soc. Bull, 96(3) (2017) 16-23.

[22] F. Sarraf, E. Abbatinali, L. Gorjan, T. Sebastian, P. Colombo, S.V. Churakov, F. Clemens, Effect of MgO sintering additive on mullite structures manufactured by fused deposition modeling (FDM) technology, J. Eur. Ceram. Soc., 41(13) (2021) 6677-6686. https://doi.org/10.1016/j.jeurceramsoc.2021.06.012

[23] P. Colombo, E. Bernardo, G. Parcianello, Multifunctional advanced ceramics from preceramic polymers and nano-sized active fillers, J. Eur. Ceram. Soc., 33(3) (2013) 453-469. https://doi.org/10.1016/j.jeurceramsoc.2012.10.006

[24] S. Walter, D. Suttor, T. Erny, B. Hahn, P. Greil, Injection moulding of polysiloxane/filler mixtures for oxycarbide ceramic composites, J. Eur. Ceram. Soc., 16(4) (1996) 387-393. https://doi.org/10.1016/0955-2219(95)00120-4

[25] F. Wolff, B. Ceron Nicolat, T. Fey, P. Greil, H. Münstedt, Extrusion foaming of a preceramic silicone resin with a variety of profiles and morphologies, Adv. Eng. Mater., 14(12) (2012) 1110-1115. https://doi.org/10.1002/adem.201100351

[26] L. Fiocco, E. Bernardo, Novel cordierite foams from preceramic polymers and reactive oxide fillers, Mater. Lett., 159 (2015) 98-101. https://doi.org/10.1016/j.matlet.2015.06.100

[27] D. Hotza, R. K. Nishihora, R. A. Machado, P. M. Geffroy, T. Chartier, S. Bernard, Tape casting of preceramic polymers toward advanced ceramics: A review, International Journal of Ceramic Engineering & Science 1(1) (2019) 21-41. https://doi.org/10.1002/ces2.10009

[28] A. Guo, M. Roso, M. Modesti, J. Liu, P. Colombo, Preceramic polymer-derived SiOC fibers by electrospinning, J. Appl. Polym. Sci., 131(3) (2014). https://doi.org/10.1002/app.39836

[29] Z. Yang, Z. Zhao, J. Yu, Z. Ren, Preparation of silica ceramic cores by the preceramic pyrolysis technology using silicone resin as precursor and binder, Mater. Chem. Phys., 223 (2019) 676-682. https://doi.org/10.1016/j.matchemphys.2018.11.039

[30] P. Colombo, J. R. Hellmann, Ceramic foams from preceramic polymers, Mater. Res. Innov., 6(5) (2002) 260-272. https://doi.org/10.1007/s10019-002-0209-z

[31] E. Ionescu, R. Riedel, Polymer processing of ceramics, Wiley: Hoboken, NJ, USA, 2012.

[32] P. Greil, Active-filler-controlled pyrolysis of preceramic polymers, J. Am. Ceram. Soc., 78.4 (1995) 835-848. https://doi.org/10.1111/j.1151-2916.1995.tb08404.x

[33] P. Greil, Polymer derived engineering ceramics, Adv. Eng. Mater. 2.6 (2000) 339-348. https://doi.org/10.1002/1527-2648(200006)2:6<339::AID-ADEM339>3.0.CO;2-K

[34] W. W. Yang, K. Y. Yang, M. C. Wang, M. H. Hon, Solvent debinding mechanism for alumina injection molded compacts with water-soluble binders, Ceram. Int. 29(7) (2003) 745-756. https://doi.org/10.1016/S0272-8842(02)00226-2

[35] X. Yang, C. Jia, Z. Xie, W. Liu, Q. Liu, Water-soluble binder system based on poly-methyl methacrylate and poly-ethylene glycol for injection molding of large-sized ceramic parts, International Journal of Applied Ceramic Technology, 10(2) (2013) 339-347. https://doi.org/10.1111/j.1744-7402.2011.02745.x

[36] V. A. Krauss, A. A. M. Oliveira, A. N. Klein, H. A. AlQureshi, M. C. Fredel, A model for PEG removal from alumina injection moulded parts by solvent debinding, Journal of materials processing technology, 182(1-3) (2007) 268-273. https://doi.org/10.1016/j.jmatprotec.2006.08.004

[37] M. I. Baker, S. P. Walsh, Z. Schwartz, B. D. Boyan, A review of polyvinyl alcohol and its uses in cartilage and orthopedic applications, J. Biomed. Mater. Res. Part B Appl. Biomater., 100(5) (2012) 1451-1457. https://doi.org/10.1002/jbm.b.32694

[38] T. F. McNulty, F. Mohammadi, A. Bandyopadhyay, D. J. Shanefield, S. C. Danforth, A. Safari, Development of a binder formulation for fused deposition of ceramics, Rapid Prototyp. J., 4(4) (1998) 144-150. https://doi.org/10.1108/13552549810239012

[39] M. Jafari, W. Han, F. Mohammadi, A. Safari, S. C. Danforth, N. Langrana, A novel system for fused deposition of advanced multiple ceramics, Rapid Prototyp. J., 6(3) (2000) 161-175. https://doi.org/10.1108/13552540010337047

[40] F. Clemens, J. Schulz, L. Gorjan, A. Liersch, T. Sebastian, F. Sarraf, Debinding and Sintering of Dense Ceramic Structures Made with Fused Deposition Modeling, In: International Conference on Additive Manufacturing in Products and Applications, Springer, (2020) 293-303. https://doi.org/10.1007/978-3-030-54334-1_21

[41] A. Hadian, L. Koch, P. Koberg, F. Sarraf, A. Liersch, T. Sebastian, F. Clemens, Material extrusion based additive manufacturing of large zirconia structures using filaments with ethylene vinyl acetate based binder composition, Addit. Manuf, 47 (2021) 102227. https://doi.org/10.1016/j.addma.2021.102227

[42] F. J. Clemens, A. Kerber, FDM/FFF an Alternative to CIM Manufacturing of Prototype and Small Quantities of Ceramic Part, Ceram. Appl. 8 (2020) 27-31.

[43] N. Venkataraman, S. Rangarajan, M. J. Matthewson, B. Harper, A. Safari, S. C. Danforth, G. Wu, N. Langrana, S. Guceri, A. Yardimci, Feedstock material property–process relationships in fused deposition of ceramics (FDC), Rapid Prototyp. J., 6(4) (2000) 244-253. https://doi.org/10.1108/13552540010373344

[44] A. Bellini, L. Shor, S. I. Guceri, New developments in fused deposition modeling of ceramics, Rapid Prototyp. J., 11(4) (2005) 214-220. https://doi.org/10.1108/13552540510612901

[45] A. Hadian, C. Zamani, L. Gorjan, F. J. Clemens, Thermoplastic processing and debinding behavior of NbC-M2 high speed steel cemented carbide, J. Mater. Process. Technol., 263 (2019) 91-100. https://doi.org/10.1016/j.jmatprotec.2018.08.006

[46] T. H. Ku, C. A. Lin, Shear flow properties and melt spinning of thermoplastic polyvinyl alcohol melts, Text. Res. J., 75(9) (2005) 681-688. https://doi.org/10.1177/0040517505059207

[47] J. Heiber, F. J. Clemens, T. Graule, D. Hülsenberg, Influence of varying the powder loading content on the homogeneity and properties of extruded PZT-fibers, Key Eng. Mater., 368 (2008) 11-14. https://doi.org/10.4028/www.scientific.net/KEM.368-372.11

[48] P. S. Thomas, J. P. Guerbois, G. F. Russell, B. J. Briscoe, FTIR study of the thermal degradation of poly (vinyl alcohol), Journal of thermal analysis and calorimetry, 64(2) (2001) 501-508. https://doi.org/10.1023/A:1011578514047

[49] K. McGarry, J. Zilberman, T. R. Hull, W. D. Woolley, Decomposition and combustion of EVA and LDPE alone and when fire retarded with ATH, Polymer international, 49(10) (2000) 1193-1198. https://doi.org/10.1002/1097-0126(200010)49:10<1193::AID-PI537>3.0.CO;2-0

[50] N. Chuaponpat, T. Ueda, A. Ishigami, T. Kurose, H. Ito, Morphology, thermal and mechanical properties of co-continuous porous structure of pla/pva blends by phase separation, Polymers, 12(5) (2020), 1083. https://doi.org/10.3390/polym12051083

[51] A. M. Henderson, Ethylene-vinyl acetate (EVA) copolymers: a general review, IEEE Electr. Insul. Mag., 9(1) (1993) 30-38. https://doi.org/10.1109/57.249923

Appendices

S1: PVA mass loss (%) versus time for solvent debound printed bars for 6 hour and 1, 3 and 6 days

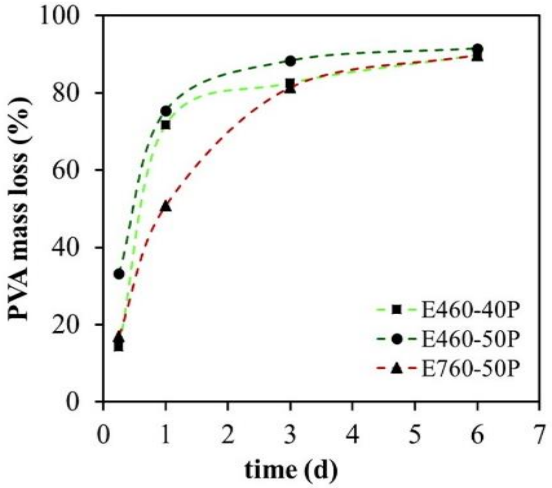

Fig. S1. Solvent debound bars for 6 hour and 1, 3 and 6 days from different EVA-PVA binder compositions. PVA mass loss (%) versus time is plotted for Elvax460 and Elvax760.

S2: XRD analysis of the sintered bars

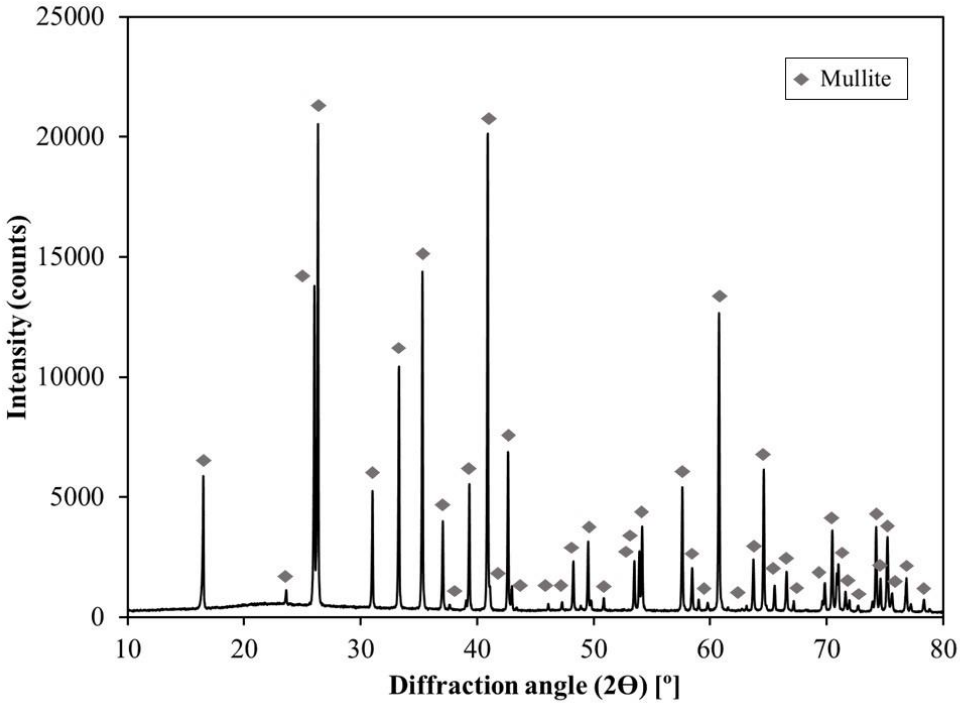

Fig. S2. XRD result of E460-50P composition after sintering at 1600 °C for 5 h.

Chapter 6- Conclusion

The objective of this PhD project was to develop fused deposition modeling (FDM) process for fabrication of polymer derived mullite ceramics, with a specific emphasis on achieving dense sintered parts with high wall thickness. In this context, the following remarks outline the research conducted during this PhD project. Further research and development for the fabrication of polymer derived ceramics (PDCs) using FDM technique are proposed in the outlook section.

6.1. Remarks

Three research questions have been outlined for this thesis in chapter 1. Regarding the research question 1, "**How sintering additives affect the densification and Mullite formation during the sintering process?**", it has been demonstrated that it is possible to promote the densification of polymer derived mullite ceramic by adding MgO sintering aid (see chapter 3). Based on the scanning electron microscopy (SEM) analysis of the mullite samples sintered at 1600°C for different durations (2.5 and 5 h) with varying amounts of MgO (0.0, 0.5, and 1.0 wt%), it could be successfully demonstrated that densification (i.e. sinterability) improved by the presence of 1.0 wt% MgO, via forming a liquid phase, when sintered the polymer derived mullite ceramic at 1600°C for 5h. Increased densification using MgO additive resulted in higher flexural strength as well and more interestingly, the impact of printing orientation on mechanical properties was diminished. Additionally, it was found by XRD analysis that using submicron alumina powder as an active filler, a small amount of MgO sintering additive (0.5 wt%) was necessary to obtain a pure mullite phase after sintering at 1600 °C for 2.5 h. Although the addition of MgO improved the sinterability of the mullite phase significantly, defects in the cross-section of sintered samples could not be avoided. Scattered macro-pores were still detected in the sintered specimens regardless of MgO content. Further investigations revealed that these defects were attributed to trapped water molecules release during crosslinking reactions (condensation). By increasing the wall thickness of printed sample from thin honeycomb structures to bar specimens with 100% infill, the problem escalated due to longer diffusion paths for the escape of gasses and closed spherical porous stucrure could be observed after sintering.

Regarding research question 2, "**How to design the thermal post-printing process to control the ceramic yield of PCP materials for silicate based ceramic materials?**", the ceramic yield

of the methyl-silsesquioxane (commercially available SILRES MK) was evaluated under air, nitrogen and argon atmospheres using different heating rates up to 800°C (see chapter 4). TG analysis results demonstrated a stable yield of 82.0 wt% after pyrolysis of SILRES MK under an inert atmosphere. The same trend was observed in air atmosphere with a heating rate of 2K/min and above. Using lower heating rates, however, yield decreased down to 69.1 wt%. To further investigate this phenomenon, GC-MS and FTIR analyses were used for two selected heating rates (0.6 and 20K/min). FTIR analysis of SILRES MK heated to 600°C with heating rates of 0.6 and 20K/min exhibited distinct composition of Si-O-Si bonds. With the higher heating rate, Si-O-Si bonds in the form of network structure were predominant. In contrast, when using a heating rate of 0.6K/min, Si-O-Si bonds in the form of cages were found to be dominant. This finding suggests that when using lower heating rates in air atmosphere, volatile unstable polyhedral silsesquioxanes (POSS) molecules are more likely to evaporate during the crosslinking process. Consequently, there is an excessive release of volatile species in the form of cages before they stabilize and form a network structure.

To evaluate the effect of heating rate on the thermoplastic processing of polymer derived mullite material, PCP- based mullite feedstocks with an Al_2O_3/SiO_2 ratio of 60/40 wt% were prepared. Mixing the feedstocks was performed at temperatures of 160°C and 190°C that - based on the rheological experiments - are below and above the crosslinking temperature of SILRES MK, respectively. Both mixtures were subjected then to debinding and pyrolysis with a heating rate of 0.6 K/min, followed by sintering at 1700°C for 5h. XRF analysis of mixture prepared at 160°C revealed a SiO_2 deficiency in obtained mullite material with an Al_2O_3/SiO_2 ratio of 61.7/37.7 wt% whereas a ratio of 59.8/39.8 wt% was achieved for the mixture prepared at 190°C. Therefore, it could be successfully demonstrated that crosslinking during the mixing process will help to avoid excessive release of POSS and stabilize the SiO_2 yield, regardless of heating rate.

To answer the third research question, "**How to optimize FDM process to fabricate dense large PDCs structures?**", and investigate the possibility to avoid structural defects in polymer derived mullite ceramics, a new approach was taken to create interconnected porous network and avoid blockage of gas products during the crosslinking process (see chapter 5). A thermoplastic binder system based on etheylene vinyl alcohol (EVA) was modified by adding a water-soluble poly vinyl alcohol (PVA) grade. Based on the experimental results, a composition of 50-50 vol% of EVA-PVA was necessary to enable the formation of an interconnected porous structure. Dissolving the PVA polymer at room temperature in water, after shaping and prior to post-processing (crosslinking and pyrolysis at elevated temperatures),

the interconnected porous channels facilitated the escape of released gases during post-processing. Introducing PVA, reduced the flexibility of the extruded feedstocks. As a result, a screw-based FDM printer was used to print the feedstock in form of pellets. The popularity of screw-based FDM printers is increasing due to the possibility to print thermoplastic materials without the restriction of spooling a ceramic feedstock filament [1-4]. The EVA-PVA binder system offers a solution to address the limitation in the thickness of PCP-based printed structures, allowing for the fabrication of bulk PDCs in air or inert atmosphere without the requirement of using filaments. In addition, it could be observed that the grade of etheylene vinyl alcohol (EVA) polymer influenced the removal of gaseous products and printability of the feedstocks to a great extent. Utilizing the suitable EVA grade with a higher ethylene vinyl acetate content and lower melt flow index, enhanced the printability of the pellets and the diffusibility of the polymer matrix during thermal debinding, respectively. Finally, by kinetic modeling, an optimization of the debinding process could be achieved. With this optimized debinding process, a controlled release of gases at a constant mass loss rate, enabled the pyrolysis of PCP and decomposition of EVA binder while avoiding structural defects such as pores, cracks and blisters.

Based on the findings in this thesis, it can concluded that for the successful MEX-AM processing of PDCs, the feedstock should be compounded above the crosslinking temperature of the PCP. According to the presented results, it is possible to use low heating rates for the thermal debinding process without changing the SiO_2 yield. A low heating rate is needed to avoid blisters, cracks and bubbles during the debinding process of ceramics shaped by thermoplastic shaping methods like MEX-AM. An EVA-PVA binder system with a volume ratio of 1:1 is needed to generate an interconnected porous network and avoid closed spherical pores in the microstructure of the sintered mullite ceramics. Finally, 1 wt.% of MgO sintereing additive is required to improve the sinterability of the polymer derived mullite ceramic. This preparation method has the potential to manufacture silicate objects with diverse shapes, employing a range of thermoplastic shaping technologies like pressing, extrusion, injection molding and 3D printing.

6.2. Outlook

According to the findings from chapter 5, even though the occurrence of structural defects resulting from crosslinking and pyrolysis of MK, as well as the thermal decomposition of the

binder system, could be prevented, further works remains to be done. Debinding program developed for this study was based on a low conversion rate (0.04%/min) with a total duration of 72 hours to ensure a slow decomposition of organic binders. In this way, the investigation was mainly focused on the effectiveness of interconnected porous networks (due to PVA leach out) on transporting the crosslinking gases from MK. As a result, debinding program needs to be further optimized, by employing kinetics modeling with higher conversion rates, leading to a shorter debinding step, thereby enhancing processing speed and reducing energy consumption. Furthermore, samples of varying wall thickness can be printed, debound, and sintered in order to determine the maximum achievable thickness for a defect-free object, using the approach presented in this thesis.

Application of screw-based FDM printers in this thesis, has become increasingly popular among research studies for additive manufacturing (AM) of ceramic and metallic compositions. This approach allows the utilization of pellets and granules [5] or ink and pastes [6], instead of spooled filaments, thereby eliminating the costs associated with filament fabrication and making it more attractive for industrial applications. Additionally, it expands the selection of materials available for 3D printing [7]. However, some challenges arised while working with such printers during this PhD study. Inconsistent extrusion of the feedstock using screw based FDM printers led to over-extrusion and under-extrusion of the material in different areas and layers of the print and printing failures remained after sintering the sample. To avoid the print defects in the structure, there is still a need to optimize the printing parameters. This issue may be solved by using the dynamic infill approach, developed by Hadian et al. to eliminate print failures [8].

According to the literature, many different polymer derived silicate ceramics and composites have been synthesized by introducing active and inert fillers to the PCP matrix such as calcium-based silicate ceramics ($CaO{\cdot}SiO_2$, $2CaO{\cdot}SiO_2$) [9], forsterite ($2MgO{\cdot}SiO_2$) [10], mullite ($3Al_2O_3{\cdot}2SiO_2$) [11], zircon ($ZrO_2{\cdot}SiO_2$) [12], willemite ($2ZnO{\cdot}SiO_2$) [13], yttrium mono-silicate ($Y_2O_3{\cdot}SiO_2$) [14], and ternary silicates such as akermanite ($2CaO{\cdot}MgO{\cdot}2SiO_2$) [15], diopside ($CaO{\cdot}MgO{\cdot}2SiO_2$) [16], hardystonite ($2CaO{\cdot}ZnO{\cdot}2SiO_2$) [17], gehlenite ($2CaO{\cdot}Al_2O_3{\cdot}SiO_2$) [18] and cordierite ($2MgO{\cdot}2Al_2O_3{\cdot}5SiO_2$) [19]. Offered preparation method in this PhD thesis can be used to fabricate the mentioned silicates, composites, glass ceramics and beyond, with tailored composition, even when pyrolysis in air with low heating rate is required.

Although the concept of partially water-soluble binder system was initially designed to facilitate the gas transport from the printed PDC structure, the same concept can be used for the

fabrication of bulk pieces from other ceramic materials too. In addition, the same approach could be used to achieve open porosity in bioactive ceramics where higher surface area is beneficial for the vascularization, cell migration, nutrient delivery or bone ingrowth. To prove this concept, bioactive composites such as wollastonite and hardystonite ($Ca_2ZnSi_2O_7$), 45S5 and 58S bioactive glasses and akermanite ($2CaO{\cdot}MgO{\cdot}2SiO_2$) and β-$Ca_2SiO_4$ bioceramics [20] could be investigated in the future. Since each element can influence the cell performances or immune reactions and trigger the signal pathways for the formation of new bone differently, utilizing PCPs is a good candidate to easily introduce or modify effective elements within the polymer derived silicate bioceramics.

References

[1] A. Hadian, M. Fricke, A. Liersch, F. Clemens, Material extrusion additive manufacturing of zirconia parts using powder injection molding feedstock compositions, Additive Manufacturing 57 (2022) 102966.doi: https://doi.org/10.1016/j.addma.2022.102966.

[2] Q. He, J. Jiang, X. Yang, L. Zhang, Z. Zhou, Y. Zhong, Z. Shen, Additive manufacturing of dense zirconia ceramics by fused deposition modeling via screw extrusion, Journal of the European Ceramic Society 41(1) (2021) 1033-1040.doi: https://doi.org/10.1016/j.jeurceramsoc.2020.09.018.

[3] K. Rane, M. Strano, A comprehensive review of extrusion-based additive manufacturing processes for rapid production of metallic and ceramic parts, Advances in Manufacturing 7 (2019) 155-173.doi: https://doi.org/10.1007/s40436-019-00253-6.

[4] E. Tabares, M. Kitzmantel, E. Neubauer, A. Jimenez-Morales, S.A. Tsipas, Extrusion-based additive manufacturing of Ti3SiC2 and Cr2AlC MAX phases as candidates for high temperature heat exchangers, Journal of the European Ceramic Society 42(3) (2022) 841-849.doi: https://doi.org/10.1016/j.jeurceramsoc.2021.10.042.

[5] J. Gonzalez-Gutierrez, S. Cano, S. Schuschnigg, C. Kukla, J. Sapkota, C. Holzer, Additive manufacturing of metallic and ceramic components by the material extrusion of highly-filled polymers: A review and future perspectives, Materials 11(5) (2018) 840.doi: https://doi.org/10.3390/ma11050840.

[6] H. Valkenaers, F. Vogeler, A. Voet, J.-P. Kruth, Screw extrusion based 3D printing, a novel additive manufacturing technology, Proceedings of the 5th international conference on competitive manufacturing, University of Stellenbosch; Stellenbosch, 2013, pp. 97-103.

[7] J.M. Justino Netto, H.T. Idogava, L.E. Frezzatto Santos, Z.d.C. Silveira, P. Romio, J.L. Alves, Screw-assisted 3D printing with granulated materials: A systematic review, The International Journal of Advanced Manufacturing Technology 115 (2021) 2711-2727.

[8] A. Hadian, L. Koch, P. Koberg, F. Sarraf, A. Liersch, T. Sebastian, F. Clemens, Material extrusion based additive manufacturing of large zirconia structures using filaments with ethylene vinyl acetate based binder composition, Additive Manufacturing 47 (2021) 102227.

[9] Y.J. No, J.J. Li, H. Zreiqat, Doped calcium silicate ceramics: a new class of candidates for synthetic bone substitutes, Materials 10(2) (2017) 153.
[10] E. Bernardo, L. Fiocco, G.A. Giffin, V. Di Noto, P. Colombo, Microstructure Development and Dielectric Characterization of Forsterite-Based Ceramics from Silicone Resins and Oxide Fillers, Advanced Engineering Materials 16(6) (2014) 806-813.
[11] E. Bernardo, P. Colombo, E. Pippel, J. Woltersdorf, Novel mullite synthesis based on alumina nanoparticles and a preceramic polymer, Journal of the American Ceramic Society 89(5) (2006) 1577-1583.doi: https://doi.org/10.1111/j.1551-2916.2006.00963.x.
[12] Z. He, C. Jiao, H. Zhang, D. Xie, M. Ge, Y. Yang, G. Wu, H. Liang, L. Shen, C. Wang, Fabrication of a zirconia/calcium silicate composite scaffold based on digital light processing, Ceramics International 48(18) (2022) 25923-25932.
[13] H. Elsayed, A. Zocca, E. Bernardo, C.M. Gomes, J. Günster, P. Colombo, Development of bioactive silicate-based glass-ceramics from preceramic polymer and fillers, Journal of the European Ceramic Society 35(2) (2015) 731-739.doi: 10.1016/j.jeurceramsoc.2014.09.020.
[14] E. Bernardo, G. Parcianello, P. Colombo, Novel synthesis and applications of yttrium silicates from a silicone resin containing oxide nano-particle fillers, Ceramics International 38(7) (2012) 5469-5474.
[15] E. Bernardo, J.-F. Carlotti, P.M. Dias, L. Fiocco, P. Colombo, L. Treccani, U. Hess, K. Rezwan, Novel akermanite-based bioceramics from preceramic polymers and oxide fillers, Ceramics International 40(1) (2014) 1029-1035.
[16] L. Fiocco, H. Elsayed, L. Ferroni, C. Gardin, B. Zavan, E. Bernardo, Bioactive Wollastonite-Diopside Foams from Preceramic Polymers and Reactive Oxide Fillers, Materials, 2015, pp. 2480-2494.
[17] A. Zocca, G. Franchin, H. Elsayed, E. Gioffredi, E. Bernardo, P. Colombo, Direct ink writing of a preceramic polymer and fillers to produce hardystonite (Ca2ZnSi2O7) bioceramic scaffolds, Journal of the American Ceramic Society 99(6) (2016) 1960-1967.
[18] E. Bernardo, L. Fiocco, A. Prnová, R. Klement, D. Galusek, Gehlenite: Eu3+ phosphors from a silicone resin and nano-sized fillers, Optical Materials 36(7) (2014) 1243-1249.
[19] I.-H. Song, M.-J. Kim, H.-D. Kim, Y.-W. Kim, Processing of microcellular cordierite ceramics from a preceramic polymer, Scripta Materialia 54(8) (2006) 1521-1525.doi: https://doi.org/10.1016/j.scriptamat.2005.12.039.
[20] S. Fu, M. Zhu, Y. Zhu, Organosilicon polymer-derived ceramics: An overview, Journal of advanced ceramics 8 (2019) 457-478.doi: https://doi.org/10.1007/s40145-019-0335-3.

Chapter 7- Collaborations

Contents

Publications resulted from collaborations are placed in this chapter:

Publication I- Material extrusion based additive manufacturing of large zirconia structures using filaments with ethylene vinyl acetate based binder composition

Amir Hadian, Leonard Koch, Philipp Koberg, **Fateme Sarraf**, Antje Liersch, Tutu Sebastian, Frank Clemens

Accepted (peer-reviewed), Additive manufacturing (2021), Volume 47, November 2021, 102227

DOI: https://doi.org/10.1016/j.addma.2021.102227

- This study focuses on the fabrication of complex zirconia structures using fused deposition modeling (FDM). A feedstock comprising zirconia powder, EVA, and stearic acid was extruded into filaments and printed using a filament printer. To prevent defects during printing, a dynamic infill technique was utilized, resulting in void-free disks with smooth top surfaces. This study successfully printed and obtained defect-free sintered vases with a height of 120 mm using the debinding program designed via model-free kinetics.

Contribution of the PhD candidate: Using the knowledge of model-free kinetic analysis for debinding process developed during this thesis, the activation energy of binder decomposition was determined and a thermal debinding program with a consistent conversion rate of 0.1%/minute for decomposition of the thermoplastic binder was designed. By integrating solvent extraction and wicking debinding steps, sufficient thermal binder burnout was achieved.

Publication II- Material extrusion additive manufacturing of advanced ceramics: Towards the production of large components

Frank Clemens, **Fateme Sarraf**, Aurelio Borzì, Antonia Neels, Amir Hadian

Accepted (peer-reviewed), Journal of the European Ceramic Society (2023), Volume 43, Issue 7, July 2023, Pages 2752-2760

DOI: https://doi.org/10.1016/j.jeurceramsoc.2022.10.019

- This study investigated three commercial yttria-stabilized zirconia (YSZ) filaments (Fabru, SiCeram and PT+A) provided by different companies for fabricating large ceramic parts via FDM method. Results showed significant variations in flexibility and rheological properties among the filaments. A 70 mm tall cup structure with overhang features and different wall thicknesses was printed and post-processed using two of the YSZ filaments (Fabru and SiCeram) for evaluation. Despite diverse filament properties, printing the ceramic cup was possible with both brittle and flexible filaments after parameter adjustments. However, only printed cups using Fabru filaments could be sintered without defects.

Contribution of the PhD candidate: Flow behavior of three feedstocks were studied at different temperatures using a shear rate in the range of 0.1 and 1 1/s. With the help of rheology analysis, printing parameters were adjusted, and therefore, failures during printing could be avoid.

Publication I- Material extrusion based additive manufacturing of large zirconia structures using filaments with ethylene vinyl acetate based binder composition

Amir Hadian, Leonard Koch, Philipp Koberg, **Fateme Sarraf**, Antje Liersch, Tutu Sebastian, Frank Clemens

Abstract

This study demonstrates the feasibility of fabricating large complex zirconia structures using a material extrusion-(MEX) based additive manufacturing process, called fused deposition modeling (FDM) or fused filament fabrication (FFF). For this purpose, a feedstock based on ethylene-vinyl acetate and stearic acid containing 45 vol.-% zirconia powder was extruded into filaments and used for printing on a consumer-grade FDM/FFF printer. To detect structural failures after each processing step, disks made out of 4 printed layers were selected. After printing, debinding and sintering a fractography analysis of the disks was evaluated using an optical and scanning electron microscope to identify the defects. To avoid defect formation during printing, a new approach, dynamic infill technique, was employed and resulted in void-free printed disks with a smooth top surface. This approach was essential to study the origin of failures in the post-processing steps. Model free-kinetic analysis was used to investigate the activation energy of the binder decomposition and to design a thermal debinding program with a constant 0.1%/min mass loss rate of the thermoplastic binder. Based on the kinetic studies it could be demonstrated that sufficient thermal binder burnout could be achieved by integration of solvent extraction and wicking debinding steps. Using ring-on-ring test it could be observed, that an edge-initiated failure resulted in low average strength (91 MPa) of the sintered disks. Finally, printed and defect-free sintered 120 mm high vase could be successfully achieved using the model free-kinetic designed debinding program.

Publication II- Material extrusion additive manufacturing of advanced ceramics: Towards the production of large components

Frank Clemens, **Fateme Sarraf**, Aurelio Borzì, Antonia Neels, Amir Hadian

Abstract

Thermoplastic extrusion based additive manufacturing (MEX-AM), is a very interesting fabrication method for the shaping of larger ceramic parts. Commercial filaments are currently available in the market, but due to the lack of information from the suppliers, it is not easy to select the suitable filament material for the 3D printing of individual ceramic objects. In this study, three commercial yttria-stabilized zirconia (YSZ) filaments provided by Fabru GmbH, SiCeram GmbH and PT+A GmbH were investigated. According to our results, it is possible to print YSZ filaments with extremely different flexibility and rheological properties. Compared to the other two filaments, the Fabru filament resulted in significantly higher flexibility, but the extrusion pressure to print it through a 0.25 mm nozzle was significantly higher at 150 °C. Interestingly, in the SiCeram filament, a grain orientation effect could be observed. Based on STA analysis it can be assumed that for the Fabru filament, the polymer which decomposes at a high temperature can already be removed by solvent debinding (SD). Finally, 70 mm tall cup structure including overhang features and different wall thicknesses was used to evaluate the printing and post-processing of YSZ filaments